JAERI-M
83-121

EVALUATION REPORT ON CCTF CORE-I REFLOOD TEST C1-4 (RUN 13) AND C1-15 (RUN 24)

—INVESTIGATION OF THE REFILL SIMULATION AND THE NITROGEN INJECTION EFFECTS—

August 1983

Takashi SUDOH* and Yoshio MURAO

日本原子力研究所
Japan Atomic Energy Research Institute

JAERI-M レポートは，日本原子力研究所が不定期に公刊している研究報告書です。

入手の問合わせは，日本原子力研究所技術情報部情報資料課（〒319-11 茨城県那珂郡東海村）あて，お申しこしください。なお，このほかに財団法人原子力弘済会資料センター（〒319—11 茨城県那珂郡東海村日本原子力研究所内）で複写による実費頒布をおこなっております。

JAERI-M reports are issued irregularly.

Inquiries about availability of the reports should be addressed to Information Section, Division of Technical Information, Japan Atomic Energy Research Institute, Tokai-mura, Naka-gun, Ibaraki-ken 319-11, Japan.

編集兼発行　日本原子力研究所
印　　刷　日立高速印刷株式会社

JAERI-M 83-121

EVALUATION REPORT ON CCTF CORE-I REFLOOD TEST C1-4 (RUN 13) AND C1-15 (RUN 24)

—— Investigation of the refill simulation and the nitrogen injection effects ——

Takashi SUDOH* and Yoshio MURAO
Department of Nuclear Safety Research,
Tokai Research Establishment, JAERI

(Received July 9, 1983)

The tests C1-4 and C1-15 were performed with the Cylindrical Core Test Facility (CCTF) to investigate the effects of the depressurization process to simulate the refill phase, and the effects of the nitrogen to be injected after the end of the accumulator injection on the thermo-hydraulic behavior in the core and primary loop system during refill and reflood phases.

In these tests, after the lower plenum was filled to 0.9m level with saturated water at 0.6 MPa, the accumulator water was injected into three intact cold legs in the depressurization period from 0.6 MPa to 0.2 MPa. The water in the lower plenum voided during the depressurization and the significant steam condensation occurred in or near the intact cold legs. The condensation caused high steam flow rate in the intact loops and the lower plenum flashing resulted in suppressed core water accumulation. The slightly lower core heat transfer coefficient due to the less core water caused the higher turnaround temperature and the longer quench time than those of the normal reflood test without the depressurization process.

The nitrogen injection followed the accumulator injection was allowed in the test C1-15. However, significant effects of the nitrogen injection was not observed.

The work was performed under contract with the Atomic Energy Bureau of Science and Technology Agency of Japan.

* NEDAC

Keywords: PWR, LOCA, ECCS, Reflood, Refill, Nitrogen, Heat-transfer, Reactor Safety, Quench, Turnaround

JAERI－M 83－121

大型再冠水円筒第1次炉心試験Cl－4（RUN 013），Cl－15（RUN 024）評価報告書
― リフィル模擬および窒素注入効果の検討 ―

日本原子力研究所東海研究所安全工学部
須藤　高史*・村尾　良夫

（1983年7月9日受理）

円筒炉心試験装置で行なわれたCl－4，Cl－15試験は，リフィル後期を模擬した減圧過程および蓄圧注入系からの窒素ガス注入模擬を含んでおり，それらのリフィル期および再冠水期における炉心や1次系システム内の熱流動挙動に与える影響を調べることを目的とした。

これらの試験では，システムを0.6MPaに加圧し，下部プレナム内に飽和水を0.9mまで満たし，このシステムを0.2MPaまで減圧させつつ，蓄圧系注水を3健全ループコールドレグに行った。減圧器では，下部プレナム水フラッシングが生じ，健全コールドレグ近傍では，顕著な蒸気凝縮が生じた。蒸気凝縮により，健全ループ中の蒸気流は増大し，下部プレナムフラッシングにより，炉心蓄水は抑えられた。炉心低蓄水のため熱伝達率が低くなり，減圧過程を含まない通常の再冠水試験と比べ，炉心最高温度は高く，クエンチ時間は長くなった。

Cl－15では減圧過程に加えて窒素ガス注入も行われたが顕著な効果はみられなかった。

本報告書は，電源開発促進対策特別会計法に基づき，科学技術庁からの受託によって行った研究の成果である。

＊　原子力データセンタ

Contents

目　　次

Tables and figures list

1. Introduction

The tests C1-4 (RUN 13) and C1-15 (RUN 24) including the refill phase, the so-called refill tests, were performed with the Cylindrical Core Test Facility (CCTF)[1].

The objectives of the CCTF program are:

a. Demonstration of ECCS behavior during refill and reflood period.

b. Verification of reflood analysis codes.

c. Collection of information to improve the thermohydrodynamics model in the analysis codes, such as models of, (a) multi-dimensional core thermohydrodynamics including the radial power distribution effect, fallback effect and spatial oscillatory behavior, (b) flow behavior in the upper plenum and hot legs, (c) behavior of accumulated water at the bottom of the upper plenum including possible counter-current flow and sputtering effect, (d) hydrodynamic behavior of the injected ECC water and the water passing through the steam generator, (e) multi-dimensional thermohydrodynamics behavior in the hot annular downcomer, and (f) overall oscillatory behavior in the system.

Thereflood phase follows the refill phase in a postulated loss-of-coolant accident (LOCA) of a pressurized water reactor (PWR), so that the initial condition for the reflood phase is not static. However, for the reflood experiments, it was very difficult to establish the transient initial condition, especially in the method for injecting subcooled ECC water into the simulated primary system which was filled with saturated steam, because the injection generated unrealistic condensation effects in the system[2),3)]. Therefore, in the normal reflood test in CCTF, the system pressure was maintained at the predetermined value and at first, the accumulator water was injected directly into the lower plenum to reduce the effect of condensation on the system. After a certain amount of water was accumulated in the core, and the steam generation in the core was considered to prevent the significant condensation effect in the system, the accumulator injection port was siwtched from the lower plenum to the cold legs.

Under more realistic initial condition, the tests C1-4 and C1-15 were conducted in CCTF. In these tests, the pressures in the system and the containment tanks were pressurized at 0.6 MPa and the saturated water was filled to 0.9m height in the lower plenum. When the system depressurization

was initiated, the accumulator water was injected only into the intact cold legs. The water in the lower plenum was allowed to flash during the depressurization period. The nitrogen gas was injected into the system just after the end of accumulator injection in C1-15.

The objective of this work is to study the effects of the depressurization process and the nitrogen gas injection on the system behavior in reflood phase.

The experimental facility and conditions are described in Section 2. For the first objective the results of C1-4 are compared in Section 3 with those of C1-2 which was conducted under the nominally same test condition as those for C1-4 except the ECC injection location and the system depressurization. The results of C1-15 are also compared with those of C1-4 in Section 3 for the second objective.

2. Experimental Conditions

2.1 Facility design

The facility design is detailed in the reference 1. The facility consists of a pressure vessel and four primary loops, as shown in Fig. 2.1.

To simulate the system effect during refill and reflood phase of a postulated PWR LOCA, the following items were considered as the design criteria:

(1) The elevations of the components are maintained to be as close to those of a PWR as possible.

(2) The lengthes of the flow pathes in the components are also preserved.

(3) The flow areas of the components are scaled down in propotion to the scaling factor of core flow area.

(4) The facility has three intact loops and one broken loop which simulates double-ended cold leg break.

The reference reactor is the Trojan reactor in USA, but the Ohi reactor in Japan is also referred partly.

The pressure vessel contains the core, upper and lower plenum, and downcomer. The core has thirty-two 8×8 bundles which simulate 15×15 fuel assembly in which unheated rods are included. The core configuration is shown in Fig. 2.2.

The core is full height and has 1824 electrically heated rods, as shown in Fig. 2.3. The axial power distribution is chopped cosign. There are high, medium and low power heaters in a bundle.

The downcomer is an annulus as shown in Fig. 2.2. The core baffle region area in a PWR is scaled and included in the simulated downcomer flow area to reduce the small-gap effect in the downcomer. Thus, the gap size of the annulus is 61.5 mm.

The internals in the upper plenum consist of control rod guide tubes, support columns, short stubs, orifice plates and open holes, as shown in Fig. 2.4 and Fig. 2.5. These internals simulate those of a 17×17 type PWR. The radial dimensions of them are scaled down in comformity to the scaling of the bundle array size.

The primary loop arrangement is shown in Fig. 2.1. Each loop consists of a hot leg and a cold leg piping, an active steam generator, and a pump simulator, as shown in Fig.2.6. U-tubes in the steam generator are about 5 m shorter than the actual ones and those of two loops are housed in a single shell.

2.2 Test conditions and procedure

A summary of the specified and measured system conditions are listed in Table 2.1 for C1-4, in Table 2.2 for C1-15 and in Table 2.3 for C1-2. Most of the initial conditions are nearly identical to those for C1-2, the reference test. The differences are as follows.

- System pressure

  The system pressure was initially 0.6 MPa for C1-4 and C1-15 while it was 0.2 MPa for C1-2.

- Primary piping wall temperature

  Saturated steam was filled in the primary system and the containment tanks prior to the experiment initiation. The primary piping wall temperature was maintained at the saturation temperature, which was 431 K for C1-4 and C1-15 and 391 K for C1-2.

- Water temperature stored in the lower plenum

  Saturated water was stored in the lower plenum prior to the initial system pressure caused the temperature difference of the saturated water.

The test procedure was described in detail in the reference 1. Then the differences of the procedure between C1-4, C1-15 and C1-2 are mainly presented below.

After establishing the specified initial conditions including saturated water filling in the lower plenum to the specified water level of 0.9 m and electric power was supplied to the core heaters. When the heater temperature reached the specified value, the accumulator injection was initiated to the intact cold leg for C1-4 and C1-15, and directly to the lower plenum for C1-2. For C1-4 and C1-15, system depressurization was initiated simultaneously with the accumulator injection by opening the pressure regulation valve of the containment-2, and the system pressure was then maintained at 0.2 MPa. For C1-2, the system pressure was maintained at 0.2 MPa throughout the transient. When the calculated water level in the core reached 0.5 m above the bottom of the core, for C1-2, the accumulator injection port was switched from the lower plenum to the intact cold legs. At 14 seconds after the calculated reflood initiation time, the accumulator injection was replaced with the simulated low pressure coolant injection (LPCI) for C1-4 and C1-2. For C1-15, the accumulator was considered to be empty at 14 seconds after calculated reflood initiation and nitrogen gas was then injected during about 10 seconds.

LPCI initiated after the nitrogen gas injection.

Figure 2.7 compares the ECC flow rates between C1-4 and C1-2. For C1-4, the accumulator injection rate is increased with the time due to the primary system depressurization. For C1-2, the accumulator injection port was at the lower plenum at first and switched to the cold leg at the time indicated by an arrow in the figure. The LPCI rate was the same for C1-4 as for C1-2.

The pressures at the containment and the upper plenum are compared in Fig. 2.8. The containment depressurization for C1-4 ends at about 30 seconds after flooding while the containment pressure for C1-2 remains nearly steady.

Table 2.1 Run condition for C1-4

	Estimated	Measured
Power		
Total (MW) :	9.37	9.31
Linear (KW/m) :	1.4	1.39
Radial Power Distribution :	1.02:1.0:0.82	1.03:1.0:0.82
Decay Type : ANS x 1.2 + Actinide (30 sec after Scram)		
Pressure (kg/cm^2a)		
System :	6.0→2.0	6.02 → 2.0
Steam Generator Secondary :	52	50
Temperature (°C)		
Downcomer Wall :	198	185
Primary Piping Wall :	158	157
Steam Generator Secondary :	265	264
Peak Clad at ECC Initiation :	518	518
Peak Clad at BOCREC :	600	654
Lower Plenum Filled Liquid :	158	149
ECC Liquid :	35	35
Water Level (m)		
Lower Plenum :	0.9	0.82
Steam Generator Secondary :	7.4	7.4
Injection Rate (m^3/hr)		
Accumlator :	251	195
LPCI :	30	30.7

Table 2.2 Run condition for C1-15

	Estimated	Measured
Power		
Total (MW) :	9.41	9.40
Linear (KW/m) :	1.4	1.4
Radial Power Distribution :	1.06:1.0:0.82	1.07:1.0:0.82
Decay Type : ANS x 1.2 + Actinide (30 sec after Scram)		
Pressure (kg/cm^2a)		
System :	6.0 → 2.0	6.06 → 2.08
Steam Generator Secondary :	52	53
Temperature (°C)		
Downcomer Wall :	198	175
Primary Piping Wall :	158	157
Steam Generator Secondary :	265	264
Peak Clad at ECC Initiation :	494	507
Peak Clad at BOCREC :	600	689
Lower Plenum Filled Liquid :	158	150
ECC Liquid :	35	40
Water Level (m)		
Lower Plenum :	0.9	0.86
Steam Generator Secondary :	7.4	7.5
Injection Rate (m^3/hr)		
Accumlator :	251	237
LPCI :	30	29.8
Injection Duration Time (sec)		
Accumulator : Water	24	} 35.5
Nitrogen Gas	10	

Table 2.3 Run condition for C1-2

	Estimated	Measured
Power		
Total (MW) :	9.41	9.40
Linear (KW/m) :	1.41	1.41
Radial Power Distribution :	1.148:1.079:0.886	1.153:1.079:0.885
Decay Type : ANS x 1.2 + Actinide (30 sec after Scram)		
Pressure (kg/cm^2a)		
System :	2.0	1.96
Steam Generator Secondary :	52	53.6
Temperature (°C)		
Downcomer Wall :	198	166
Primary Piping Wall :	119	120
Steam Generator Secondary :	265	263
Peak Clad at ECC Initiation :	502	516
Peak Clad at BOCREC :	600	597
Lower Plenum Filled Liquid :	119	114
ECC Liquid :	35	38.8
Water Level (m)		
Lower Plenum :	0.9	0.88
Steam Generator Secondary :	7.4	7.2
Loop Seal Section :	1.5	1.48
Injection Rate (m^3/hr)		
Accumlator :	278/251	285/254
LPCI :	30	30.2

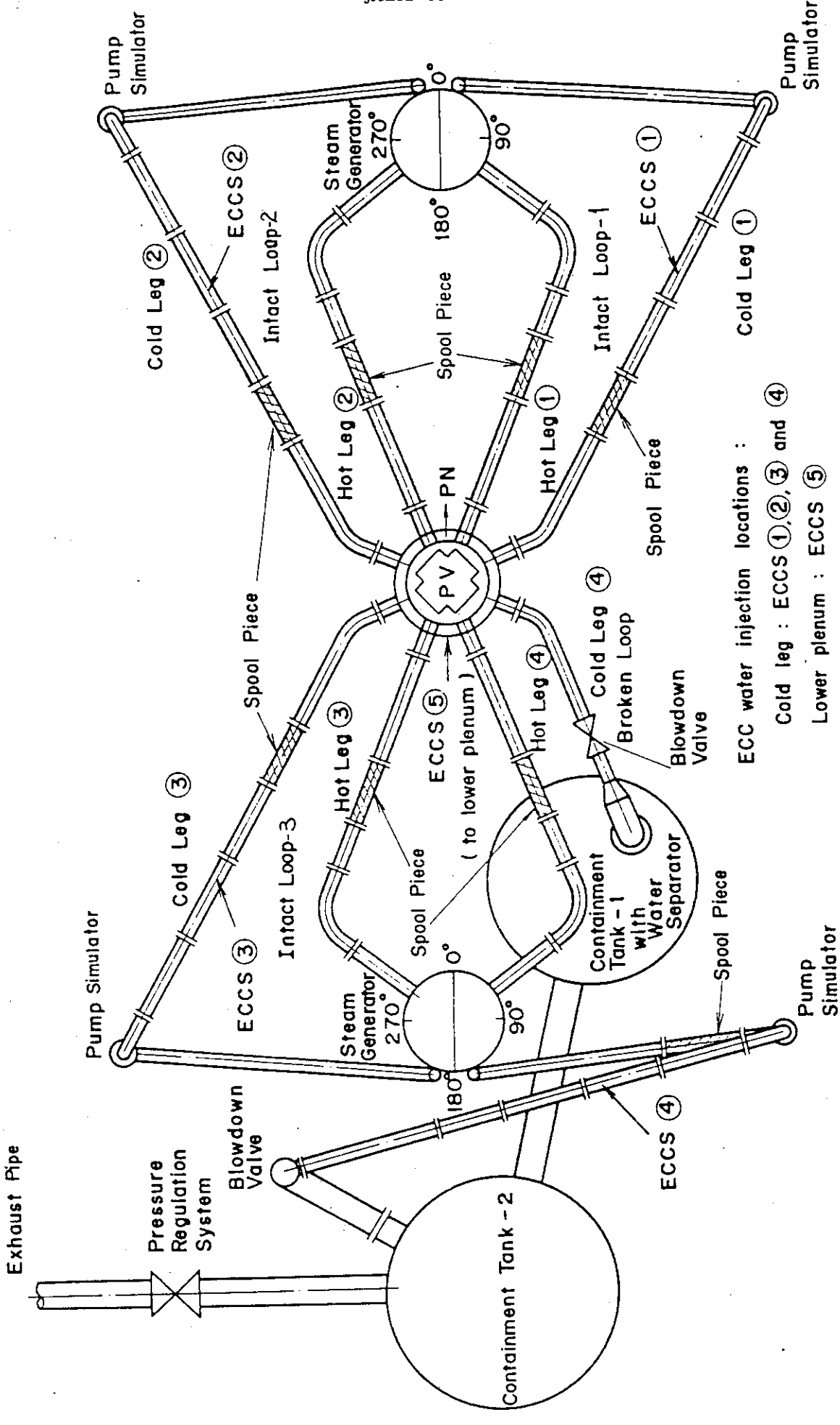

Fig.2.1 Primary loop piping

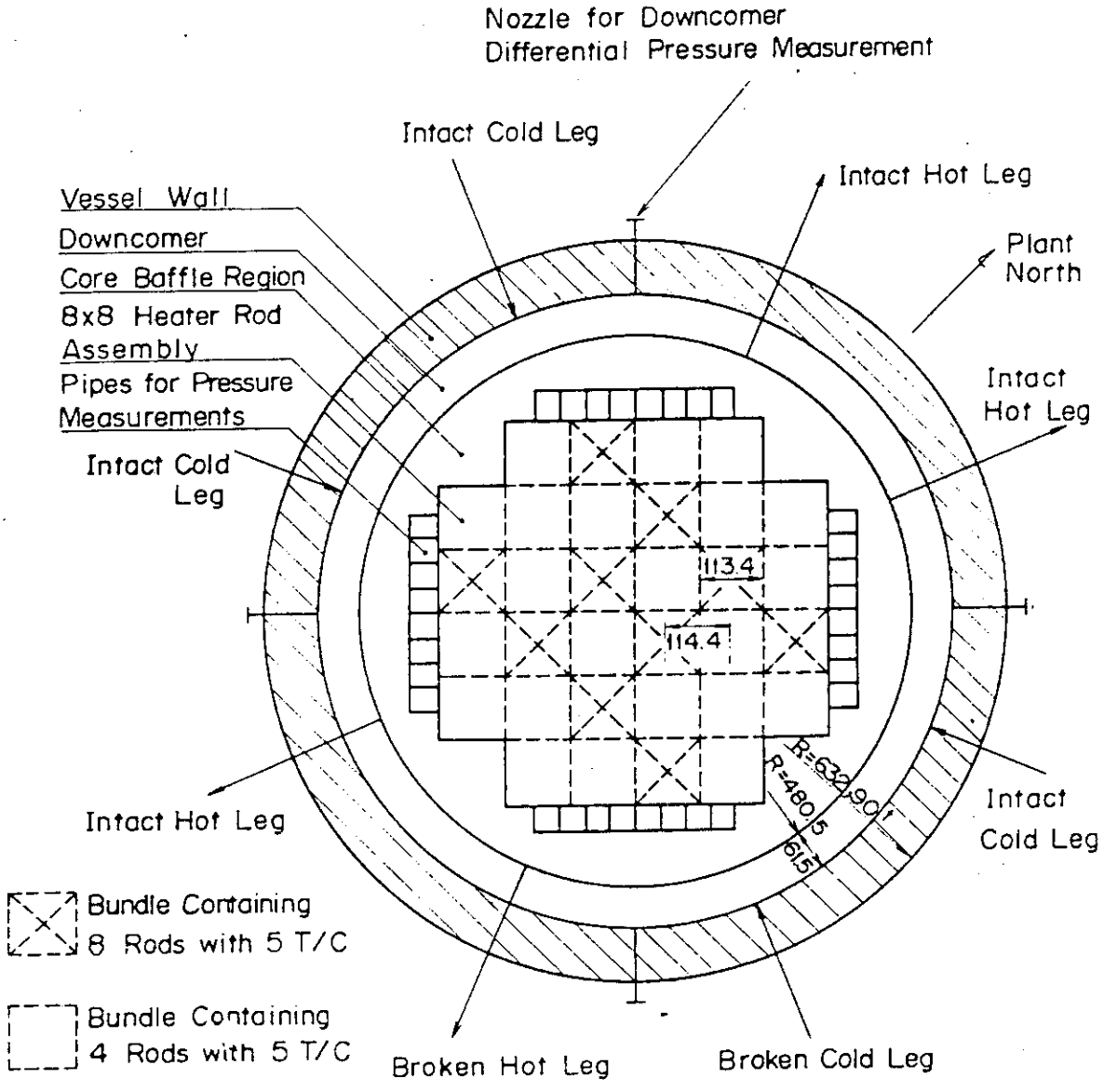

Fig.2.2 Cross section of pressure vessel

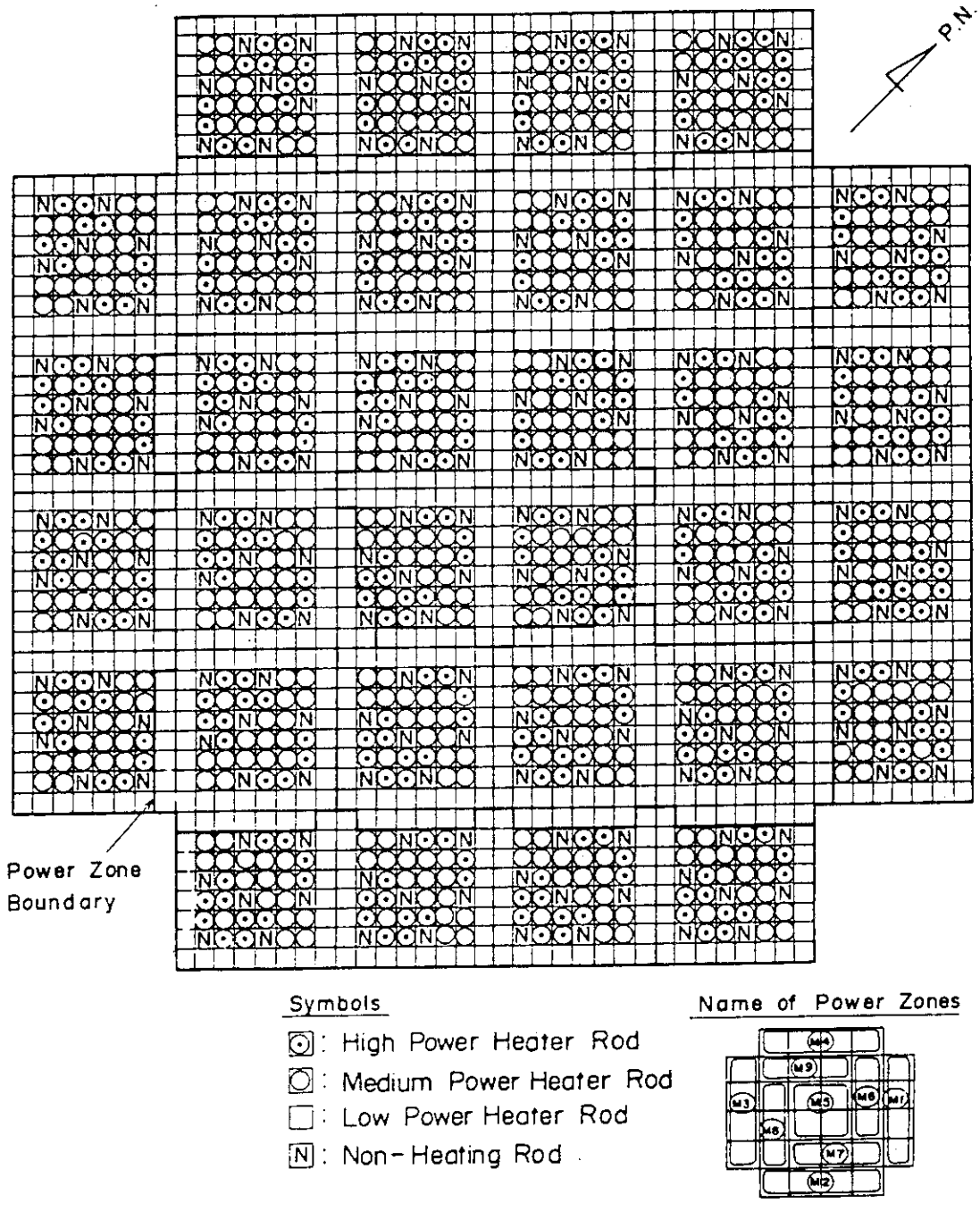

Fig.2.3 Configuration of rods in core

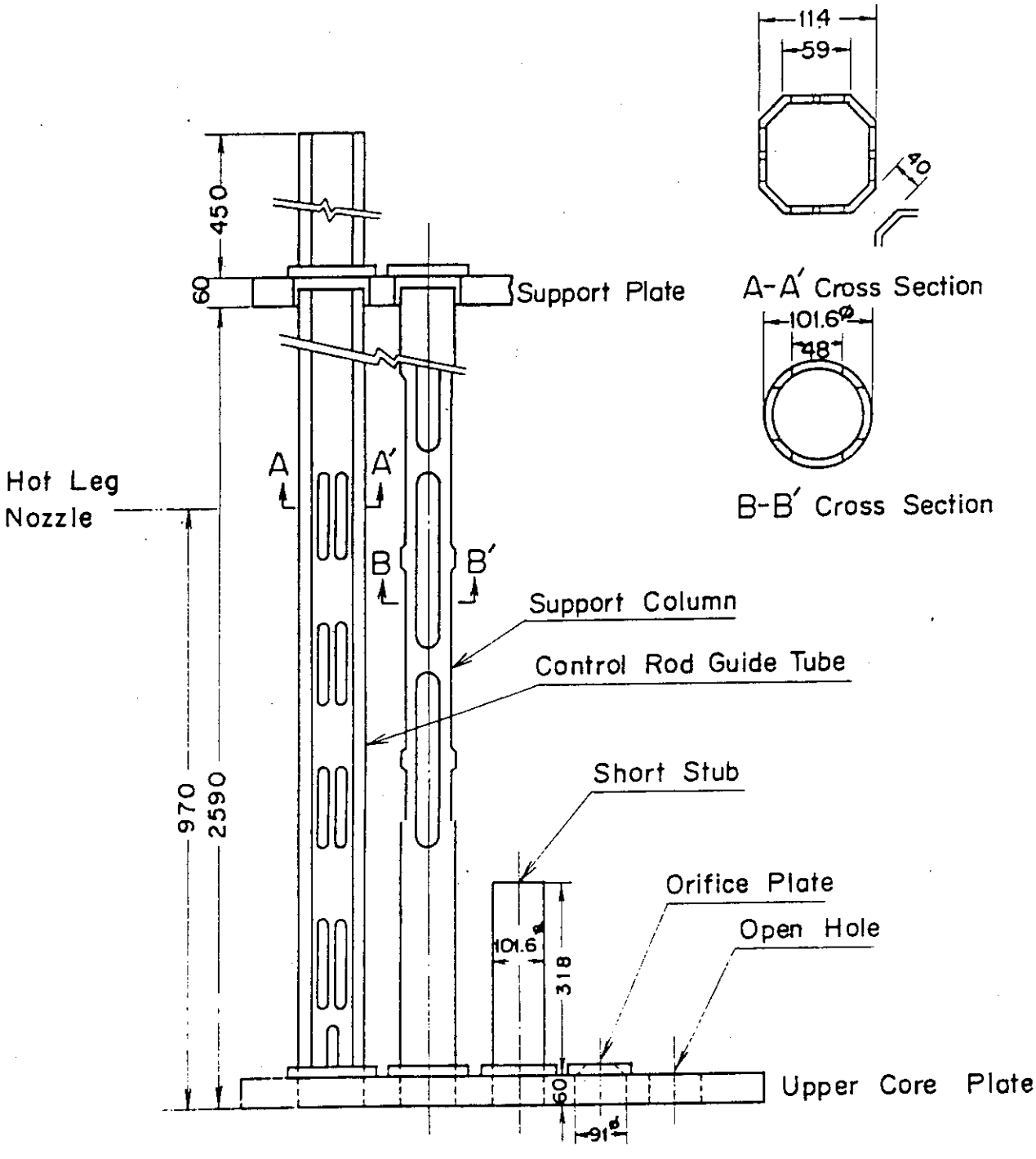

Fig.2.4 Conception of internals

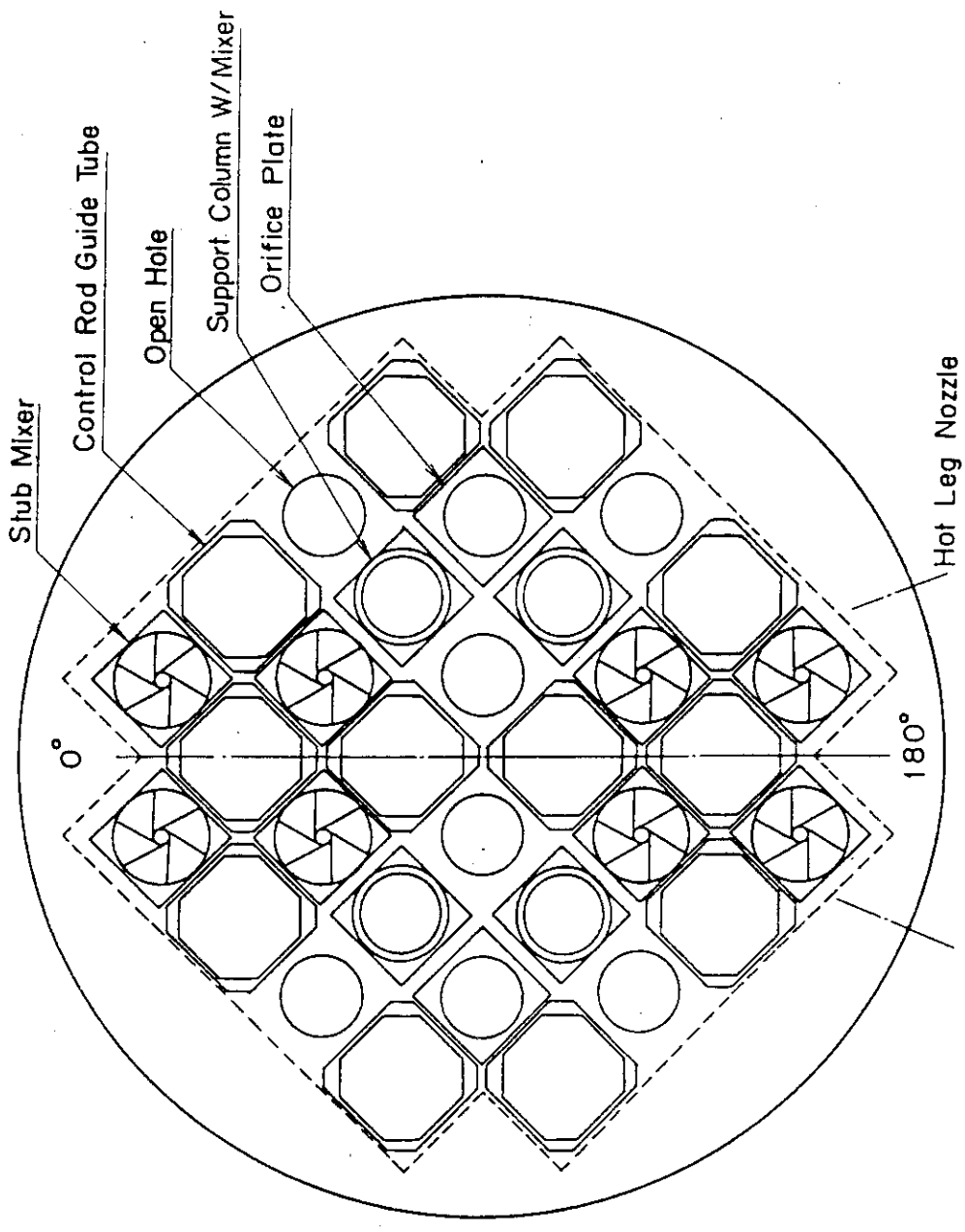

Fig.2.5 Arrangement of internals

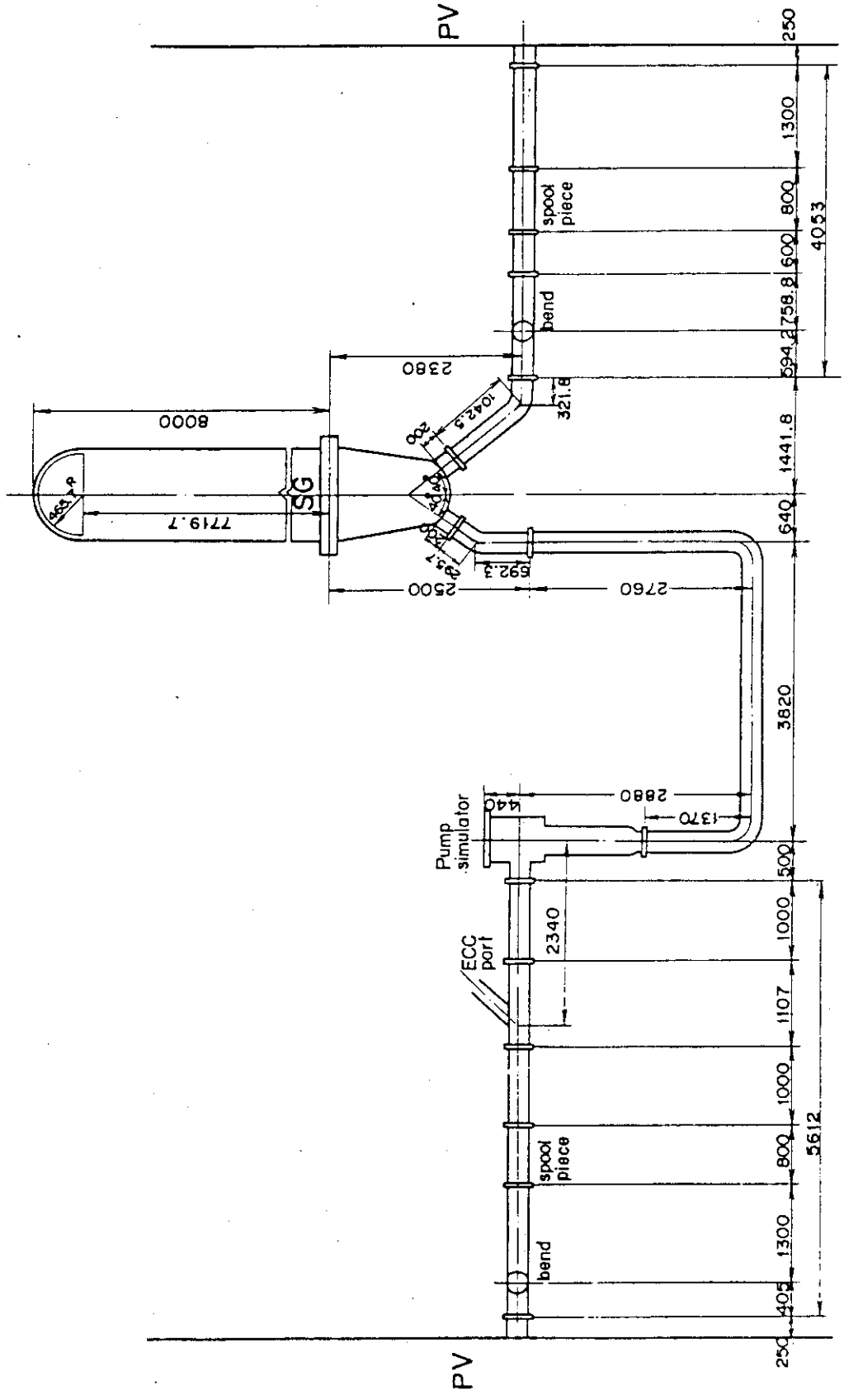

Fig.2.6 Primary loop

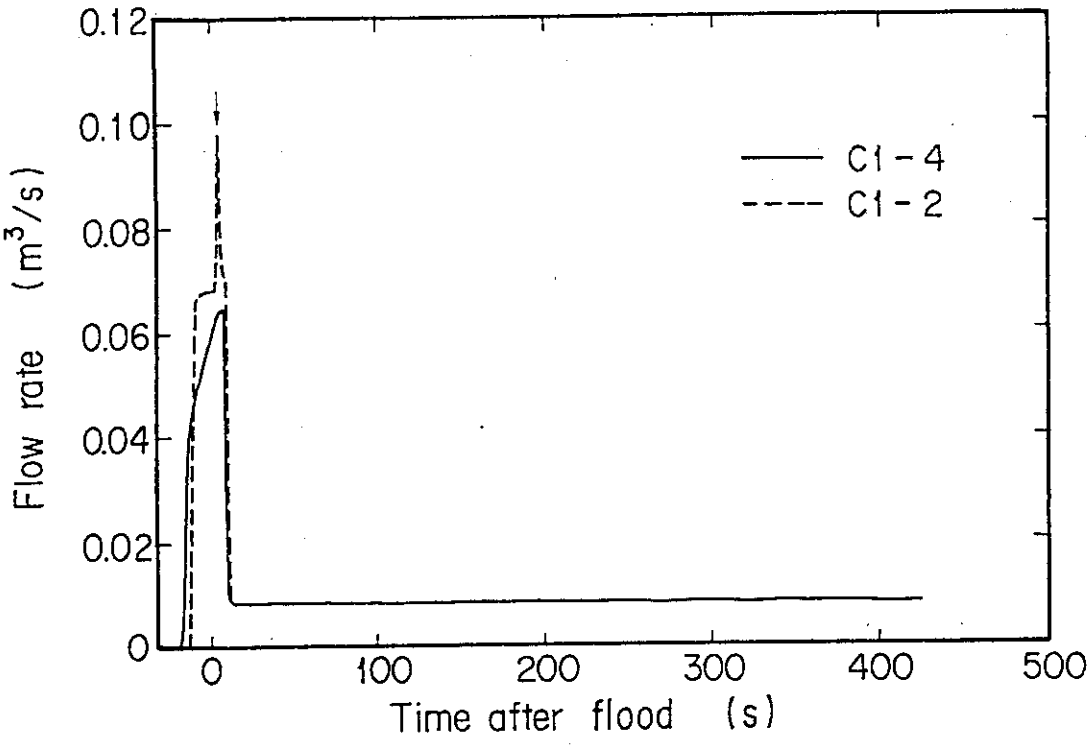

Fig.2.7 Total ECC flow rate

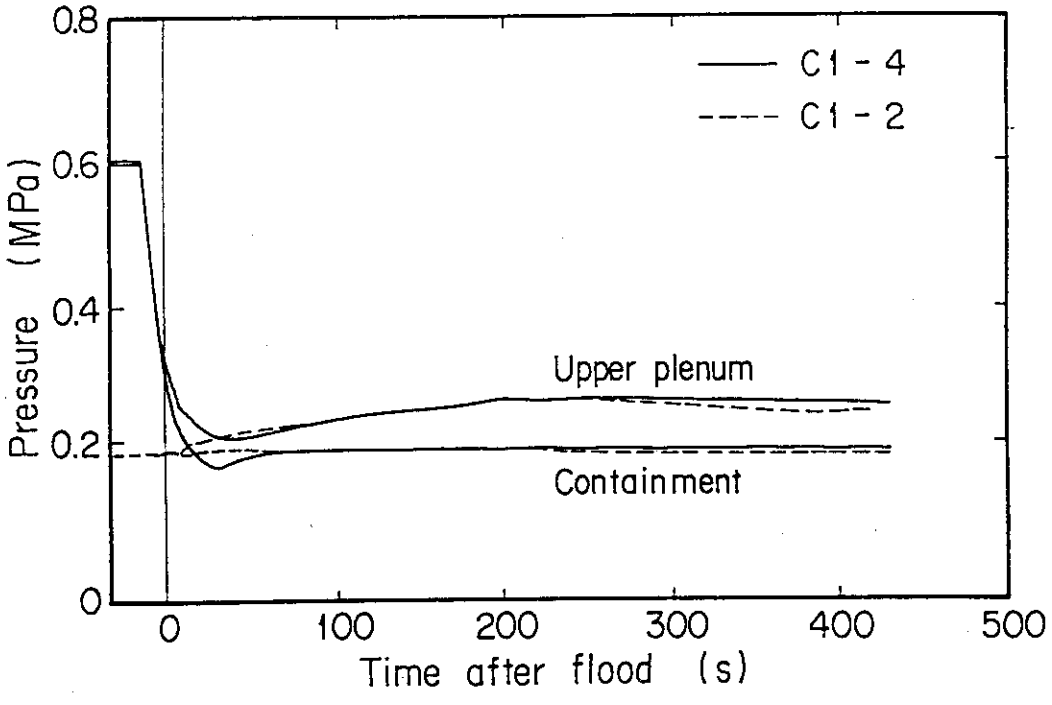

Fig.2.8 Pressure in containment and upper plenum

3. Experimental Results and Discussions

The significant phenomena observed in the C1-4 and C1-15 experiments are discussed in this section. Comparisons are made between the C1-4 results and the reference test (C1-2) results in Section 3.1 and 3.2.

Since the initial conditions and the test procedure for these experiments were nominally the same as each other, the differences in the experimental results were due to the differences in the containment pressure history and the accumulator injection location. The containment pressure for the present test (C1-4) decreased from 0.6 MPa to 0.2 MPa while that for the reference test was maintained at about 0.2 MPa. The accumulator water was injected into the intact cold legs for C1-4. While for C1-2, at first, that was injected into the lower plenum, then the injection port was switched to the intact cold legs.

In addition, the effects of the nitrogen injection are investigated by comparing the results of C1-15 with those of C1-4 in Section 3.3. The initial conditions and the test procedure for C1-15 were the same as those for C1-4 except the nitrogen injection after terminating the accumulator injection.

Summary of the discussion is presented in Section 3.4.

3.1 System behavior

3.1.1 Downcomer and core differential pressures.

For C1-4, containment pressure was initiated to decrease when the accumulator injection began. The injection rate increased during the injection period due to the pressure decrease at the injection port.

Figures 3.1 shows the downcomer, the core, and the lower plenum differential pressure histories. Saturated water was filled in the lower plenum before the experiment initiation. The injected water penetrates to the lower plenum at about 2.8 seconds after the injection initiation and accumulates there. The lower plenum is subdivided into two sections by the core barrel skirt to the elevation of 0.88 m from the bottom of the lower plenum.

The differential pressure across the downcomer is larger than that across the lower plenum, even before the flooding initiation. This fact means the more water accumulation in the downcomer side of the lower plenum than that in the core side.

In comparison with the result of C1-2, shown in the figure, the water accumulation rate in the downcomer is significantly higher for C1-4 than for C1-2. The higher water accumulation rate is reduced when the simulated LPC injection was replaced with the accumulator injection at about 8 seconds after flood. The differential pressure decreases from 25 seconds through 41 seconds, then it increases gradually and approaches to the saturated value. This will be discussed in this section. The differential pressure in the downcomer is smaller for C1-4 than for C1-2 before 250 seconds. The core water accumulation for C1-4, shown in the figure, initiates before the differential pressure across the lower plenum reaches the nearly constant value. This fact shows that flashing occurs in the lower plenum due to the system depressurization and the water swells, then reaches the bottom of the core earlier than the expected lower plenum fill time. The steam void is collapsed when the system depressurization slows down at about 10 seconds. At that time, the lower plenum differential pressure reaches the nearly saturated value, and the step-wise increase of the water accumulation in the core is observed. Then the core water mass continues to increase gradually. In comparison with the result of C1-2, the water accumulation is less for C1-4 than for C1-2, however, after 200 seconds, that is the same as the result of C1-2. The lower downcomer differential pressure for C1-4 results in the lower water accumulation mass in the core before 200 seconds.

The comparison of the upper plenum defferential pressure are shown in Fig. 3.2. The water accumulation in the upper plenum is also much less for C1-4 than for C1-2. However, the increasing rate of the water accumulation is not so different between C1-4 and C1-2 except first 65 seconds.

Firure 3.3 presents the axial differential pressure distribution in the downcomer. For C1-2, the water begins to accumulate when each lower section is filled. For C1-4, the water accumulation in each section except the uppermost section initiates before each lower section is filled. This indicates that the water swells because of the void generation in the accumulated water caused by the system depressurization.

The decrease of the differential pressure between 2.68 and 4.43 m elevations is observed in the period from 25 seconds through 41 seconds. This tendency is similar to the total downcomer differential pressure response shown in the former figure. In this period, the differential pressure in the upper section increases. The wall surface temperatures of the downcomer

are shown in Fig. 3.4. The temperature at the 2.4 m elevation is nearly the same as the saturation temperature, but those above the 2.4 m elevation show significant subcooling during the accumulator injection period. They recovers from about 10 seconds to 25 seconds due to the lower water injection rate at the cold leg. The depressurization is slowing down after about 10 seconds and terminates at 45 seconds. This slow depressurization and the significant water subcooling allow the void collapse in the accumulated water in the downcomer, in the result, the differential pressure in each section increases to the nearly saturated value at about 10 seconds. When the wall surface temperature of the downcomer at 3.8 m elevation returns to the saturation temperature at about 25 seconds, the void is generated again in the downcomer due to the depressurization. The depressurization is very slow in this period, so that the voiding occurs only in the upper part of the downcomer. This steam voiding reduces the differential pressure between 2.68 m and 4.48 m elevations, and pushes up water into the upper section. Because the depressurization terminated at about 45 seconds and the vessel pressure increases gradually after that, the steam void should be crashed again. The differential pressure between 2.68 m and 4.43 m elevations recoveres.

3.1.2 Loop behavior

Figure 3.5 shows the loop differential pressures. For the refill test, C1-4, when the pressure regulation valve of the containment tank was open, the system depressurization initiated. The steam in the vessel was discharged through the broken loop otherwise through the broken cold leg nozzle via the downcomer and via the intact loops. This figure shows the steep increases of the differential pressures in the borken loop and the intact loops after the initiation of the depressurization.

At 30 seconds, the containment tank depressurization terminated, then the differential pressures of both the broken and the intact loops decrease. Steam was generated in the core after flooding. This steam was discharged through the broken and the intact loops to the containment tank. The steam generation in the core continued to increase early in the transient, and caused the increases of the loop differential pressures after 47 seconds.

The results of the reference test, C1-2, are also presented in this figure by the dotted lines for comparison. As described above, the significantly large loop differential pressures for C1-4 are observed early in the transient, while the differential pressures for C1-2 increase

gradually after flooding. And each differential pressure for C1-4 is a little smaller than for C1-2 from 50 seconds to about 200 seconds. This is caused by the lower downcomer differential pressure, as shown in the previous figure. However, the tendencies and values of those for C1-4 are similar to those for C1-2 after 200 seconds.

Figure 3.6 shows the differential pressure for C1-4 between the pump outlet and the cold leg nozzle. During the accumulator injection period, it can be seen that the differential pressure is oscillatory and indicates a negative value. The flow observation with movie cameras revealed that the intact cold leg nozzle was filled with the injected water in the accumulator injection period and steam flow occasionally penetrated water plug and flowed through a part of the cross section of the cold leg nozzle to the downcomer. These flow behavior is explained as follows. When the cold leg nozzle was plugged by the injection water, the steam condensation was decreased due to reduced contact area of steam and water, then the differential pressure between the pump outlet and the cold leg nozzle increased. When the differential pressure increased enough to break the water plug, steam could flow through the cold leg to the downcomer, and the contact area was increased. Therefore, the steam condensation lowered the pressure and the differential pressure decreased to the negative. These flow alternation was repeated several times in the accumulator injection period.

Figure 3.7 shows the intact loop differential pressure and the pump orifice differential pressure for C1-4 again with expanded time scale. The oscillations of both, before the termination of the accumulator injection showed by an arrow, are explained by the water plugging and the break of it as described above. When the accumulator injection was terminated, the loop differential pressure increases suddenly and the pump orifice differential pressure decreases at that time. It indicated that the cold leg was plugged again. After that, since the water plug was broken finally, the steam flow in the cold leg recovered. However, the steam condensation was not so significant as before due to the reduced ECC flow rate, hence, the steam flow was reduced. The break of the water plug and the less steam flow rate in the loop caused the steep decrease of the loop differential pressure, as shown in the figure. This steep decrease of the loop differential pressure resulted the step-wise increase of the core differential pressure at that time, as shown in Fig. 3.1.

Figure 3.8 shows the pump differential pressures in the intact and

the broken loops. The tendencies of them are the same as those of the total loop differential pressures. Large differential pressure is observed in the intact loop during the accumulator injection period. It is considered that when the large amount of the subcooled water was injected into the intact cold legs, the steam condensation occurred near the injection port and lowered the cold leg pressure, as the result, the steam flow through the intact loop increased and the differential pressure through the intact loop pump was caused to be large during the accumulator injection period. That decreases suddenly when the accumulator injection was terminated. Figure 3.9 shows the differential pressure through the intact cold leg nozzle. The relatively large oscillation and the occasional negative values are observed during the accumulator injection period.

The total loop mass flow rate is presented in Fig. 3.10. The high flow rate is maintained during the accumulator injection period. The intact and the broken loop mass flow rates are shown in Fig. 3.11. The C1-4 results are nearly the same as the C1-2 results after about 50 seconds, though the much higher flow rates for C1-4 are observed before 50 seconds. This high flow rate in the broken loop was caused by the system depressurization. During the accumulator injection period, the flow rate in the intact loop for C1-4 is significantly greater than that in the broken loop. The condensation near the cold leg must have increased the steam flow in the intact loops.

The upper plenum pressure is shown in Fig. 3.12. It can be seen that after the ECC injection rate was reduced, the depressurization is slowing down. This was caused by the decreased intact loop flow rate. As described above, the accumulator injection caused the significant steam condensation in or near the intact cold legs and increased the flow rates in the intact loops, as the result, it controls the system depressurization.

Figure 3.13 shows the comparison of the fluid temperatures in the inlet and the outlet plenum of the steam generator. The outlet temperature for C1-4 is about 15 K higher than that for C1-2. Figure 3.14 presents the comparison of the secondary fluid temperatures. It can be seen that the initial temperature in the lower part of the secondary fluid is higher for C1-4 than C1-2. This fact allows the higher outlet temperature for C1-4.

3.2 Core behavior

The comparison of the flooding rates to the core between C1-4 and C1-2 is shown in Fig. 3.15. The flooding rate was obtained from the mass balance

calculation. During the accumulator injection period, the flooding rate for C1-4 is lower than that for C1-2. After that, no significant differences are observed in this figure.

The fluid temperatures at the core inlet are compared in Fig. 3.16. For C1-2, at first, the subcooled accumulator water was directly injected to the lower plenum during 16 seconds, then the injection port was changed to the cold leg, so that significant amount of the subcooled water was accumulated in the lower plenum. For C1-4, the accumulator water was injected only to the cold leg. The subcooled water was mixed with steam in the cold leg and reached the lower plenum through the hot downcomer. This difference of the injection port between C1-4 and C1-2 seems to allow the higher fluid temperature at the core inlet for C1-4.

The comparison of the void fractions in the core is shown in Fig. 3.17. In the lower half of the core, the void fraction of each elevation for C1-4 is higher than that C1-2 before that reaches the saturated value. This is not clear in the upper half of the core. The flooding rate and the loop mass flow rate C1-4 are nearly the same as those for C1-2 after about 50 seconds. Consequently, the higher fluid temperature at the core inlet for C1-4 contributed the higher void fraction in the lower half of the core. The void fraction in the lowest core elevation for C1-4 is significantly higher in an early transient than that for C1-4. This is due to the lower water accumulation for C1-4 caused by the higher intact loop differential pressure in the early transient.

Figure 3.18 shows the comparison of the heat transfer coefficient on the maximum powered rod midplane. The tendency is similar to each other, though the value of the heat transfer coefficient is smaller for C1-4 than for C1-2. The higher void fraction seems to cause the lower heat transfer coefficient. As a result, the turnaround temperature, shown in Fig. 3.19, are higher for C1-4. And quench times, shown in Fig. 3.20 are also longer, however, this is not so significant.

3.3 Comparison of the test results between C1-15 and C1-4

The initial conditions were nominaly the same for C1-15 as C1-14. The difference was only that the nitrogen gas in the accumulator was injected into the system for C1-15, while, it was not allowed for C1-4. The ECC injection rate, shown in Fig. 3.21, indicates that the accumulator injection lasts about 3 seconds longer for C1-15 than for C1-4. For C1-15, the nitrogen gas injection from the accumulator was expected to continue

during 10 seconds. The ECC injection rate into each intact loop for C1-15 is shown in Fig. 3.22. After the accumulator injection was terminated, the oscillation is observed in each loop injection rate, and this oscillation disappears for Loop-3 after about 35 seconds, though injection rates for the other loops are still oscillatory. And the injection rate for Loop-3 is about 6.39×10^{-4} m^3/s on the average. Since the total LPCI flow rate after the accumulator injection was 8.33×10^{-4} m^3/s, the most of the LPC water was injected into Loop-3 cold leg and the small residual was injected into the Loop-1 and Loop-2 cold legs. The ECC water was injected into the system via the header which is installed above the system. It is considered that the nitrogen gas was accumulated in the header and skewed the water distribution to each intact loop.

Figure 3.23 compares the pressure in the upper plenum and the containment-2. They are very similar to each other right after the initiation of the system depressurization. However, the depressurization is faster for C1-15 than for C1-4 near the end of the depressurization due to the longer significant steam condensation period caused by the later termination of the accumulator injection for C1-15. The depressurization period for C1-15 is about 25 seconds shorter than that for C1-4.

Figure 3.24 shows the comparison of the differential pressures in the downcomer, the lower plenum and the core. For C1-15, the water accumulation in the downcomer is much more than that of the lower plenum in an early transient as seen in the C1-4 results. The one of differences between the C1-15 and C1-4 results is that the downcomer differential pressure for C1-15 reaches the saturated value within the accumulator injection period, on the contrary, that for C1-4 is significantly lower than the saturation value. The longer accumulater injection period for C1-15 allows to store the more water in the downcomer. The core water mass suddenly increases at about 15 seconds, and the accumulated mass in the core for C1-15 is larger than that for C1-4 through 200 seconds.

Figure 3.25 shows the differential pressures of the total loop and the pump orifice for C1-15. During the accumulator injection period, the behavior of them is the same as that for C1-4, that is, the water plugging effect is observed. The sudden decrease of the total loop differential pressure results the step-wise increase of the core water mass at 15 seconds. This phenomenon is also the same as that for C1-4. Figure 3.26 shows the comparison of the differential pressure through the broken cold leg nozzle.

Both show the sudden increase just after the termination of the accumulator injection due to the increased steam flow caused by the less steam condensation and the water plugging in the intact cold legs as discussed in the C1-4 result. For C1-15, this increase is remarkable. It is considered that the overflowed water from the downcomer caused this increase and the injected nitrogen gas also promoted it. The injected nitrogen into the intact cold legs is discharged to the containment through the upper part of the downcomer and the broken cold leg nozzle. The mixture of nitrogen, steam and the overflowed water must increase the pressure loss in the broken cold leg nozzle.

The intact loop mass flow rates for C1-15 and C1-4 are compared in Fig. 3.27. The high mass flow rate is observed during the accumulator injection period in both experiments due to the significant condensation in the cold leg. For C1-15, the mass flow rate in Loop-3 is higher than that in Loop-1 after the ECC injection rate reduction, as shown in Fig. 3.28. The skewed distribution of the ECC water to the cold legs seems to affect the steam flow rate in each loop. That is, the steam condensation in the intact cold leg was greater in Loop-3 than in Loop-1 due to the higher ECC injection rate and resulted in the higher steam flow rate in Loop-3.

Figure 3.29 shows the comparison of the broken loop mass flow rates between C1-15 and C1-4. The larger pressure loss in the broken cold leg nozzle allows the higher steam flow rate for C1-15.

The comparison of the flooding rate is presented in Fig. 3.30. The flooding rate was calculated with the mass balance of the core. The larger mass flow rates in the intact loops and the broken loop result in the higher flooding rate for C1-15 through about 100 seconds.

Figure 3.31 shows the comparison of the heat transfer coefficient on the maximum powered rod midplane. The slightly higher heat transfer coefficient is observed for C1-15. Therefore, the turnaround temperatures, shown in Fig. 3.32, are lower for C1-15 than for C1-4. The quench times in the core high power region are compared in the Fig. 3.33. The quench times for C1-15 are slightly shorter than those for C1-4.

3.4 Summary of discussion

The discussion in Section 3.1, 3.2 and 3.3 is summarized as follows:

Comparison between C1-4 and C1-2

1. The difference in the experimental conditions was in the system pressure and the accumulator injection location. The containment pressure for C1-4 decreased from 0.6 MPa to 0.2 MPa while that for C1-2 was nearly constant at 0.2 MPa during the transient. The accumulator water was injected into the cold leg for C1-4, while, it was injected into the lower plenum for C1-2, prior to the cold leg injection.
2. The accumulator injection rate was lower for C1-4 than for C1-2 because of the higher cold leg pressure during the injection period.
3. The depressurization ended at about 30 seconds. The water swelling in the lower plenum was observed in the C1-4 experiment due to the system depressurization.
4. This fact caused the earlier initiation of the water accumulation in the core than the expected fill time of the lower plenum. The steam void in the lower plenum collapsed when the system depressurization slowed down at about 10 seconds.
5. The core differential pressure was smaller for C1-4 than for C1-2 before 200 seconds. That for C1-4 increased suddenly at about 10 seconds due to the steep decrease of the loop differential pressure and continued to increase gradually after that. That for C1-4 was equal to that for C1-2 after 200 seconds. The smaller downcomer differential pressure for C1-4 contributed to the less water accumulation in the core before 200 seconds except in an early transient.
6. The downcomer differential pressure increased steeply during the accumulator injection period. Steam void was generated due to the depressurization, however, collapsed by the cold water penetration. After reducing the ECC injection rate, void was generated again in the upper part of the downcomer. This void also collapsed when the depressurization terminated. After about 250 seconds, the differential pressure in the downcomer for C1-4 was very similar to that for C1-2.
7. The upper plenum water accumulation was less for C1-4 than C1-2, though the accumulation rate was not so different between the experiments except in an early transient.

8. During the accumulator injection period, the significant condensation occured in the intact cold leg and allowed the high steam flow rate in the intact loop. Therefore, the condensation affected the system depressurization. After the accumulator injection was terminated, the depressurization was slowing down. The reverse flow in the cold leg nozzle due to the condensation was not significant. The induced large pressure loss in the intact loop suppressed the core water accumulation and allowed the injected water to accumulate mainly in the downcomer in an early transient, as described in Item 5 and 6. The water plugging in the cold leg was observed and affected the steam flow rate in the loop and the differential pressures in the loop components. When the water plug was finally broken at about 10 seconds, the differential pressure of the intact loop decreased suddently, as a result, the core water mass steeply increased, as described in Item 5.
9. The differential pressure in the broken loop for C1-4 was higher before 50 seconds after BOCREC than that for C1-2 due to the system depressurization. That in the intact loop for C1-4 was also higher before 50 seconds due to the condensation in and near the cold leg.
10. The differential pressures and the mass flow rates in the intact and the broken loops for C1-4 were nearly the same as those for C1-2 after 50 seconds.
11. The steam temperature in the outlet plenum of the steam generator was about 15 K higher for C1-4 than for C1-2. The initial temperature of the secondary water in the lower part of the steam generator was higher for C1-4 than for C1-2. This higher water temperature allowded the higher steam temperature for C1-4.
12. The flooding rate for C1-4 was not so different from that for C1-2, except in an early transient. The C1-2 result showed the higher flooding rate immediately after flooding. During 40 seconds after the termination of the depressurization, the flooding rate for C1-4 was slightly higher than that for C1-2.
13. The water temperature at the core inlet was very close to the saturation temperature for C1-4 while that for C1-2 was lower than the saturation temperature.
14. The void fraction in the core was higher for C1-4 than for C1-2. It was significant in the lower half of the core before the void fraction in each core elevation reached the steady value. A potential cause

of this fact was the higher water temperature at the core inlet for C1-4.

Comparison of C1-15 with C1-4

1. Both experiments included the system depressurization phase. The nitrogen injection after the accumulator injection was allowed for C1-15 but not for C1-4.
2. The accumulator injection period was about 3 seconds longer for C1-15. Consequently, the total mass of the injected accumulator water was more for C1-15.
3. After the nitrogen injection, the distribution of the ECC water injection rate to the cold legs skewed. Most of the LPC water was injected to Loop-3. The accumulated nitrogen in the header of the ECC line caused this fact.
4. The upper plenum depressurization ended during the accumulator injection period for C1-15. The longer accumulator injection period promoted the depressurization, and the pressure decay terminated 25 seconds shorter for C1-15 than for C1-4.
5. The water accumulation was much more in the downcomer side than in the core side for C1-15, as observed in C1-4 experiment. When the accumulator injection was terminated, the water level in the downcomer was very close to the overflow line for C1-15 whereas it was significantly lower than the overflow line for C1-4.
6. After the termination of the accumulator injection, the stepwise increase of the core water mass was caused by the steep decrease of the intact loop diferential pressure due to the water plug break in the cold leg, as seen in the C1-4 results.
7. When the nitrogen was inj-cted into the system, the broken cold leg defferential pressure increased suddenly. The mixture flow of the nitrogen, the steam and the water caused the large pressure deop in the broken cold leg. No significant effect of the nitrogen injection on the system and the core behaviors was observed except this fact.
8. The intact loop mass flow rate for C1-15 was high during the accumulator injection period, as discussed in the C1-4 results. After that, the mass flow rate in the intact Loop-3 was higher than those of the other two loops. The more ECC water injection rate into Loop-3 caused the more steam flow due to the condensation effect.

9. The steep increase of the core water mass for C1-15 allowed the core transient to be slightly faster. The turnaround temperature was lower for C1-15 than for C1-4 and the quench time for C1-15 was also shorter.

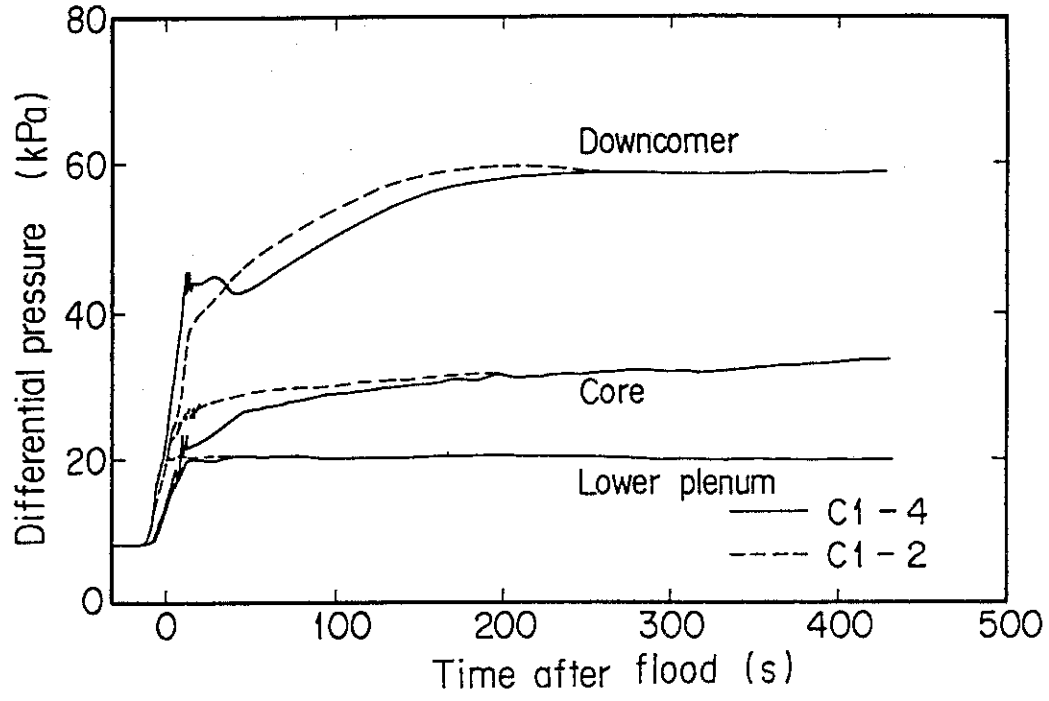

Fig.3.1 Differential pressures of downcomer, lower plenum and core

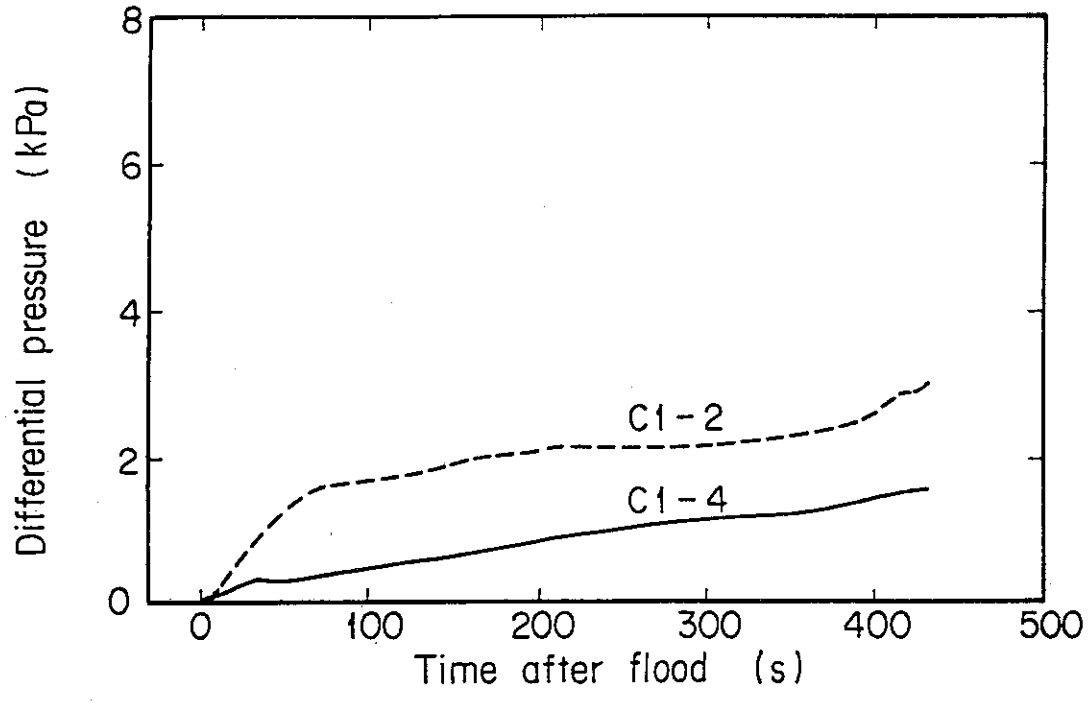

Fig.3.2 Upper plenum differential pressure

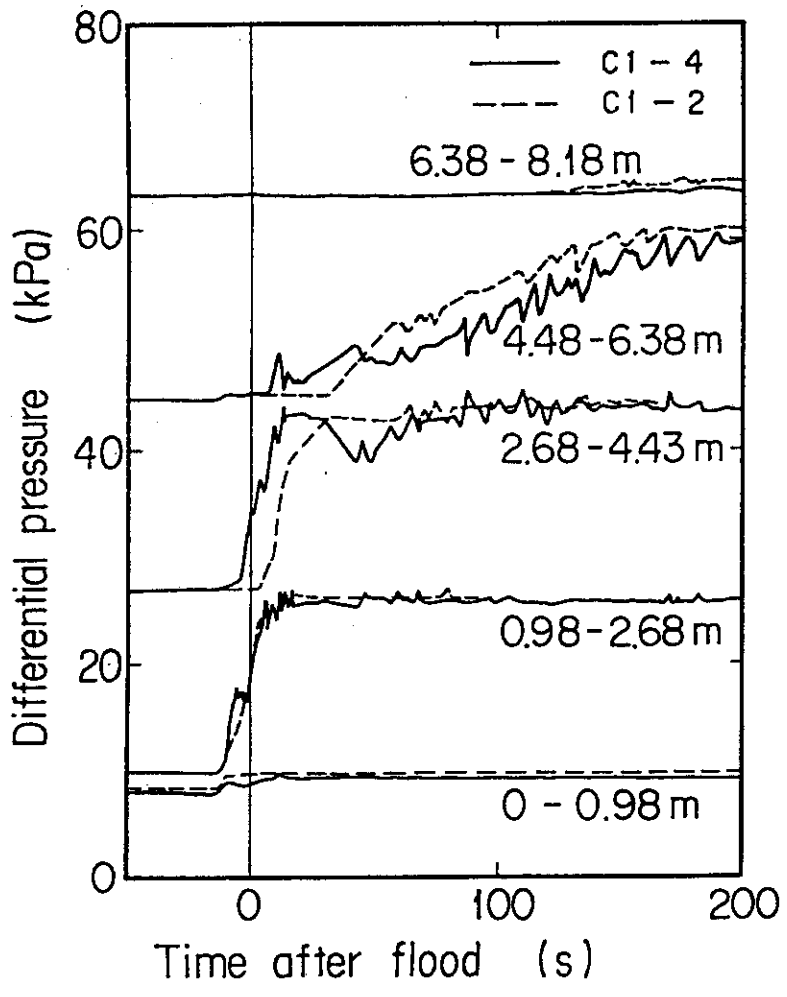

Fig.3.3 Differential pressure in downcomer

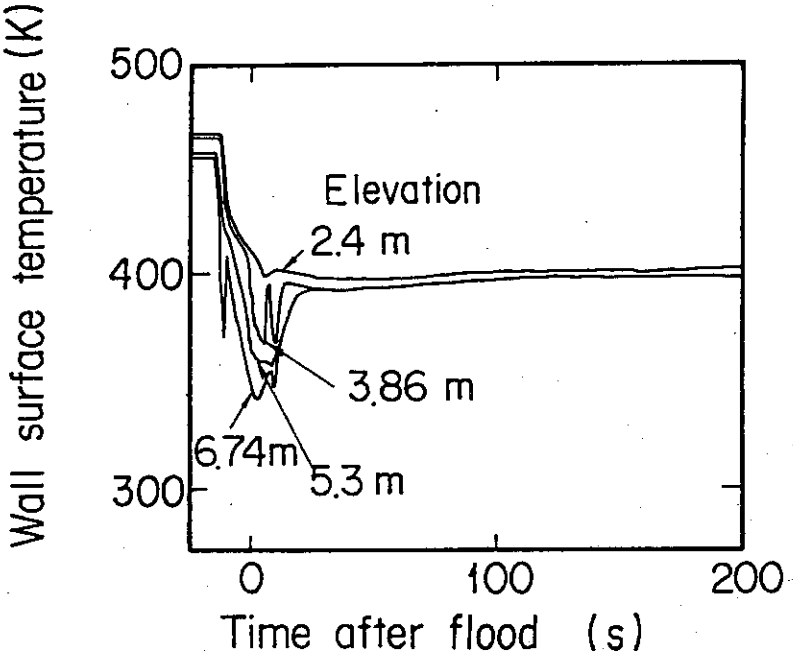

Fig.3.4 Downcomer wall surface temperature

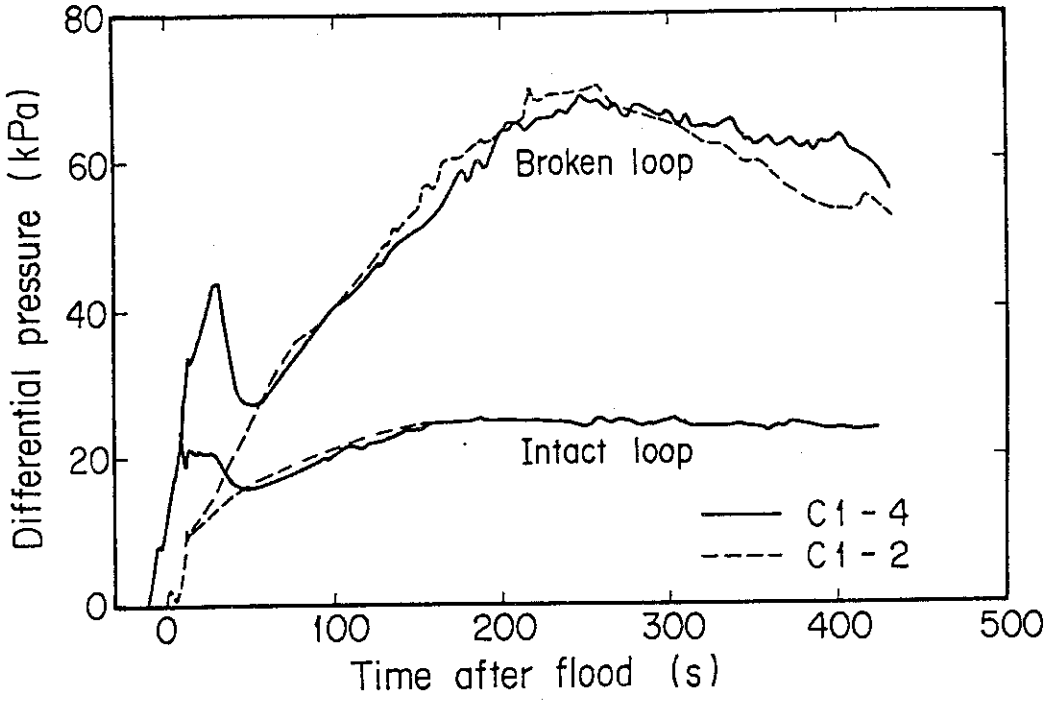

Fig.3.5 Differential pressures of intact and broken loops

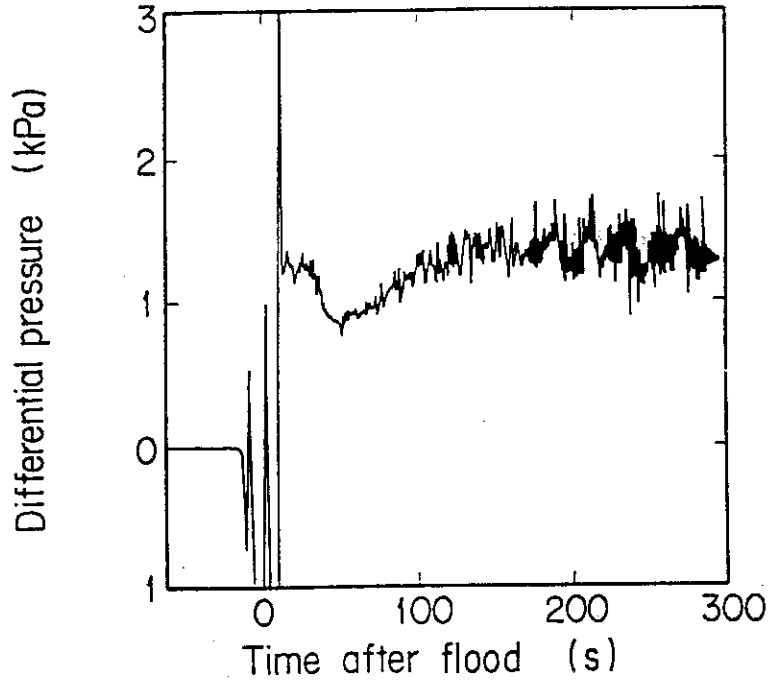

Fig.3.6 Differential pressure between pump outlet and cold leg nozzle for C1-4 intact loop

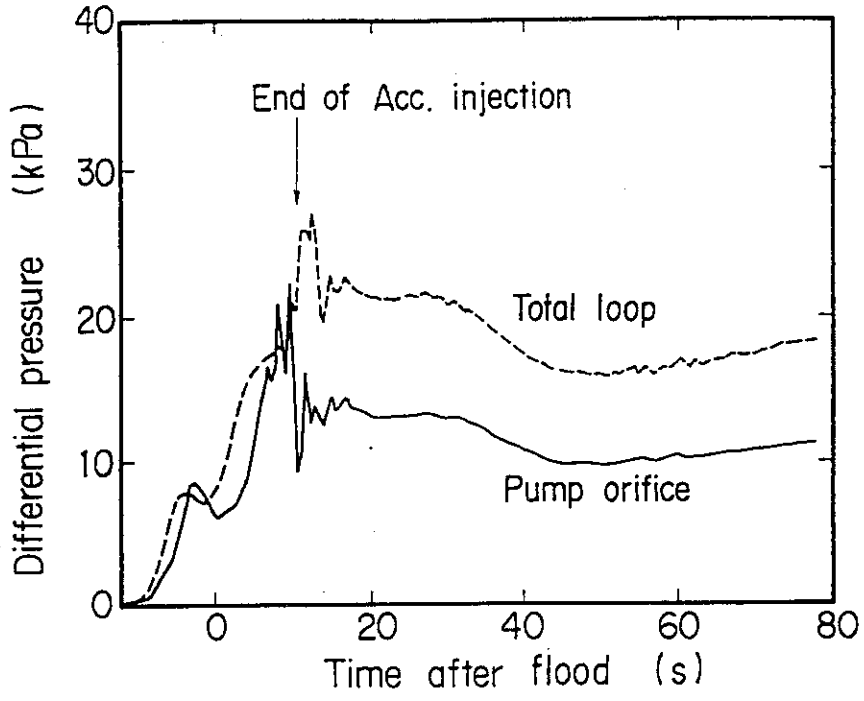

Fig.3.7 Differential pressures of total intact loop and pump orifice for Cl-4

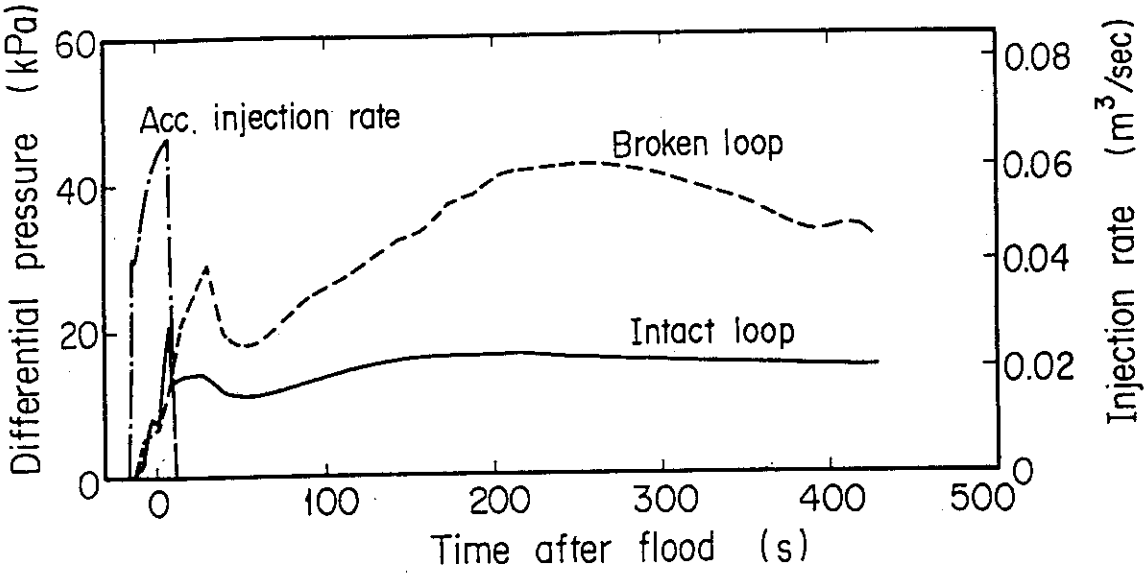

Fig.3.8 Pump differential pressure

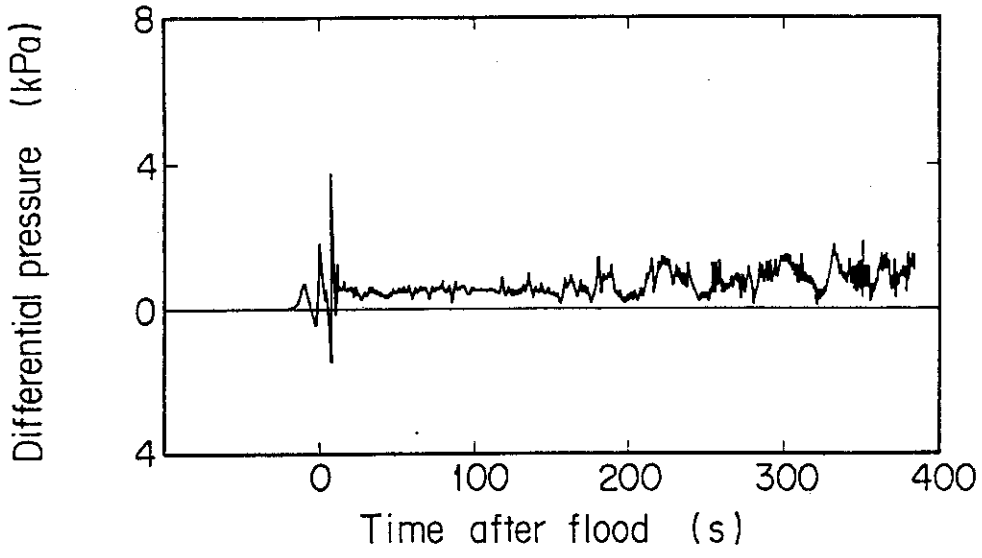

Fig.3.9 Differential pressure between upper part of the downcomer and cold leg nozzle

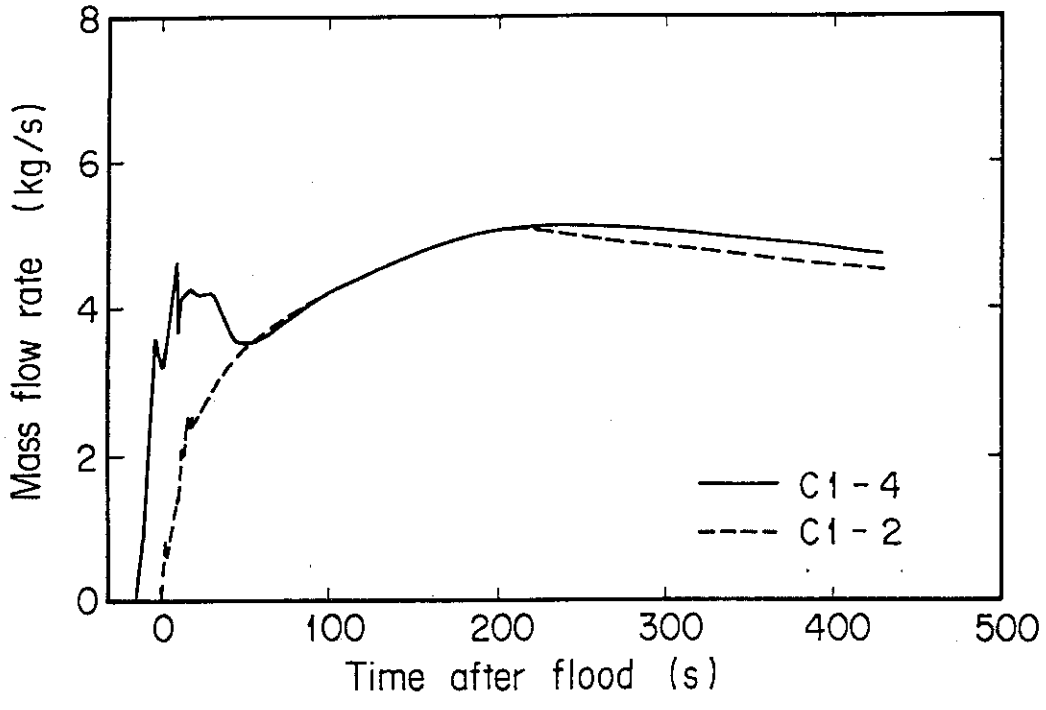

Fig.3.10 Total loop mass flow rate

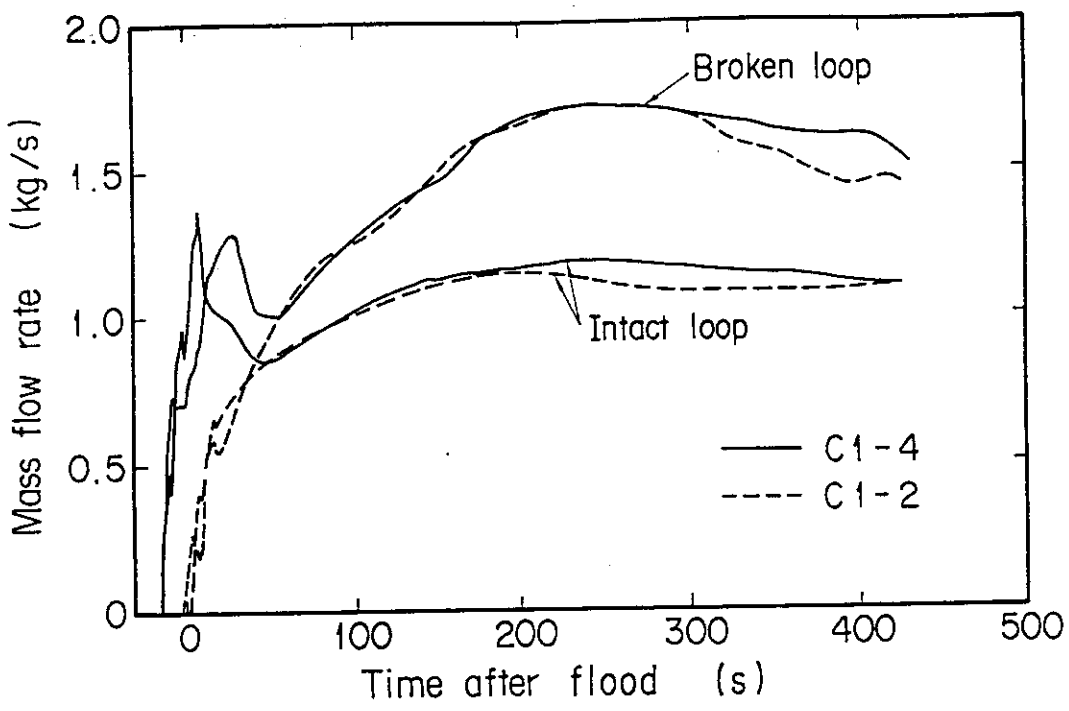

Fig.3.11 Mass flow rates in intact and broken loops

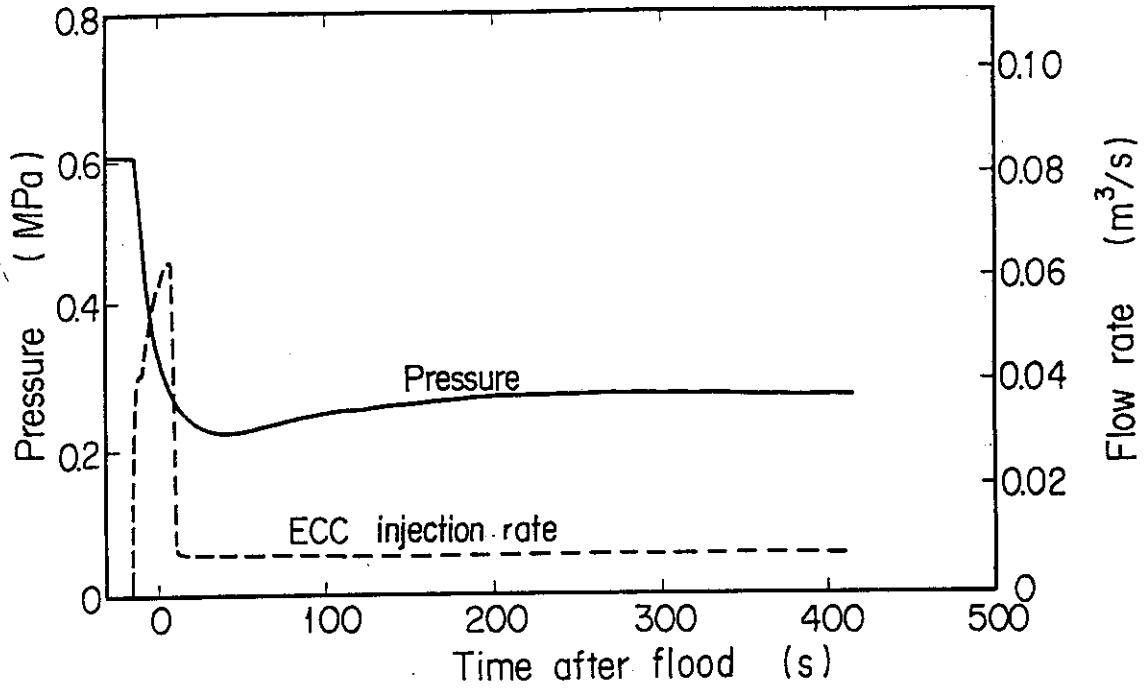

Fig.3.12 Upper plenum pressure and ECC injection rate

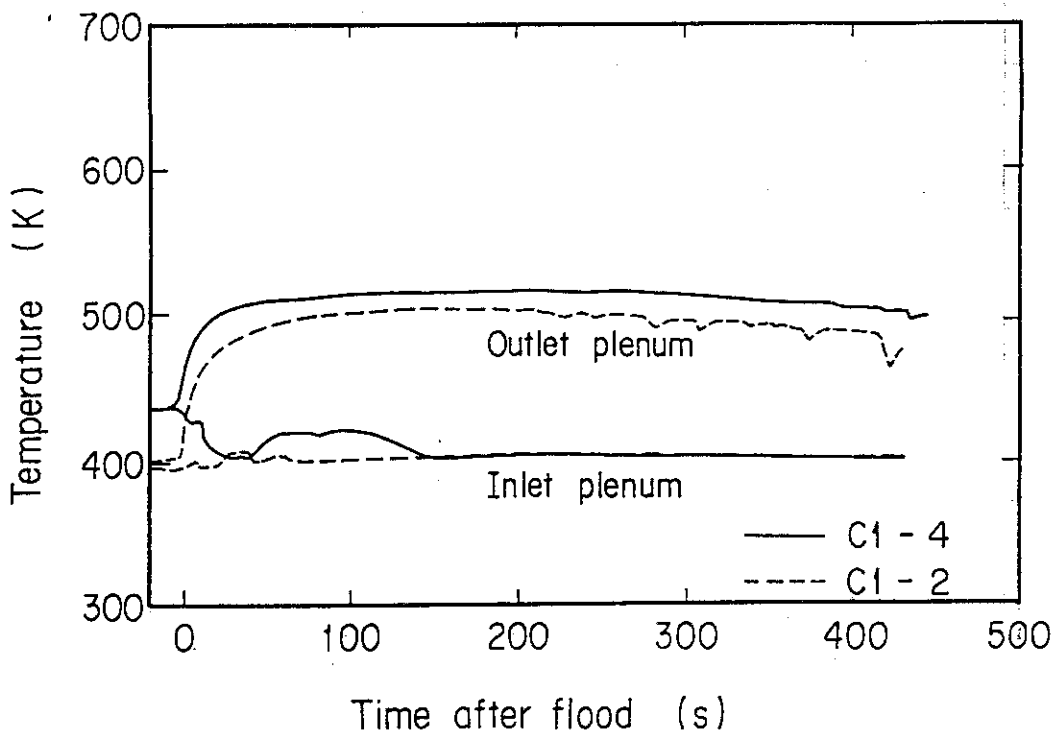

Fig.3.13 Fluid temperatures in inlet and outlet plenum of steam generator

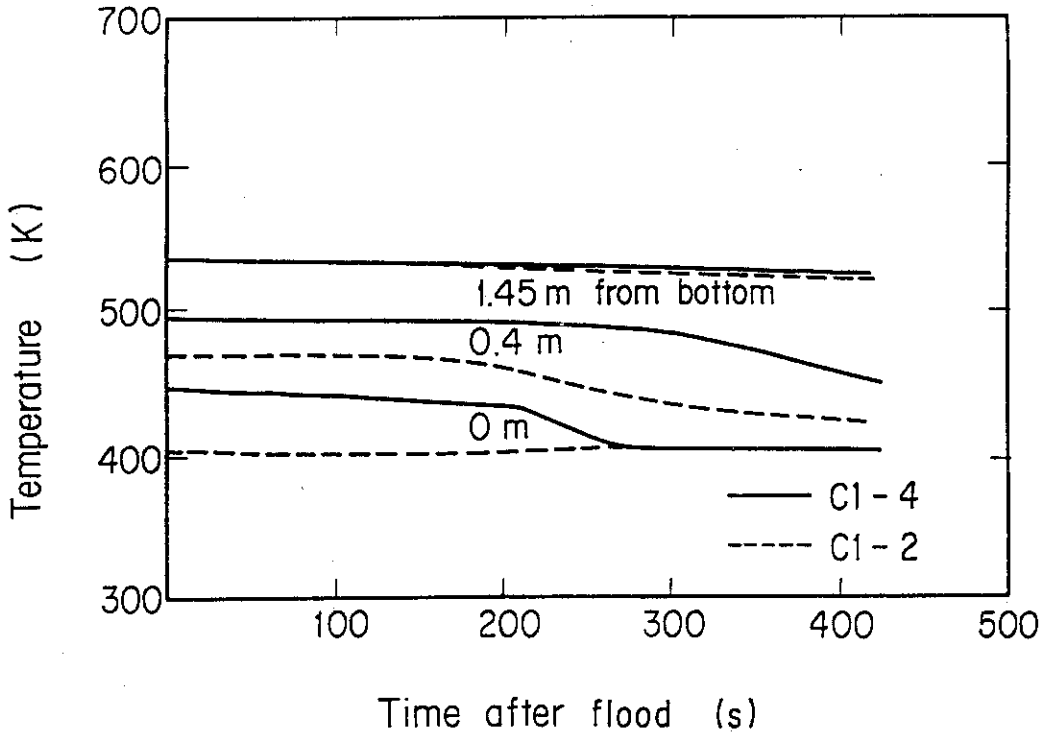

Fig.3.14 Comparison of 2ndary fluid temperatures

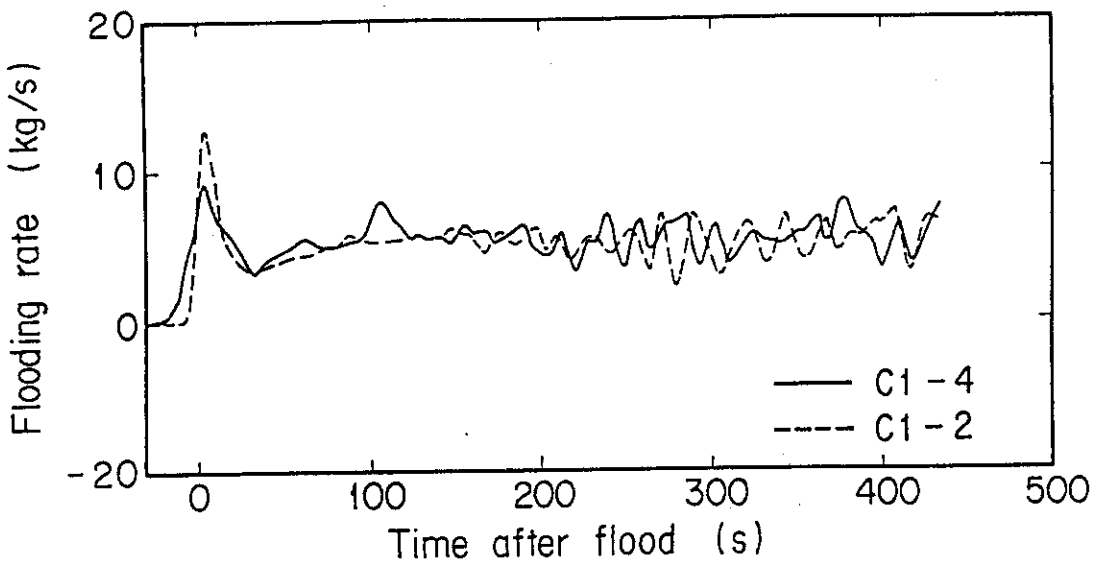

Fig.3.15 Comparison of flooding rstes

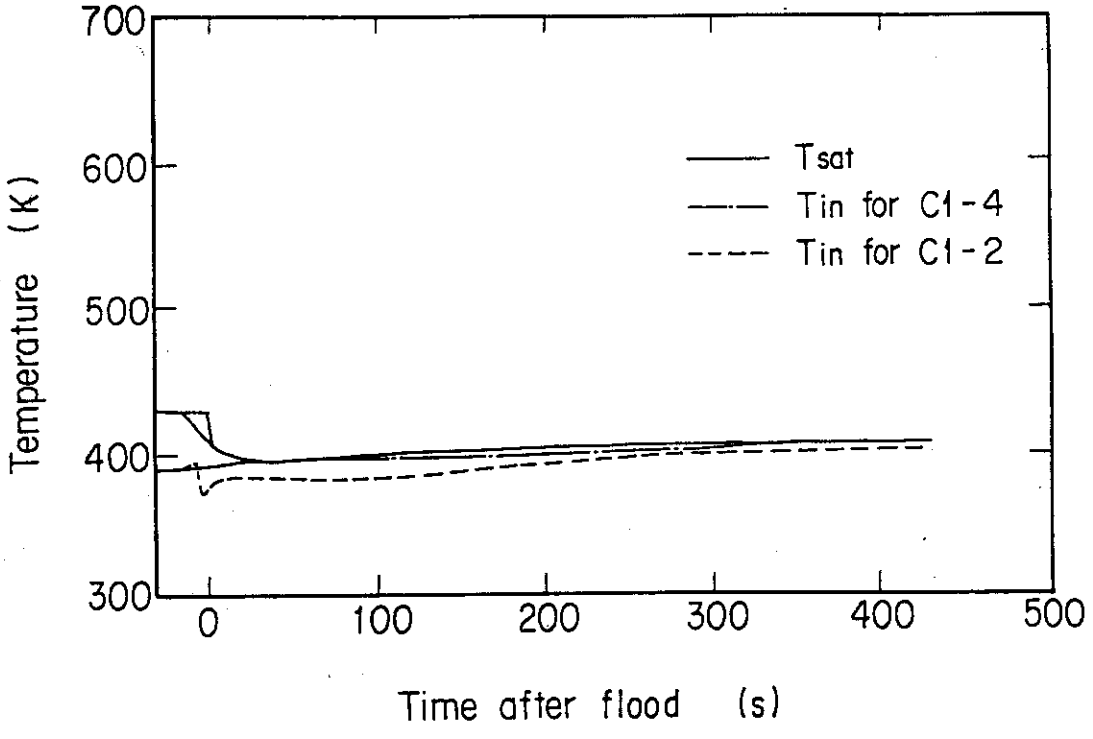

Fig.3.16 Fluid and saturation temperatures at core inlet

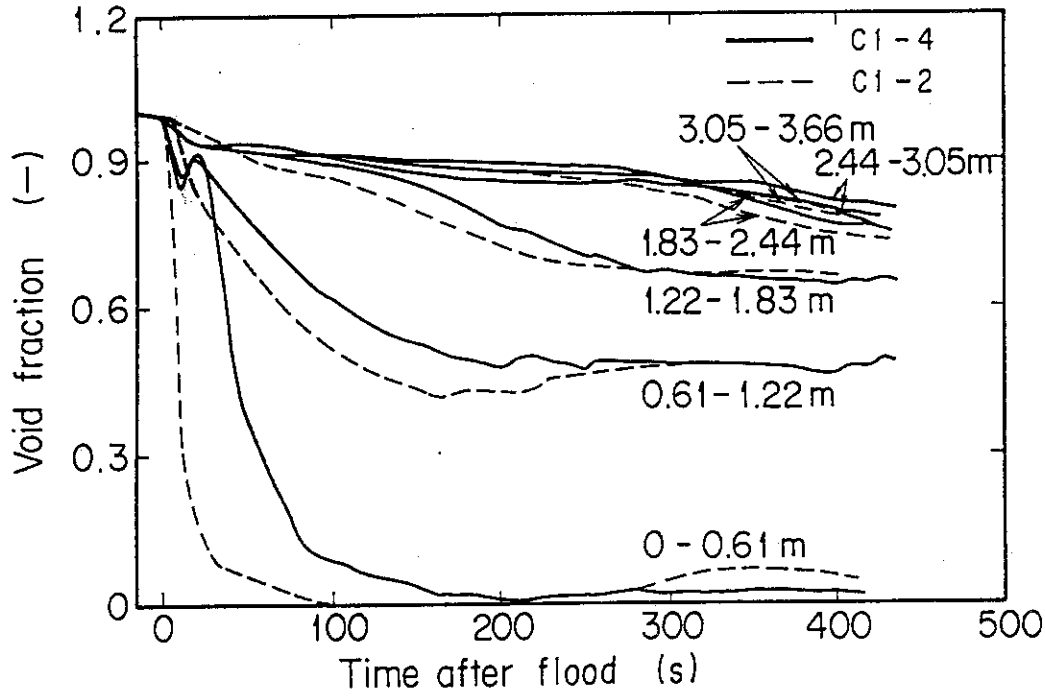

Fig.3.17 Void fractions in core

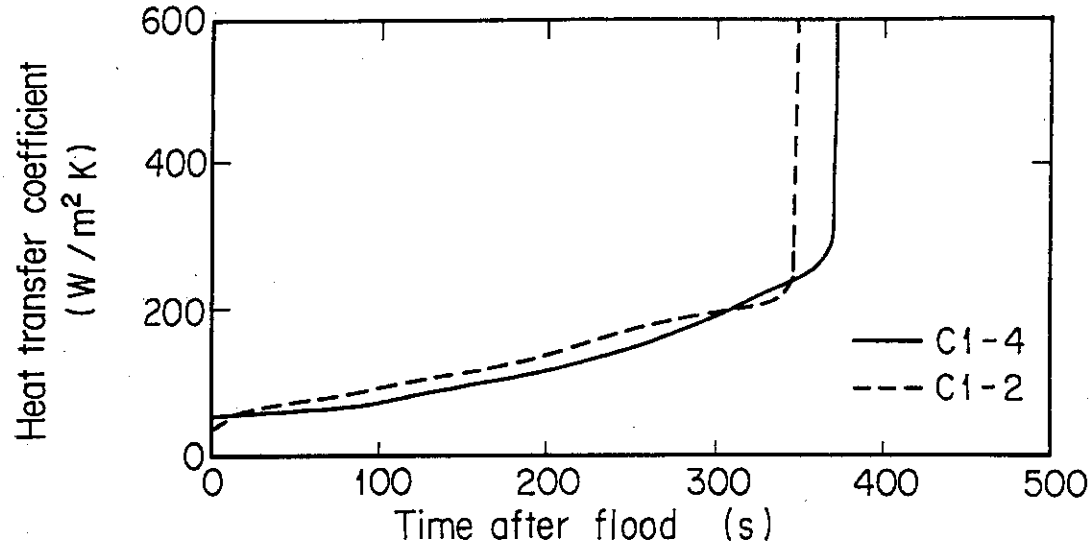

Fig.3.18 Heat transfer coefficient on maximum powered rod midplane (TE32 X 13)

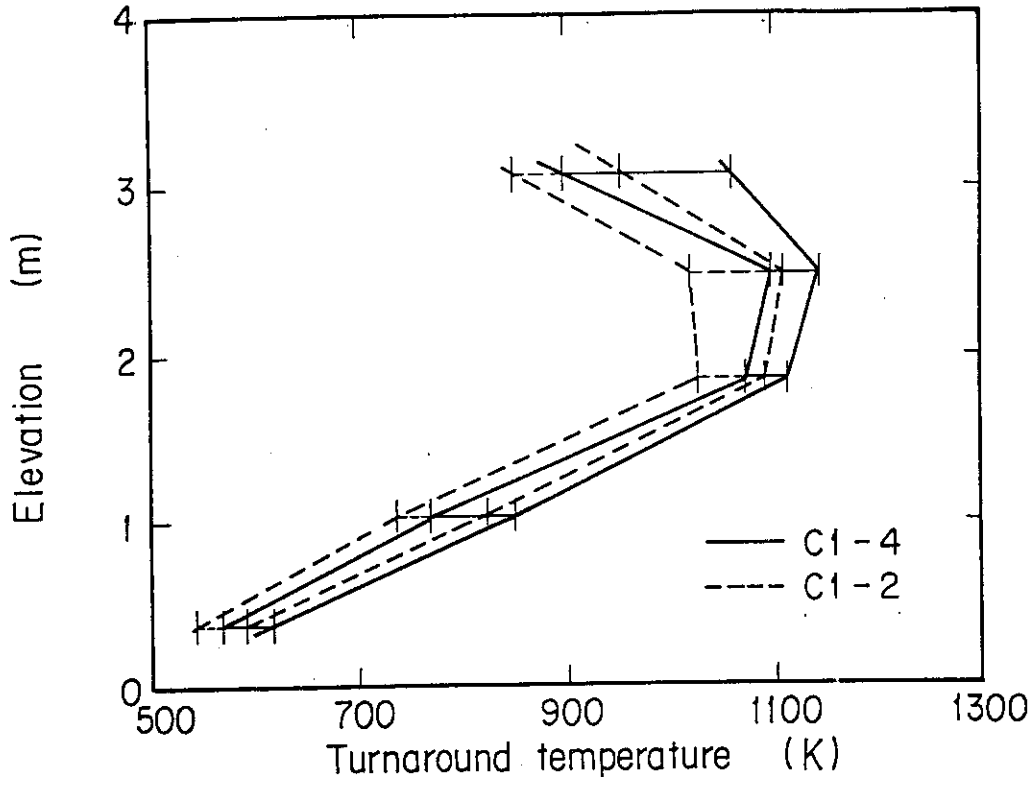

Fig.3.19 Turnaround temperature in core central region

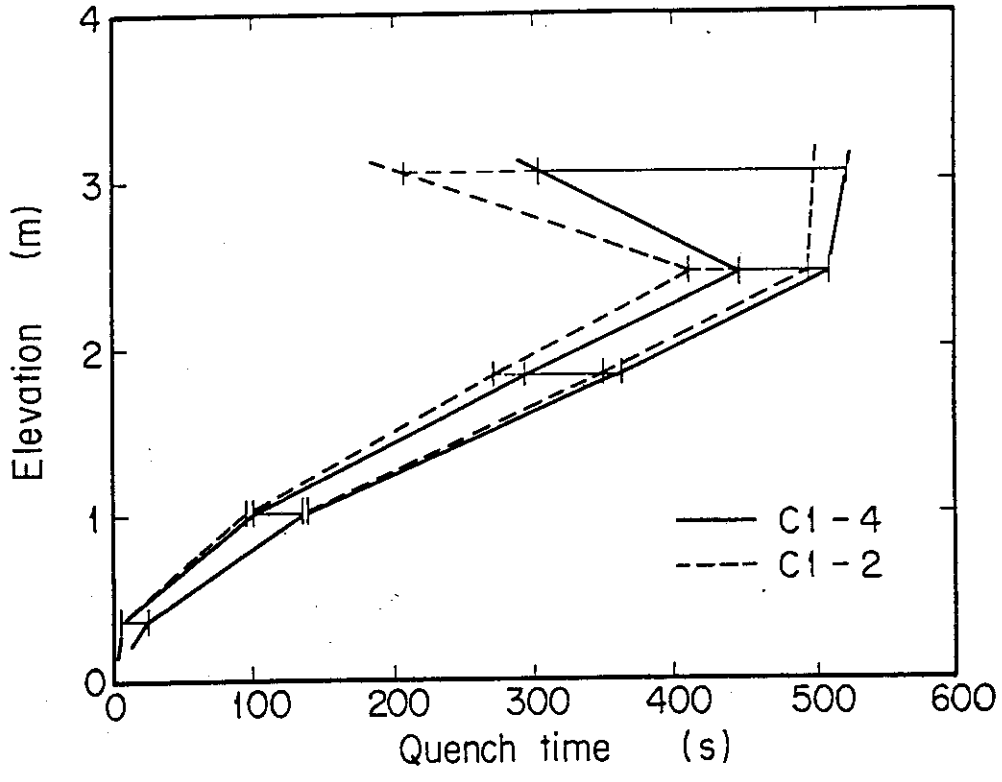

Fig.3.20 Quench time in core central region

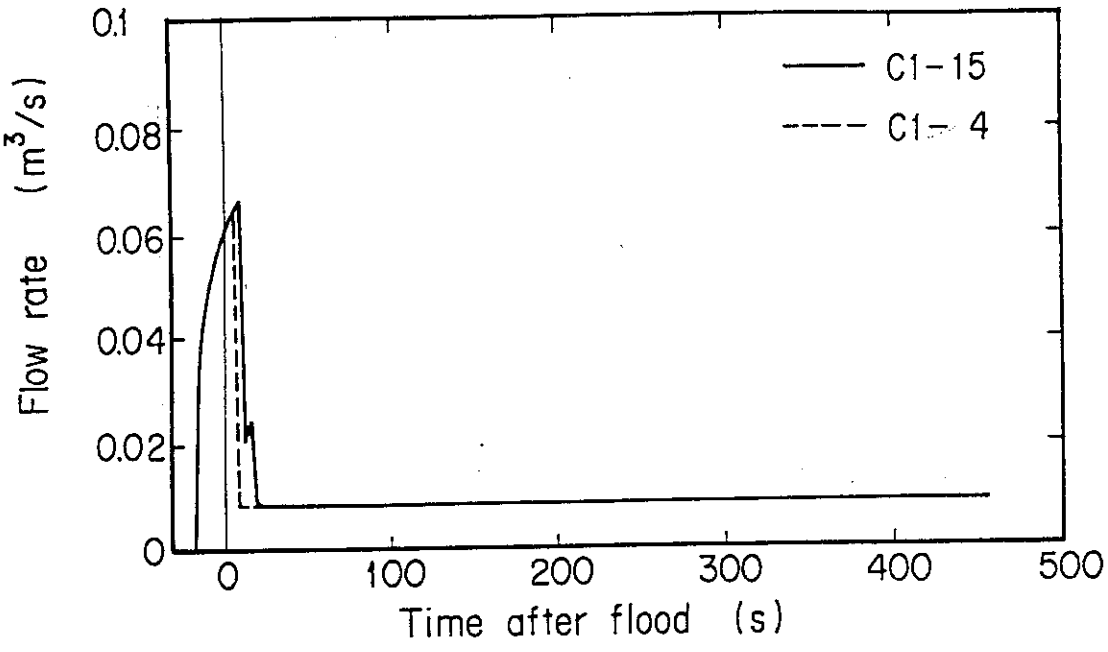

Fig.3.21 Comparison of ECC injection rate

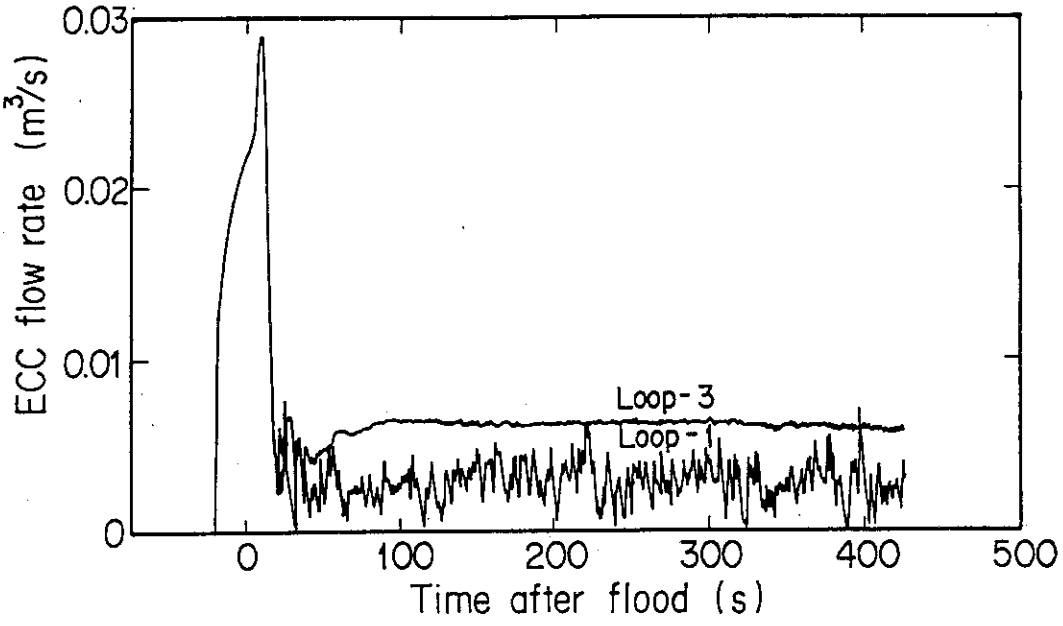

Fig.3.22 ECC injection rates into intact cold legs

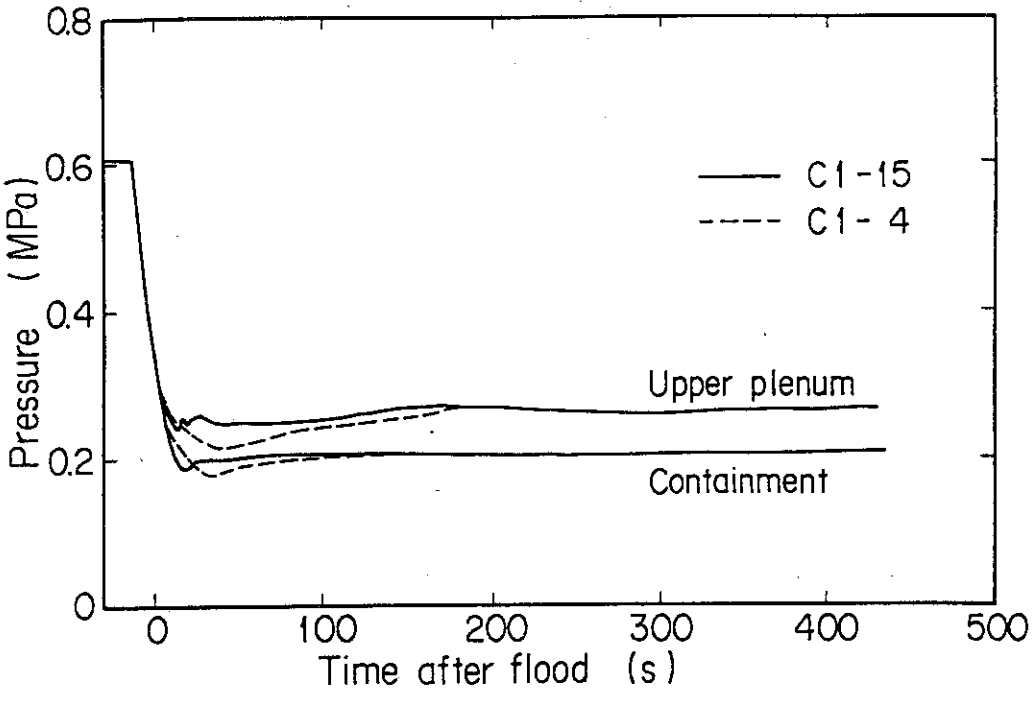

Fig.3.23 Comparison of containment and upper plenum pressure

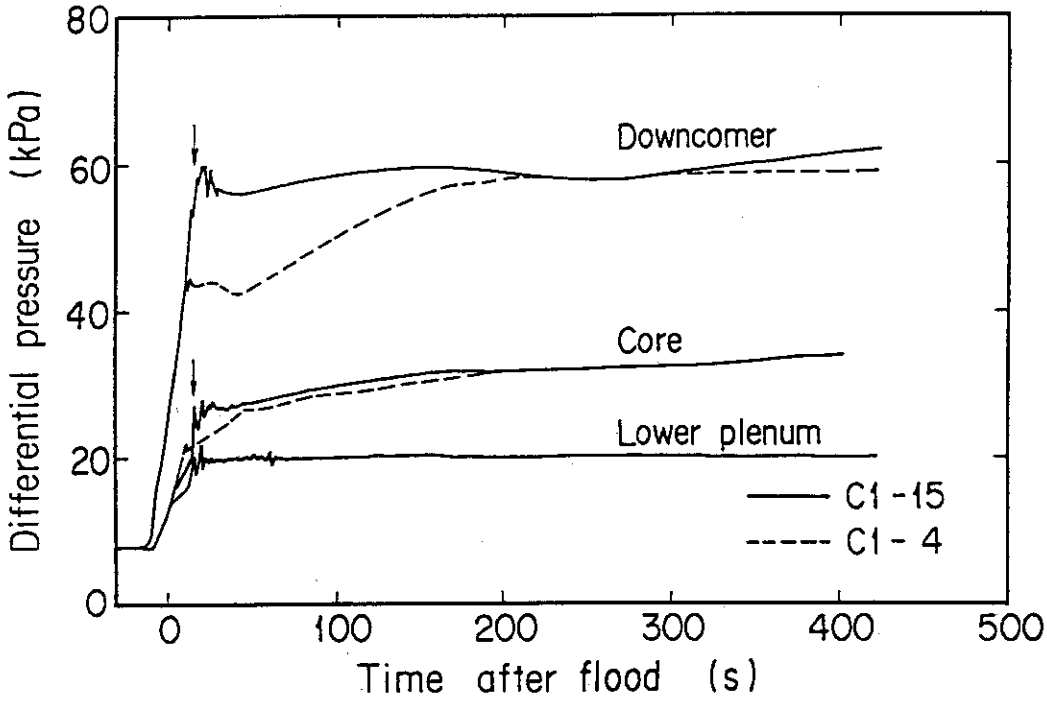

Fig.3.24 Comparison of differential pressures of downcomer, lower plenum and core

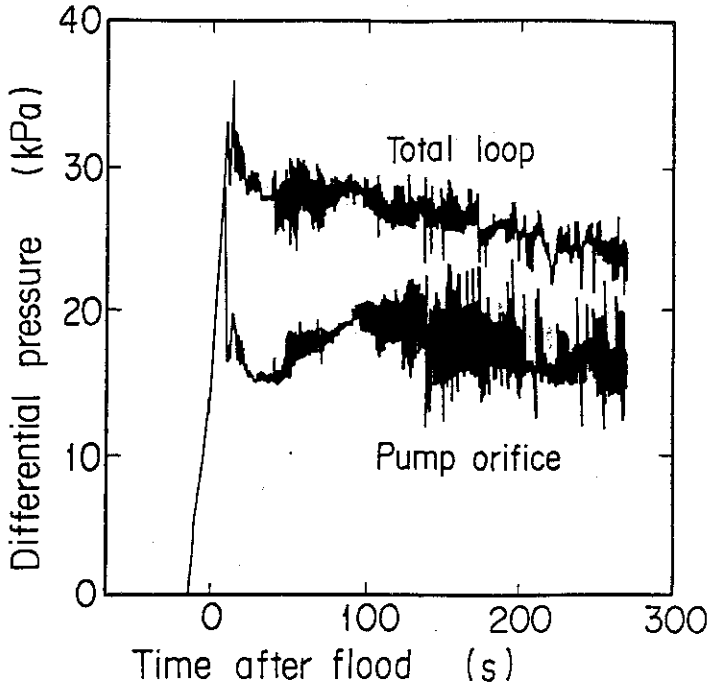

Fig.3.25 Differential pressures of total intact loop and pump orifice

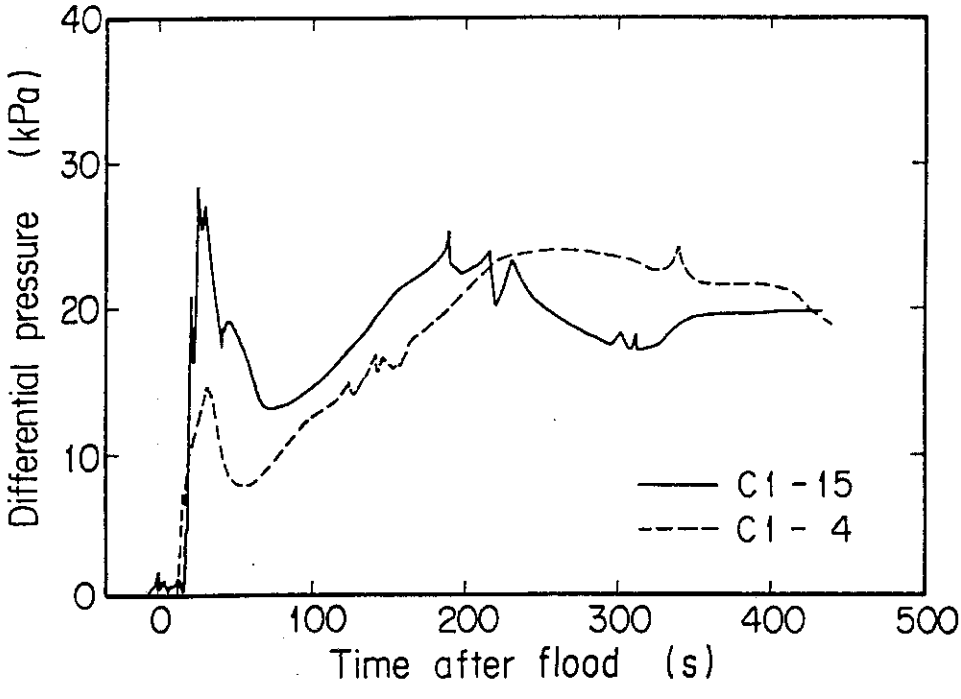

Fig.3.26 Comparison of differential pressures through broken cold leg nozzle

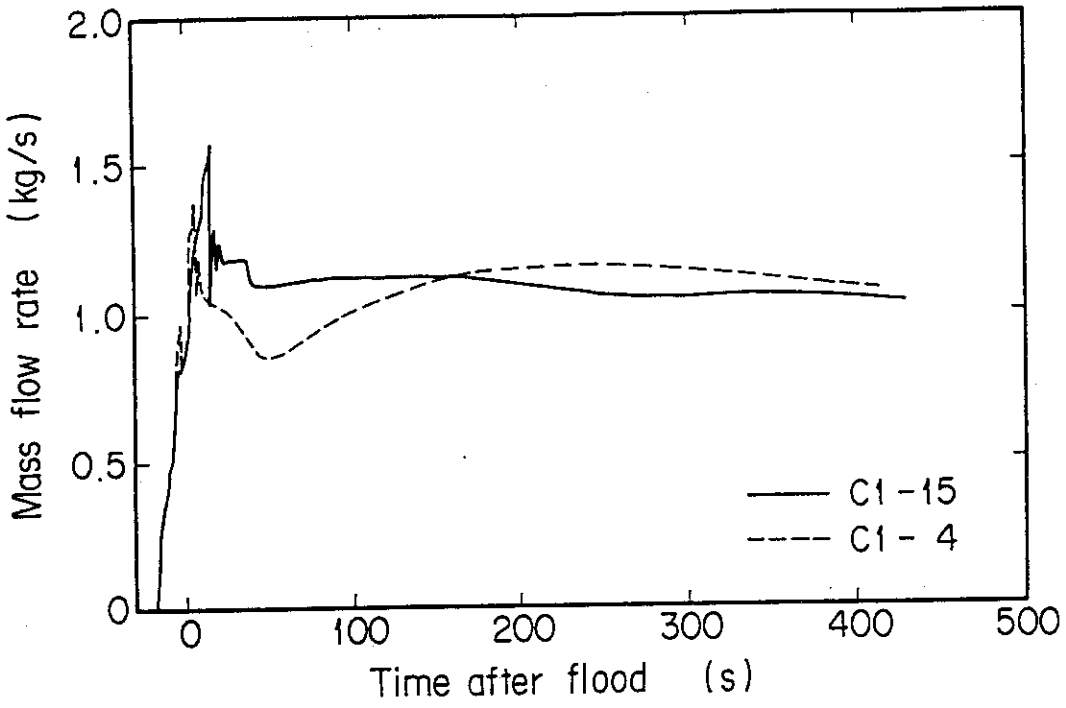

Fig.3.27 Intact loop mass flow rate

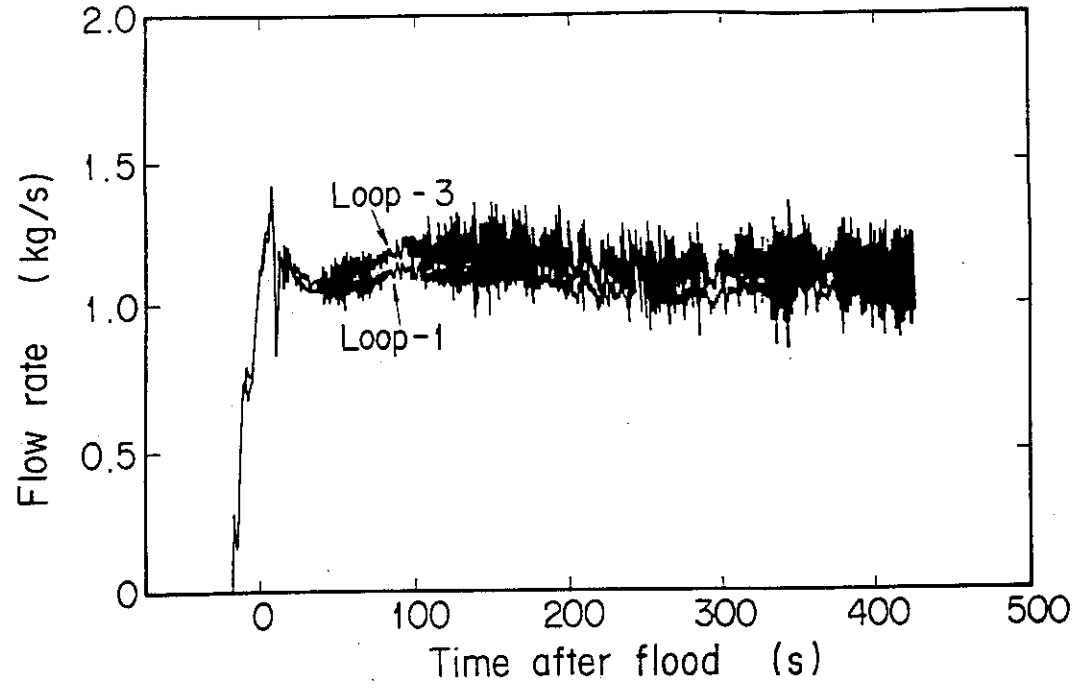

Fig.3.28 Mass flow rates in Loop-1 and in Loop-3

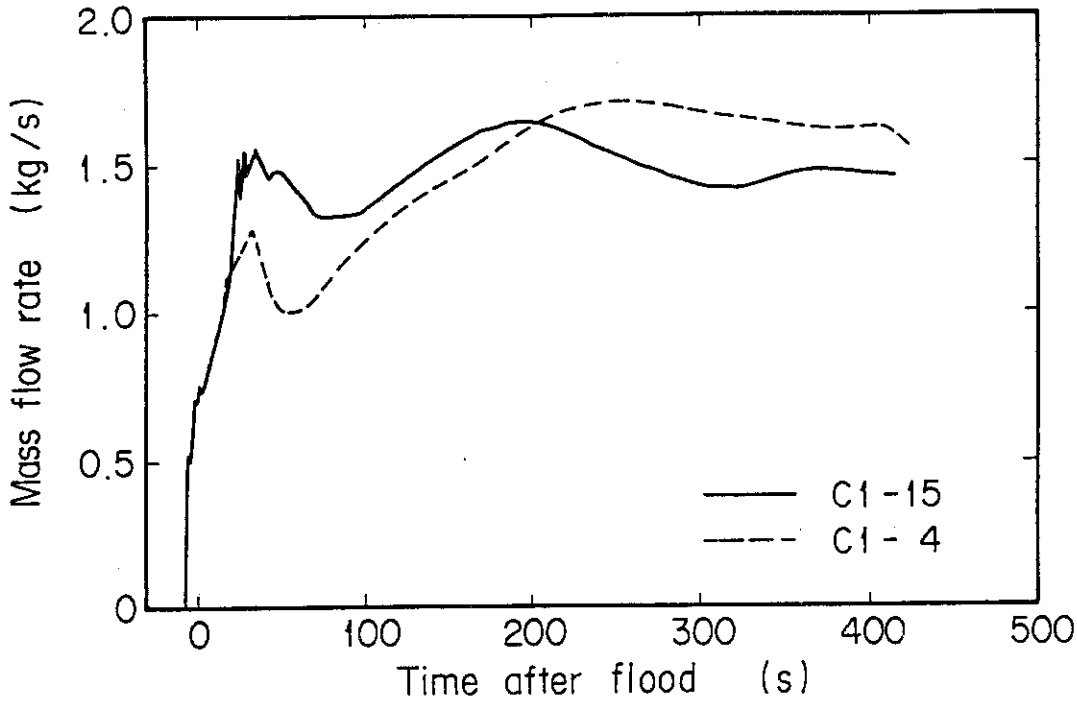

Fig.3.29 Broken loop mass flow rate

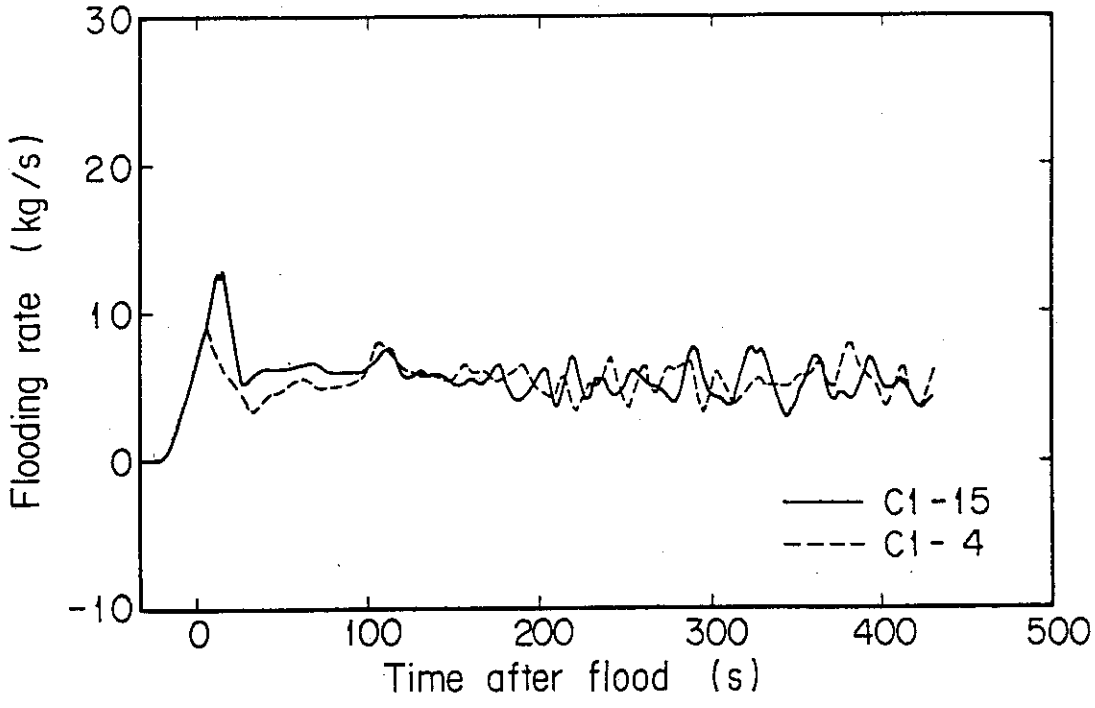

Fig.3.30 Comparison of flooding rate

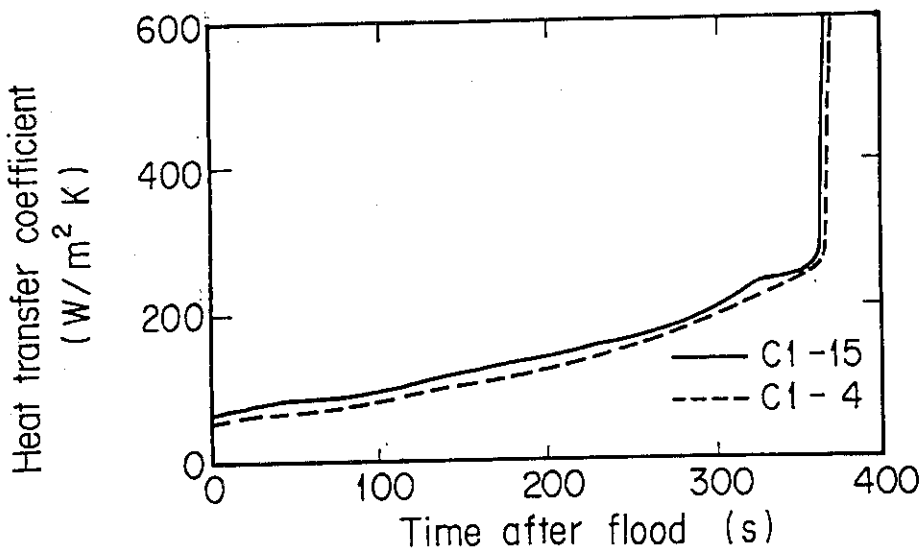

Fig.3.31 Comparison of heat transfer coefficient on maximum powered rod midplane

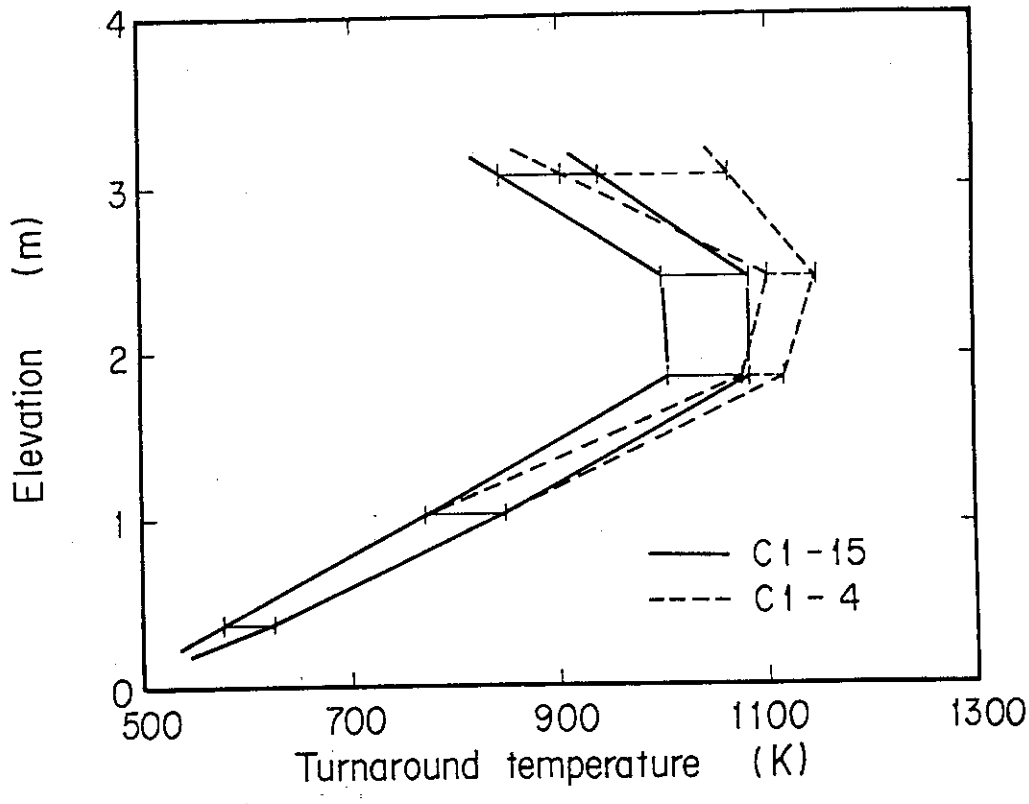

Fig.3.32 Comparison of turnaround temperatures in core central region

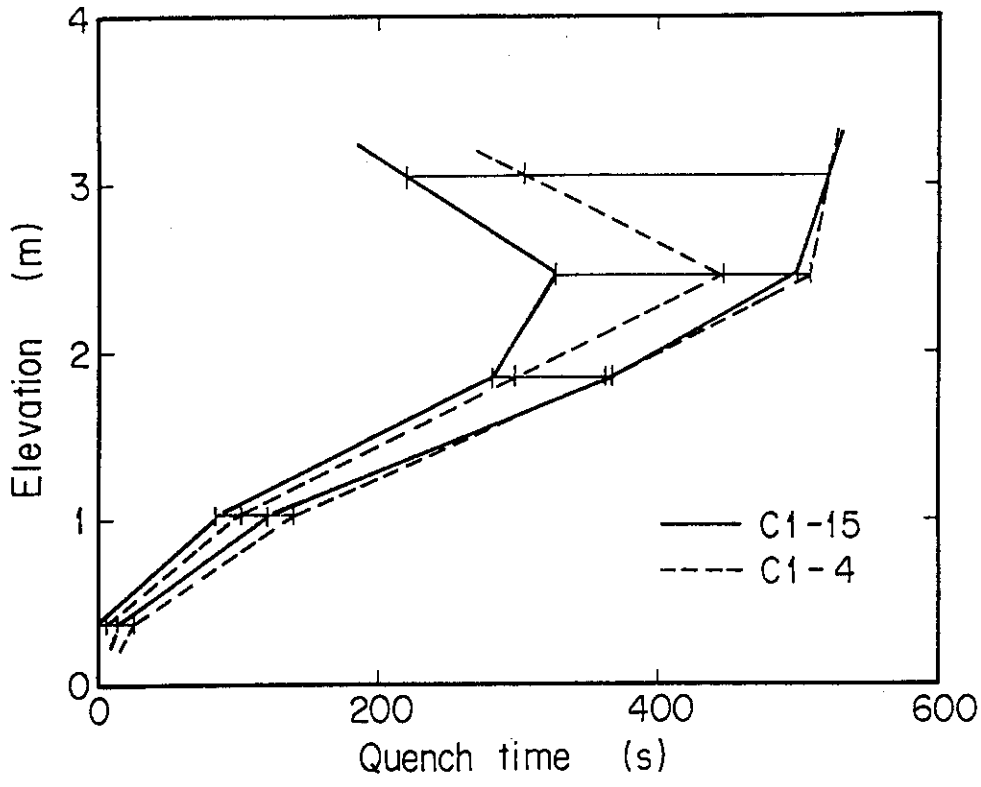

Fig.3.33 Comparison of quench times in core central region

4. Conclusions

The effects of the depressurization process on the system behavior in the reflood phase were discussed and the following conclusions were obtained:

1) The steam condensation in the intact cold legs was significant during the accumulator injection period. That increased the steam flow rate in the intact loop, as a result, controlled the system depressurization.
2) The induced high differential pressure through the intact loop during the accumulator injection period suppressed the core water accumulation.
3) The formed water plug in the cold leg induced the pressure oscillation across the intact loop. After terminating the accumulator injection, the water plug was pushed to the downcomer. That caused the water mass increase in the downcomer and resulted in the sudden increase of the core water mass.
4) The higher turnaround temperature and the longer quench time were observed in the experiment with the depressurization process than in the experiment without that due to the less core water mass caused by flashing in the lower plenum water.
5) Significant effects of the nitrogen injection were not observed except for the higher pressure drop across the broken cold leg nozzle during the injection period.
6) It is considered that the present experiment indroduced more realistical reflood initiation.

Acknowledgements

The authors are very grateful to Dr. M. Nozawa, Deputy Director General of Tokai Research Establishment, JAERI, Dr. S. Katsuragi, of Nuclear Safety Research Center, and Dr. K. Hirano, Deputy Head of Department of Nuclear Safety Research for their hearty suggestion and encouragement.

They are deeply indebted to Mr. T. Iguchi, Mr. J. Sugimoto, Dr. H. Akimoto, and Mr. T. Okubo for their analytical support. They would like to express their appreciation to Mr. H. Adachi, Dr. Y. Sudo, Mr. M. Sobajima, Mr. T. Iwamura, Mr. M. Osakabe, and Mr. A. Ohnuki for their useful discussions, Messrs. K. Sekiguchi, Y. Fukaya, N. Suzuki, T. Oyama,

4. Conclusions

The effects of the depressurization process on the system behavior in the reflood phase were discussed and the following conclusions were obtained:

1) The steam condensation in the intact cold legs was significant during the accumulator injection period. That increased the steam flow rate in the intact loop, as a result, controlled the system depressurization.
2) The induced high differential pressure through the intact loop during the accumulator injection period suppressed the core water accumulation.
3) The formed water plug in the cold leg induced the pressure oscillation across the intact loop. After terminating the accumulator injection, the water plug was pushed to the downcomer. That caused the water mass increase in the downcomer and resulted in the sudden increase of the core water mass.
4) The higher turnaround temperature and the longer quench time were observed in the experiment with the depressurization process than in the experiment without that due to the less core water mass caused by flashing in the lower plenum water.
5) Significant effects of the nitrogen injection were not observed except for the higher pressure drop across the broken cold leg nozzle during the injection period.
6) It is considered that the present experiment indroduced more realistical reflood initiation.

Acknowledgements

The authors are very grateful to Dr. M. Nozawa, Deputy Director General of Tokai Research Establishment, JAERI, Dr. S. Katsuragi, of Nuclear Safety Research Center, and Dr. K. Hirano, Deputy Head of Department of Nuclear Safety Research for their hearty suggestion and encouragement.

They are deeply indebted to Mr. T. Iguchi, Mr. J. Sugimoto, Dr. H. Akimoto, and Mr. T. Okubo for their analytical support. They would like to express their appreciation to Mr. H. Adachi, Dr. Y. Sudo, Mr. M. Sobajima, Mr. T. Iwamura, Mr. M. Osakabe, and Mr. A. Ohnuki for their useful discussions, Messrs. K. Sekiguchi, Y. Fukaya, N. Suzuki, T. Oyama,

T. Wakabayashi, Y. Niitsuma, J. Matsumoto, T. Nishikizawa, and H. Sonobe for their contribution to the facility operation, to Messrs. R.K. Fujita and D.H. Miyasaki, resident engineers from USNRC, and to Dr. P.J. Schally, resident engineer from BMFT, for their devoted help.

References

1) Murao, Y., et. al., "CCTF Core I Test Result" JAERI-M 82-073, (July 1982)
2) Waring, J.P., Hochreiter, L.E., "PWR FLECHT-SET Phase B1 Evaluation Report", WCAP-8583 (Aug. 1975)
3) Kirmse, R., et. al., "Zusammenfassende Darstellung von Wichigen Ergebnissen der PKL Versuche der Testserien IA und IB", GRS-A-360

T. Wakabayashi, Y. Niitsuma, J. Matsumoto, T. Nishikizawa, and H. Sonobe for their contribution to the facility operation, to Messrs. R.K. Fujita and D.H. Miyasaki, resident engineers from USNRC, and to Dr. P.J. Schally, resident engineer from BMFT, for their devoted help.

References

1) Murao, Y., et. al., "CCTF Core I Test Result" JAERI-M 82-073, (July 1982)
2) Waring, J.P., Hochreiter, L.E., "PWR FLECHT-SET Phase B1 Evaluation Report", WCAP-8583 (Aug. 1975)
3) Kirmse, R., et. al., "Zusammenfassende Darstellung von Wichigen Ergebnissen der PKL Versuche der Testserien IA und IB", GRS-A-360

Appendix A

Definition of Tag. IDs in Appendix B and Appendix C

Figure list

1. Definition of Tag.ID for clad surface temperatures

Notation : TENNWAM

NN : Bundle number

WA : Power zone

WA = X1, X2 : High power (Local power factor 1.1)

WA = Y1, Y2 : Medium power (Local power factor 1.0)

WA = Z1, Z2 : Low power (Local power factor 0.95)

M : Elevation

	Elevation (m)	Axial power factor
1	0.38	0.568
2	1.015	1.176
3	1.83	1.492
4	2.44	1.312
5	3.05	0.815

2. Definition of power zone and bundle number

See Fig. A-1

3. Definition of Tag.ID for void fraction

See Fig. A-2

4. Definition of Tag.ID for average linear power of heater rod in each power unit zone

See Fig. A-3

5. Definition of carry-over rate fraction (C.R.F)

$$CRF = \frac{\dot{m}_{UP} + \dot{m}_{L}}{\dot{m}_{CR} + \dot{m}_{UP} + \dot{m}_{L}}$$

The calculated data within ±25 s are averaged:

$$(CRF)_i = \frac{1}{101} \sum_{k=i-50}^{i+50} (CRF)_k$$

where

ΔP_{UP} : Average of measured data at four orientations

ΔP_{CR} : Same as above

$$\dot{m}_{UP} = A_{up} \frac{d}{dt} (\Delta P_{UP})$$

$$\dot{m}_{CR} = A_{CR} \frac{d}{dt} (\Delta P_{CR})$$

$$\dot{m}_L = \sum_{k=1}^{4} \dot{m}_{pk}$$

$\dot{m}$: mass flow rate or mass accumulation rate

ΔP: differential pressure

suffix

UP: upper plenum

CR: core

L : loop

p : primary pump

6. Definition of Tag.ID for differential pressure through downcomer, upper plenum, core and lower plenum

   See Fig. A-4

7. Definition of Tag.ID for differential pressure through intact and broken loop and broken cold leg nozzle

   See Fig. A-5

8. Definition of Tag.ID for fluid temperature in inlet and outlet plenum and secondary of steam generator

   See Fig. A-6

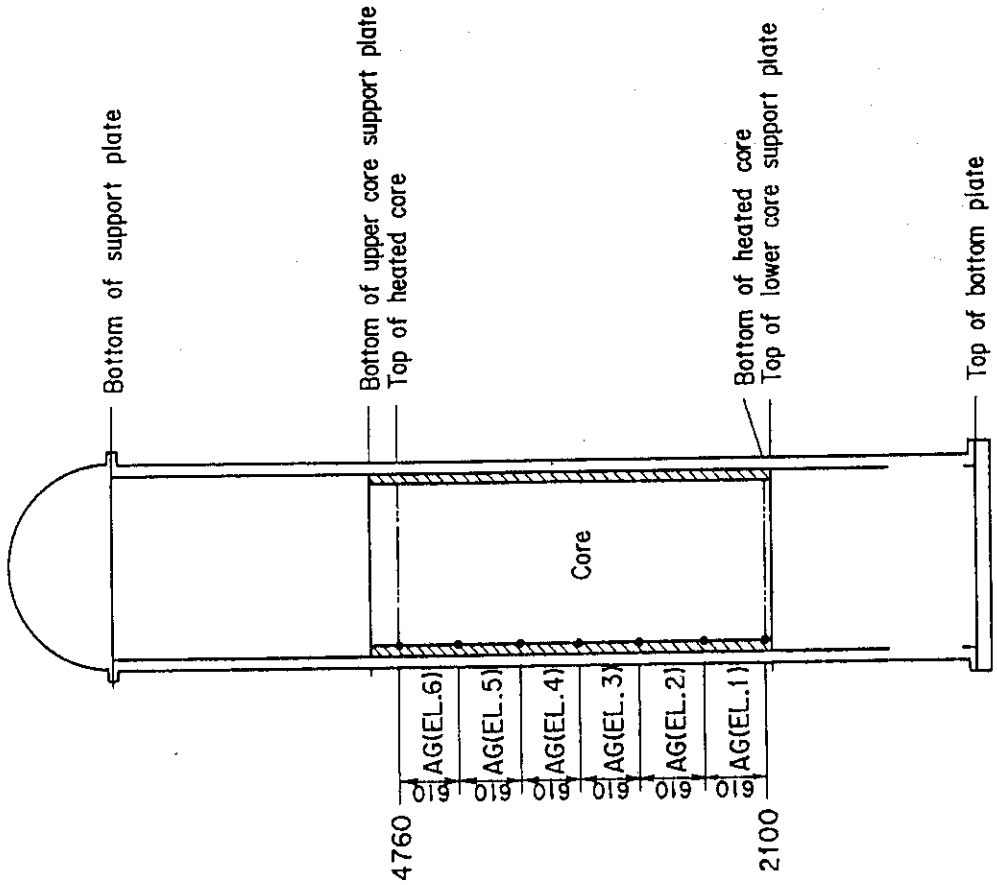

Fig.A-2 Definition of Tag.ID for void fraction (AG(EL.1) ~ AG(EL.6))

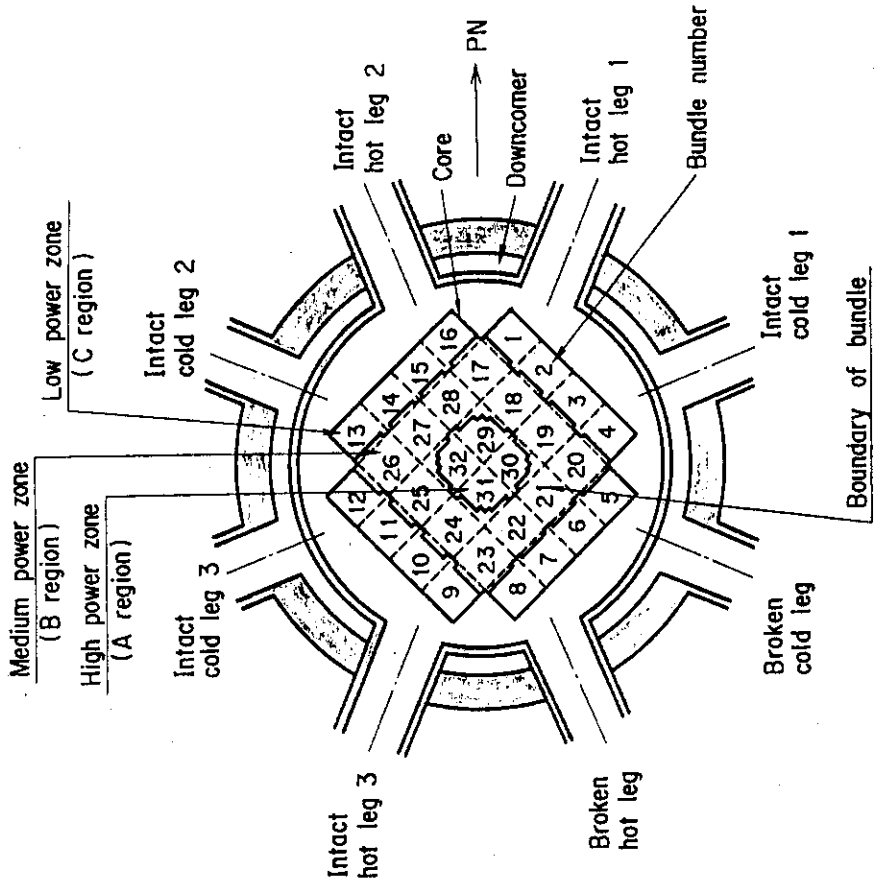

Fig.A-1 Definition of power zones and bundle numbers

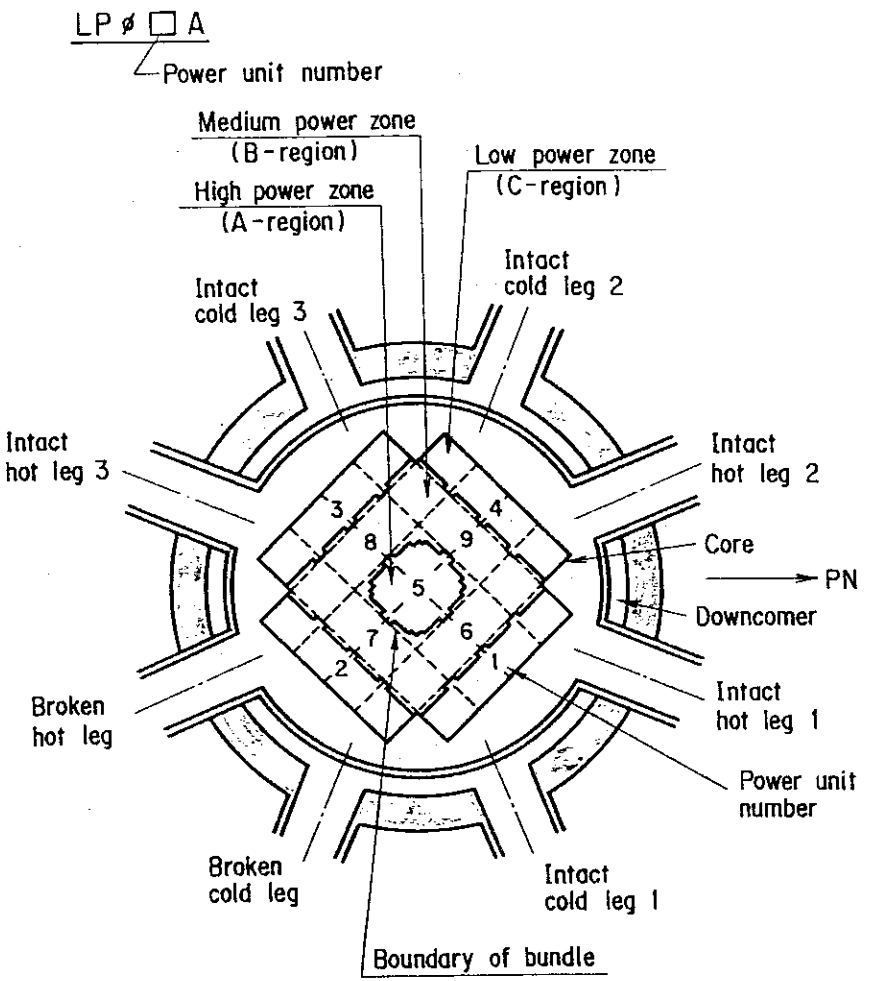

Fig. A-3 Definition of Tag. ID for average linear power of heater rod in each power unit zone (LP01A ~ LP09A)

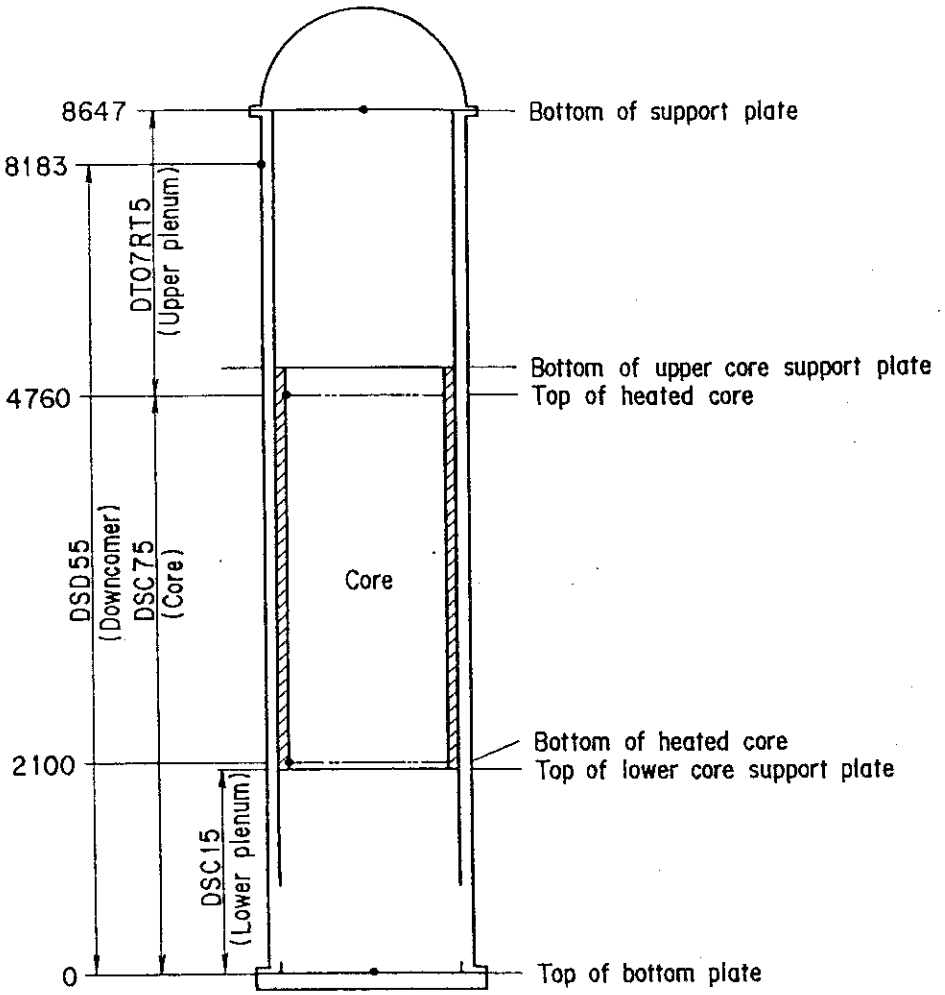

Fig. A-4 Definition of Tag. ID for differential pressure through downcomer, upper plenum, core, and lower plenum (DSD55, DTO7RT5, DSC75, DSC15)

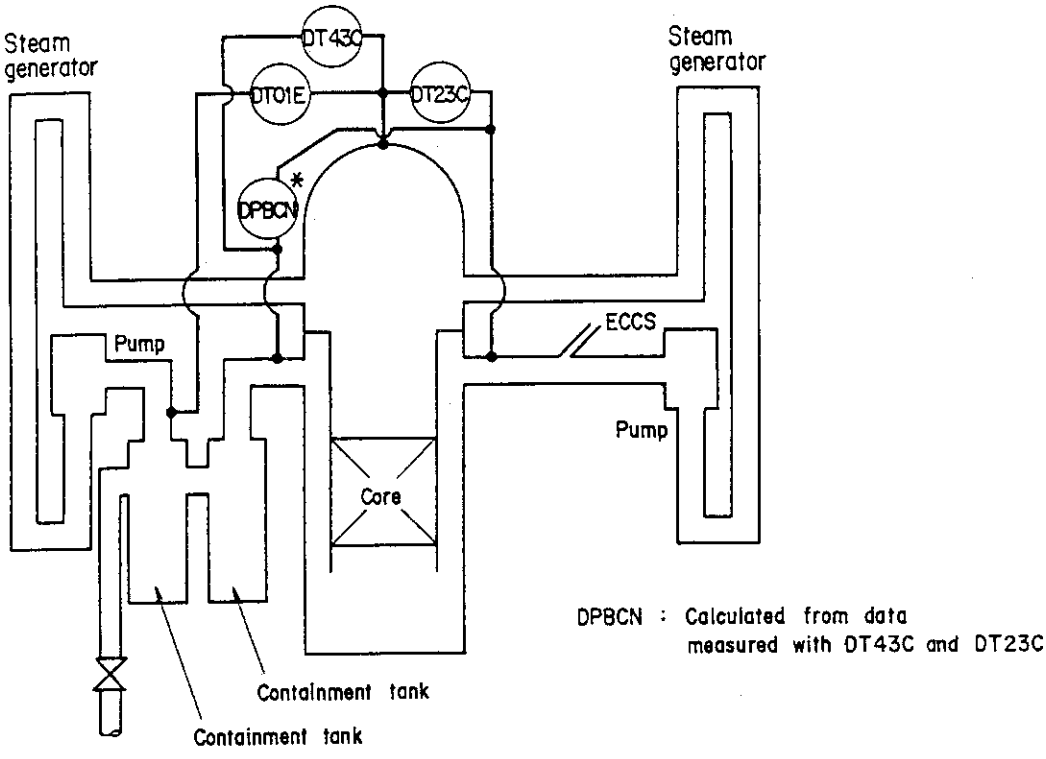

Fig. A-5 Definition of Tag. ID for differential pressure through intact and broken loop and broken cold leg nozzle (DT23C, DT01B, DPBCN)

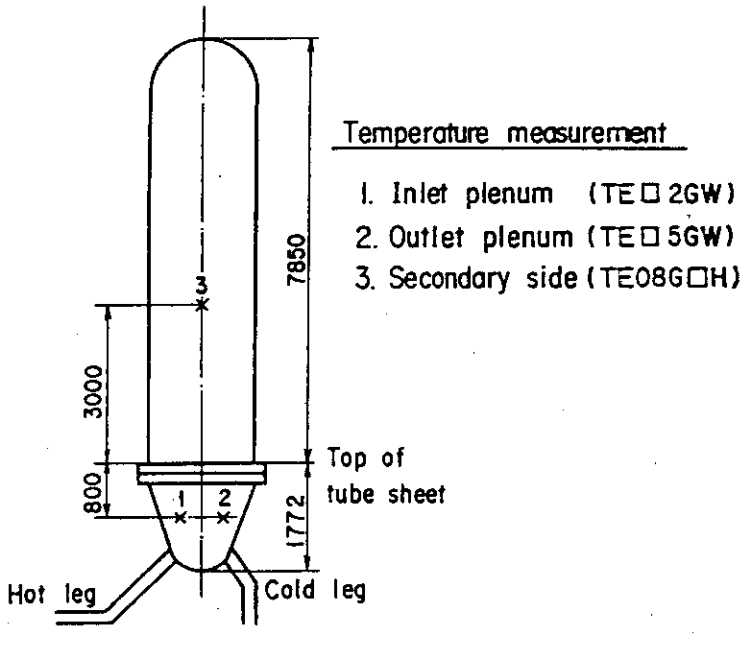

Fig. A-6 Definition of Tag. ID for fluid temperature in inlet and outlet plenum and secondary of steam generator (TE□2GW, TE□5GW, TE08G□H)

Appendix B

Main results of Test C1-4 (Run 13)

Table and Figure List

Table B-1 Summary of test conditions

1. TEST TYPE : TEST c1-4 (CCTF MAIN TEST NO.4)
2. TEST NUMBER : RUN 013 3. DATE : July 27, 1979
4. POWER : A: TOTAL: 9.31 MW; B:LINEAR: 1.4 KW/M
5. RELATIVE RADIAL POWER SHAPE :

   A: ZONE: A B C

   B: RATIO: 1.03 : 1.0 : 0.82
6. AXIAL POWER SHAPE : CHOPPED COSINE
7. PRESSURE (KG/CM^2A) :

   A: SYSTEM: 6.02 → 2.0, B: CONTAINMENT 6.02 → 2.0,

   C: STEAM GENERATOR SECONDARY: 50
8. TEMPERATURE (DEG.C) :

   A: DOWNCOMER WALL 185, B: VESSEL INTERNALS 158,

   C: PRIMARY PIPING WALL 157, D: LOWER PELNUM LIQUID 149,

   E: ECC LIQUID 37, F: STEAM GENERATOR SECONDARY 264,

   G: CORE TEMPERATURE AT ECC INITIATION 494
9. ECC INJECTION TYPE: A

   A: COLD LEG, B: LOWER PLENUM, C: LOWER PLENUM + COLD LEG
10. PUMP K-FACTOR : ∿ 15 (UNCERTAIN)
11. ECC FLOW RATES AND DURATION :

    A: ACCUMULATOR 195 M^3/HR FROM 0 TO 28 SECONDS

    B: LPCI 30.7 M^3/HR FROM 29 TO 839 SECONDS

    C: ECC INJECTION TO LOWER PLENUM : FROM — TO — SECONDS

    (VALVE OPENING AND CLOSING TIMES ARE INCLUDED IN THE INJECTION DURATION)
12. INITIAL WATER LEVEL IN LOWER PLENUM : 0.82 M.
13. POWER CONTROL : ANS x 1.2 + ACTINIDE (30 SEC AFTER SCRAM)
14. EXPECTED BOCREC TIME FROM ECC INITIATION 12 SEC
15. EXPECTED PEAK TEMPERATURE AT BOCREC 600 C

Table B-2 Chronology of events

EVENT	TIME (sec)
Test C1-4 initiated (Heater rods power on) (Data recording initiated)	0.0
Accumulator injection initiated	46.5
Power decay initiated (Bottom of core recovery)	61 (75)
Accumulator injection switched from lower plenum to cold leg	
Accumulator injection ended and LPCI injection initiated	74.5
All heater rods quenched	616
Power off	765
LPCI injection ended	885
Test C1-4 ended (Data recording ended)	1130

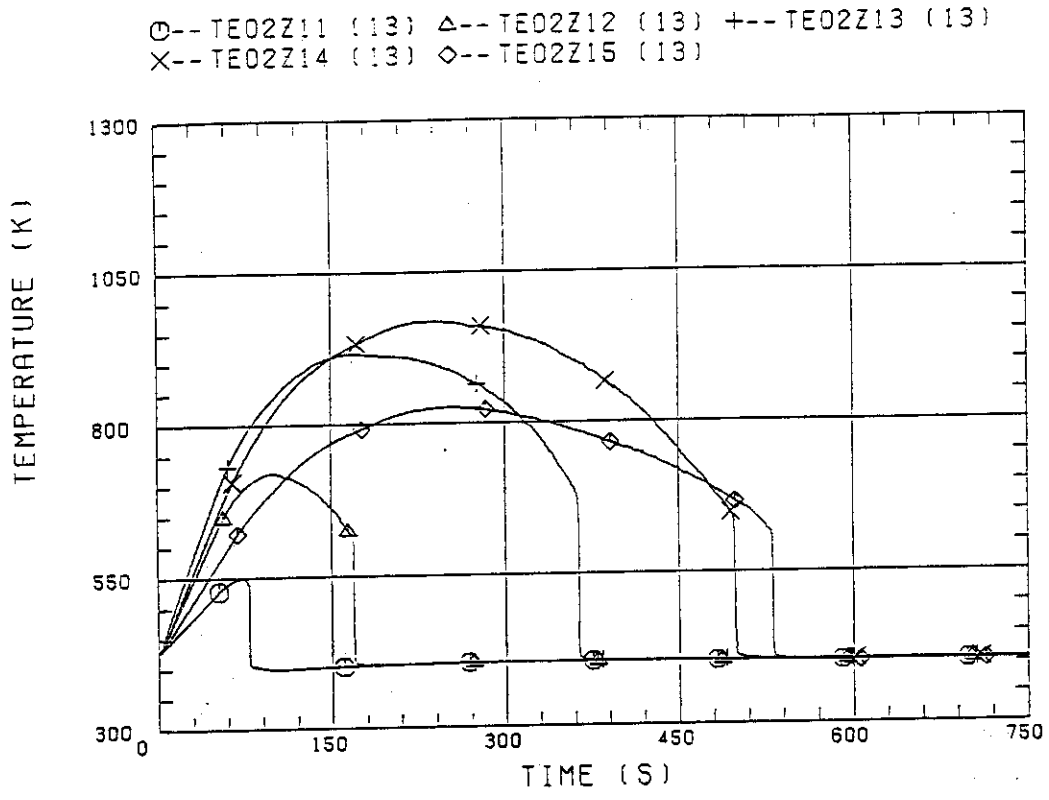

Fig. B-1 Surface temperature on low power rod (Z-rod) in medium power region (B region) (average power rod)

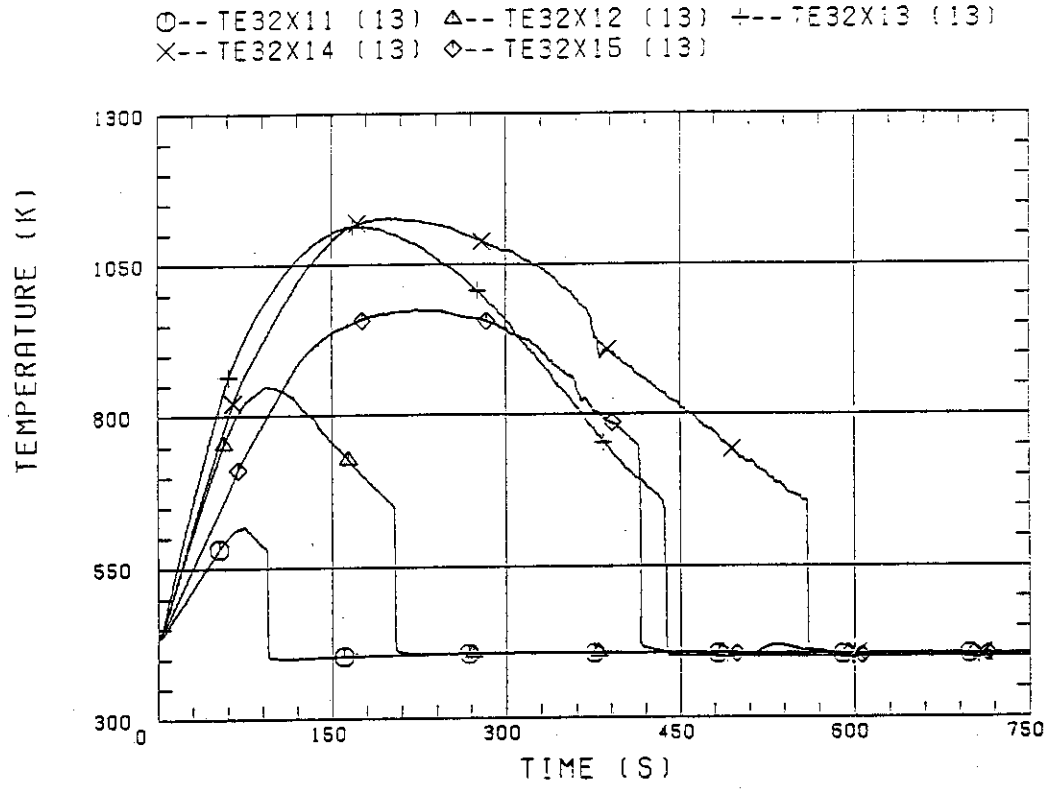

Fig. B-2 Surface temperature on high power rod (X-rod) in high power region (A region) (peak power rod)

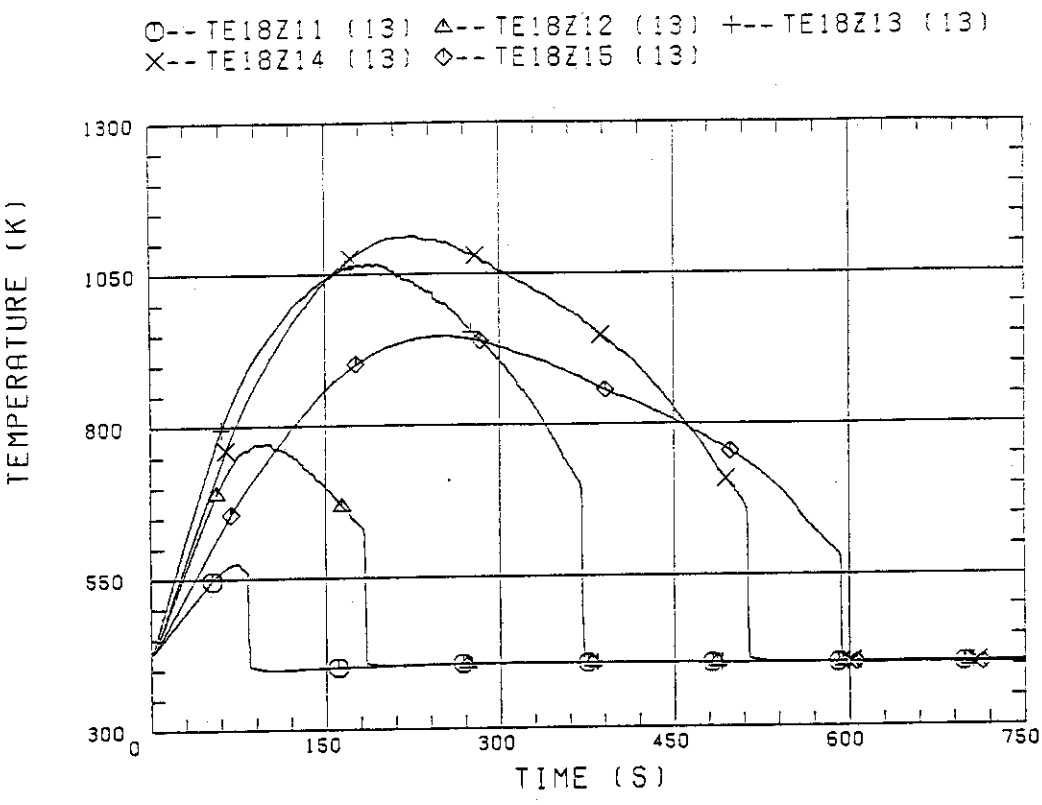

Fig. B-3 Surface temperature on low power rod (Z-rod) in low power region (C region) (lowest power rod)

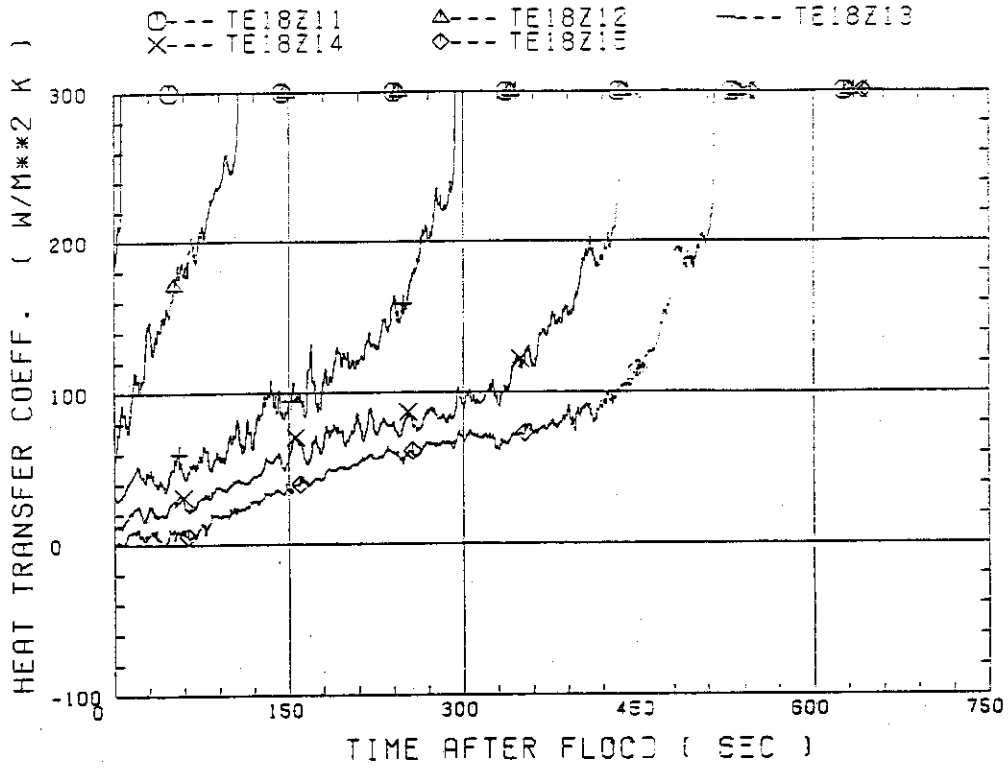

Fig. B-4 Heat transfer coefficient at midplane of low power rod (Z-rod) in medium power region (B region) (average power rod)

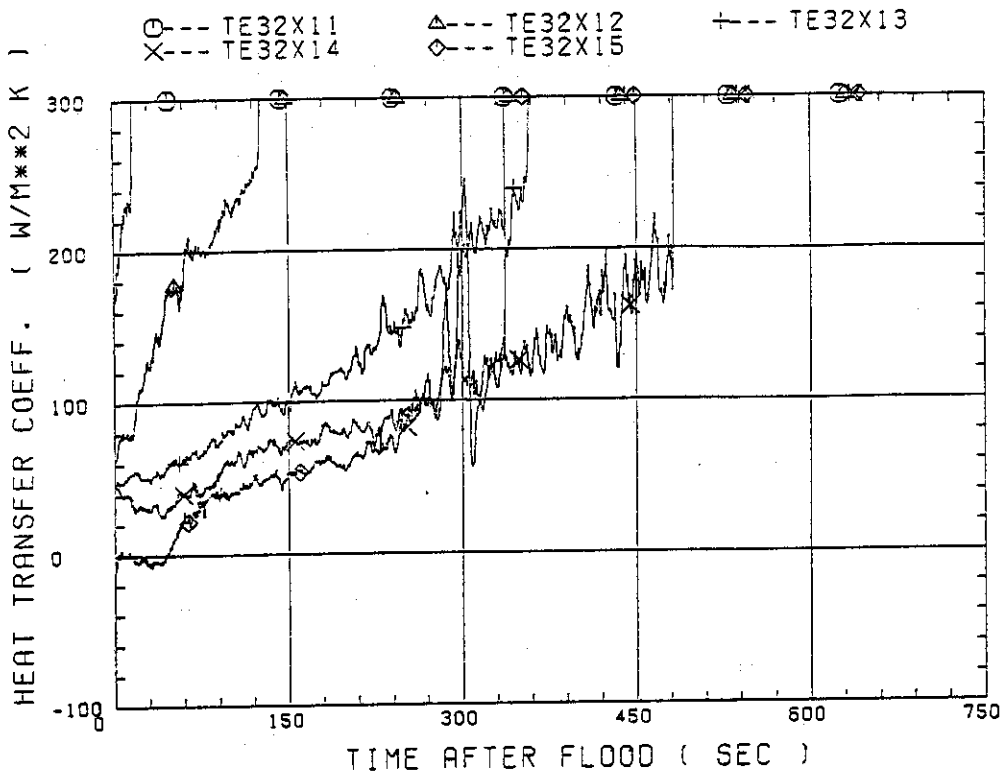

Fig. B-5 Heat transfer coefficient at midplane of high power rod (X-rod) in high power region (A region)

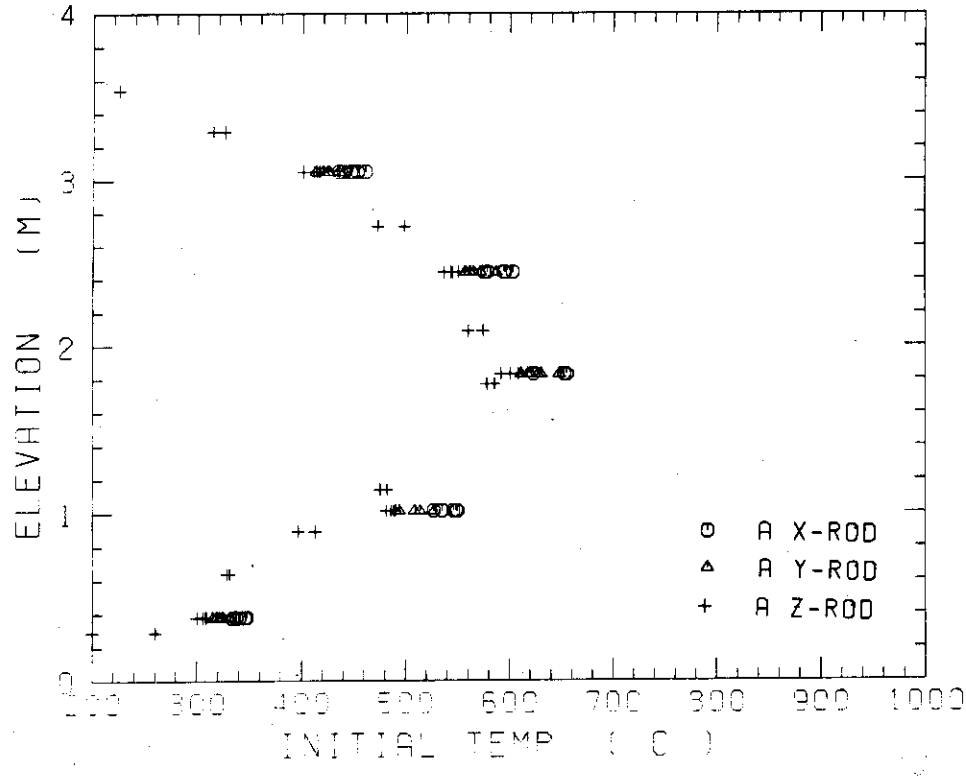

Fig. B-6 Initial rod surface temperature in high power region (A region)

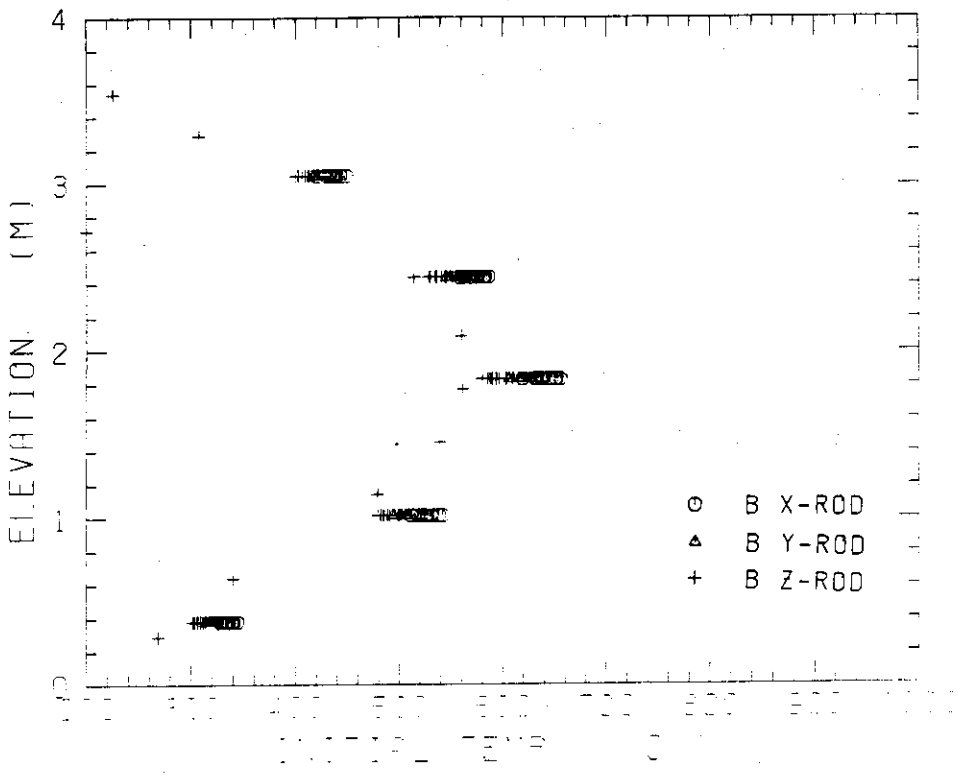

Fig. B-7 Initial rod surface temperature in medium power region (B region)

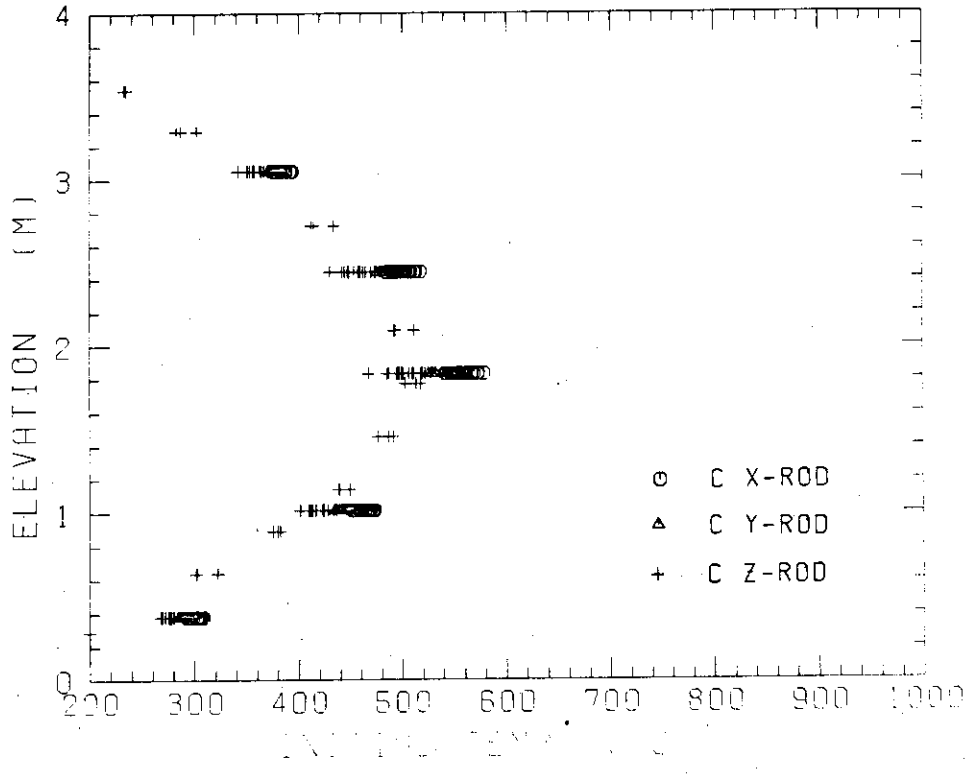

Fig. B-8 Initial rod surface temperature in low power region (C region)

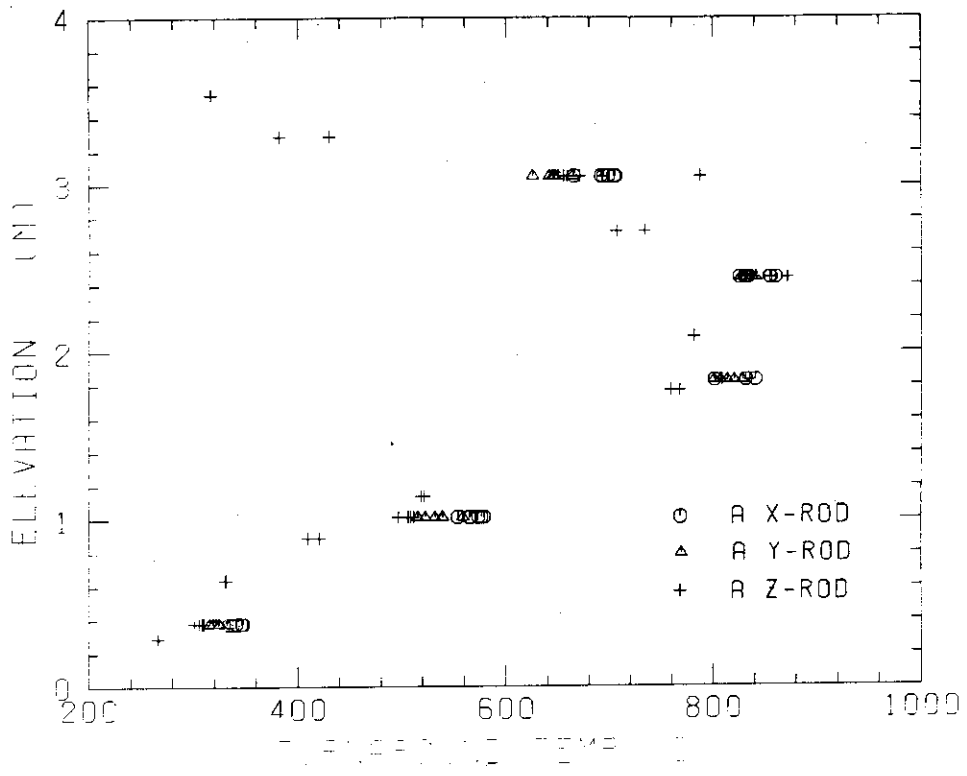

Fig. B-9 Turnaround temperature in high power region (A region)

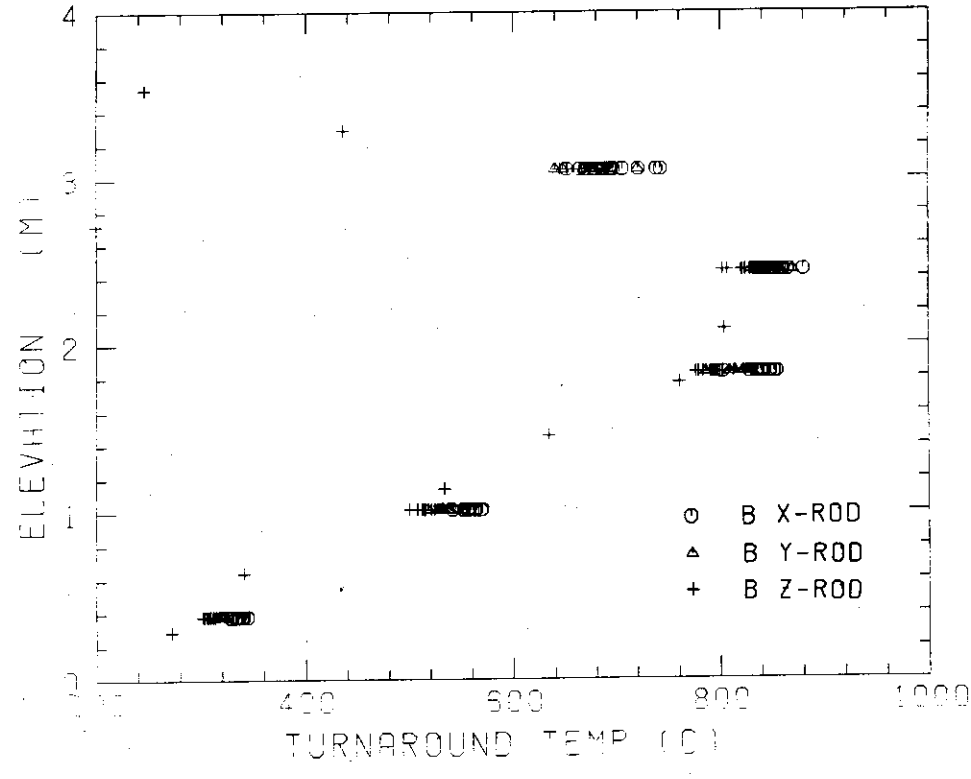

Fig. B-10 Turnaround temperature in medium power region (B region)

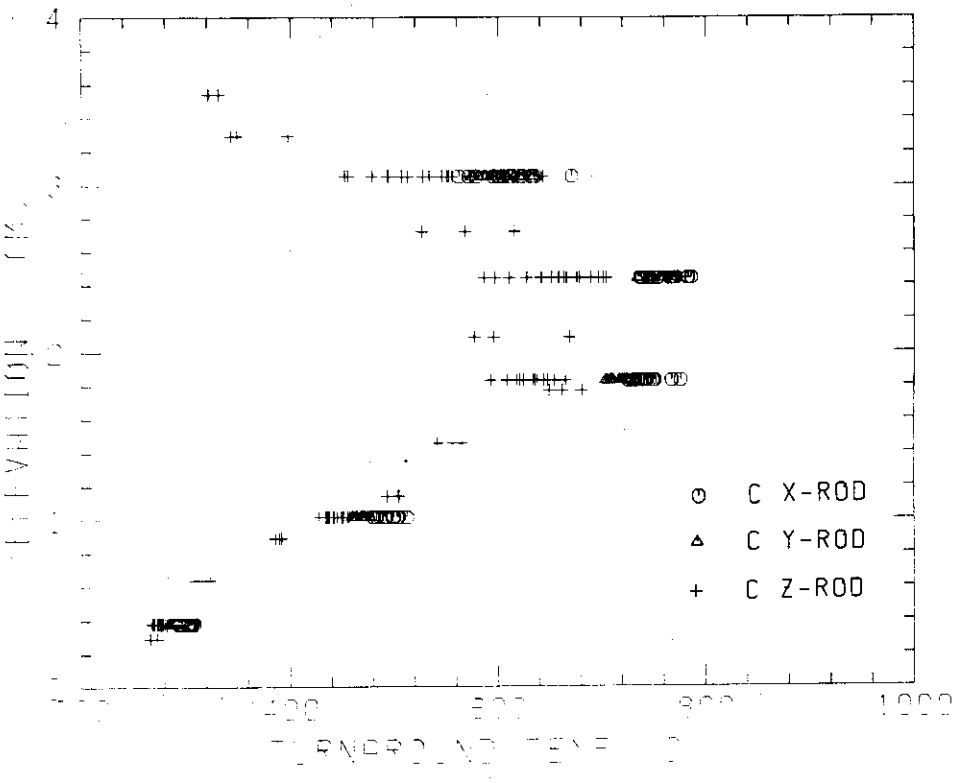

Fig. B-11 Turnaround temperature in low power region (C region)

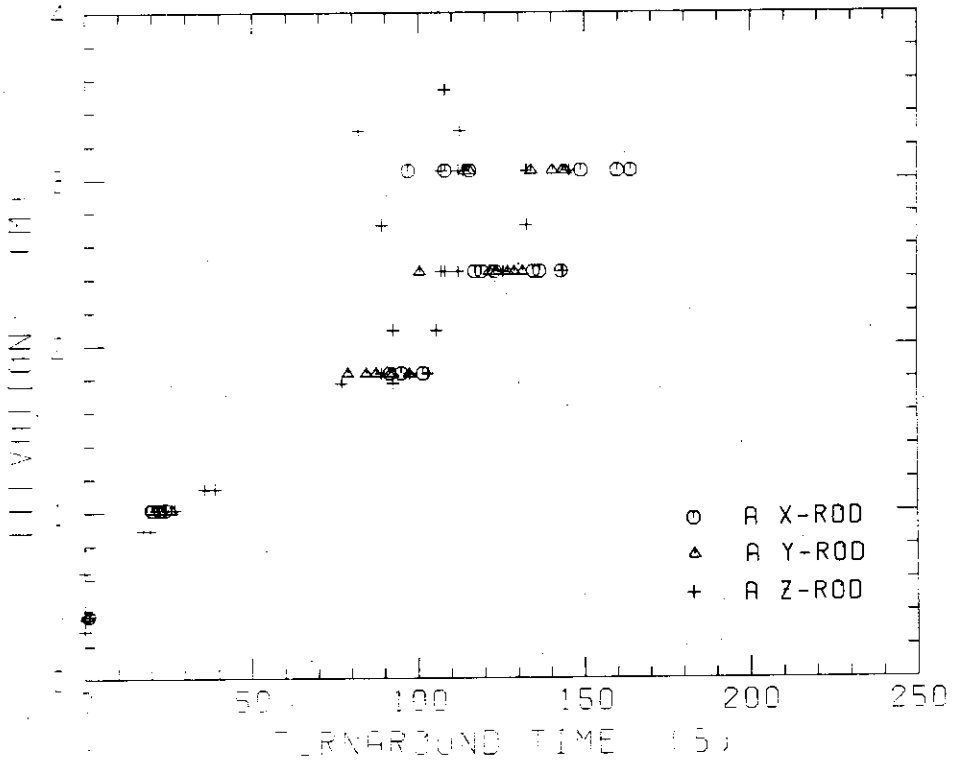

Fig. B-12 Turnaround time in high power region (A region)

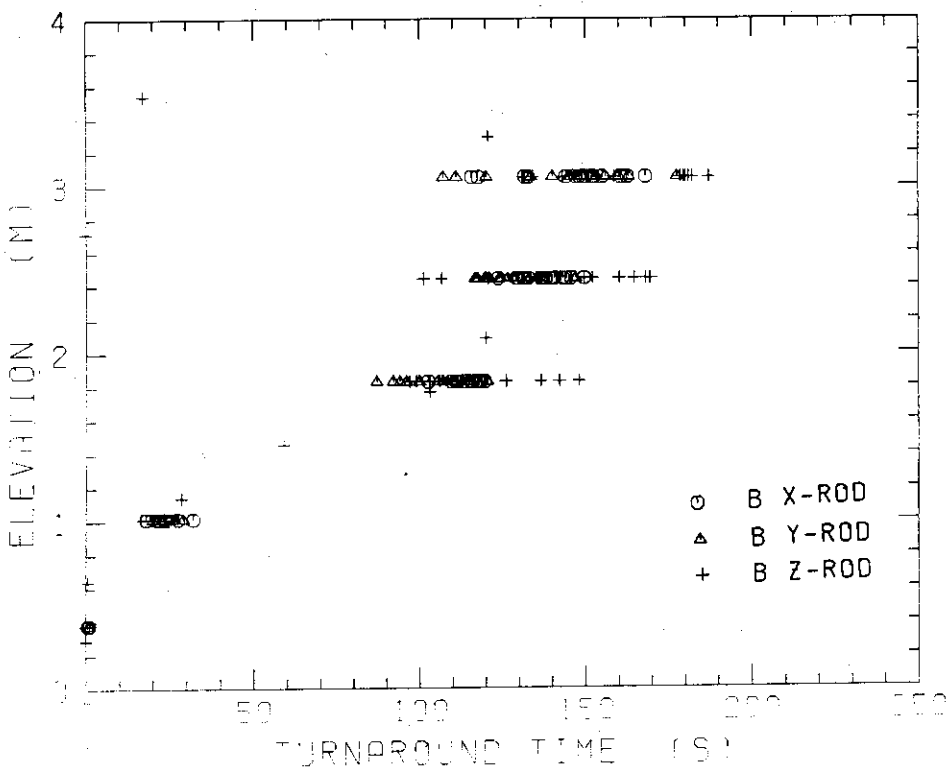

Fig. B-13 Turnaround time in medium power region (B region)

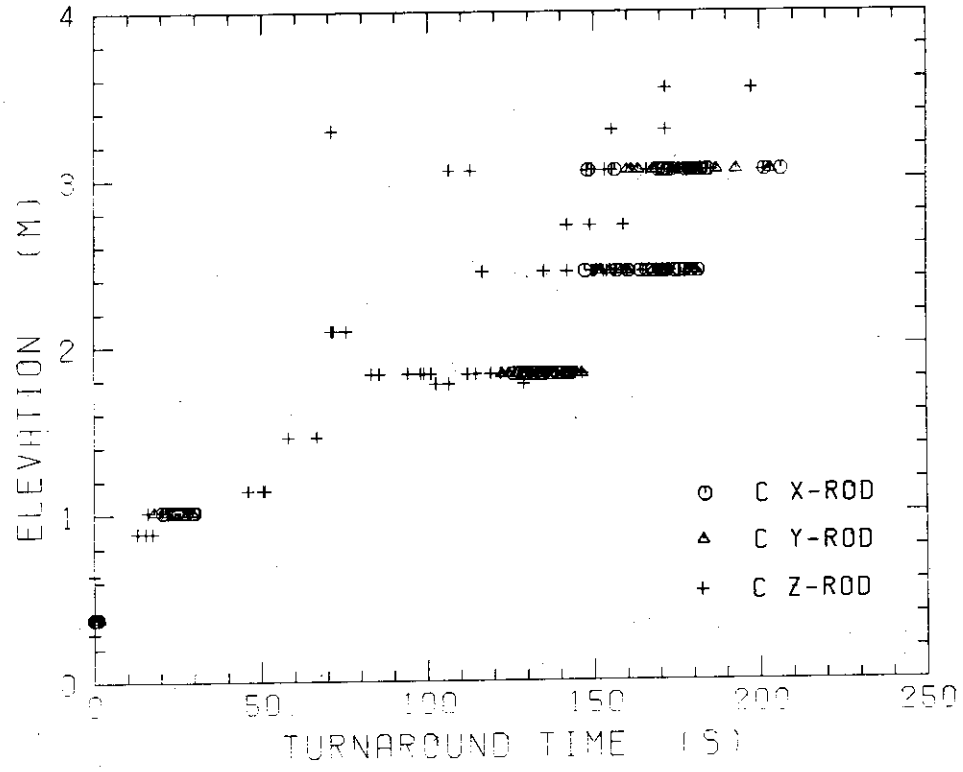

Fig. B-14 Turnaround time in low power region (C region)

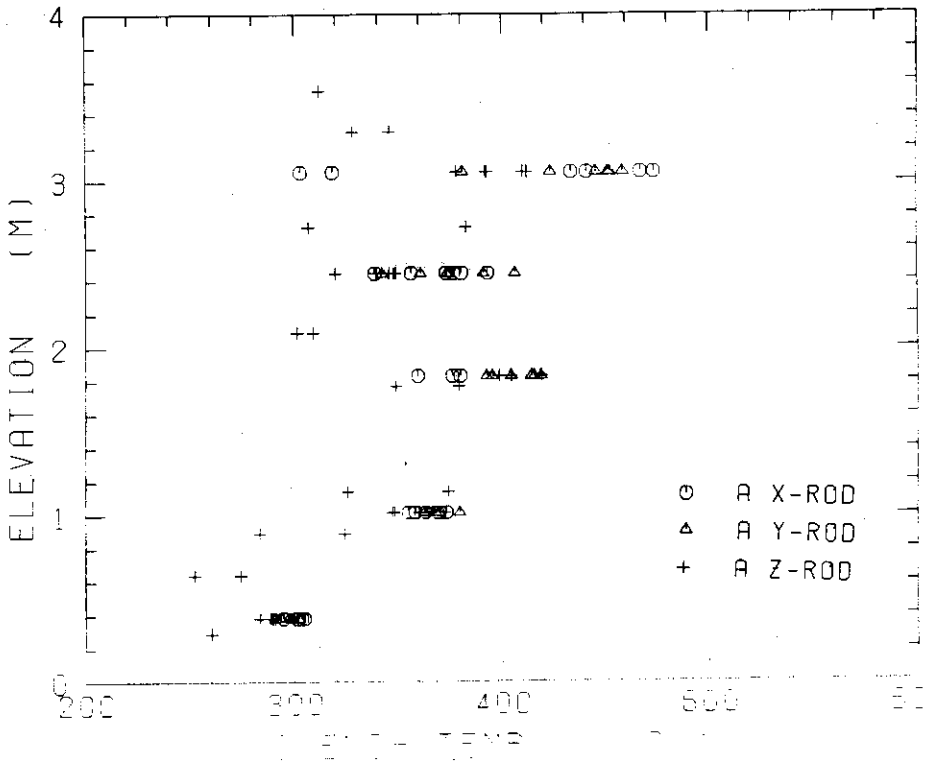

Fig. B-15 Quench temperature in high power region (A region)

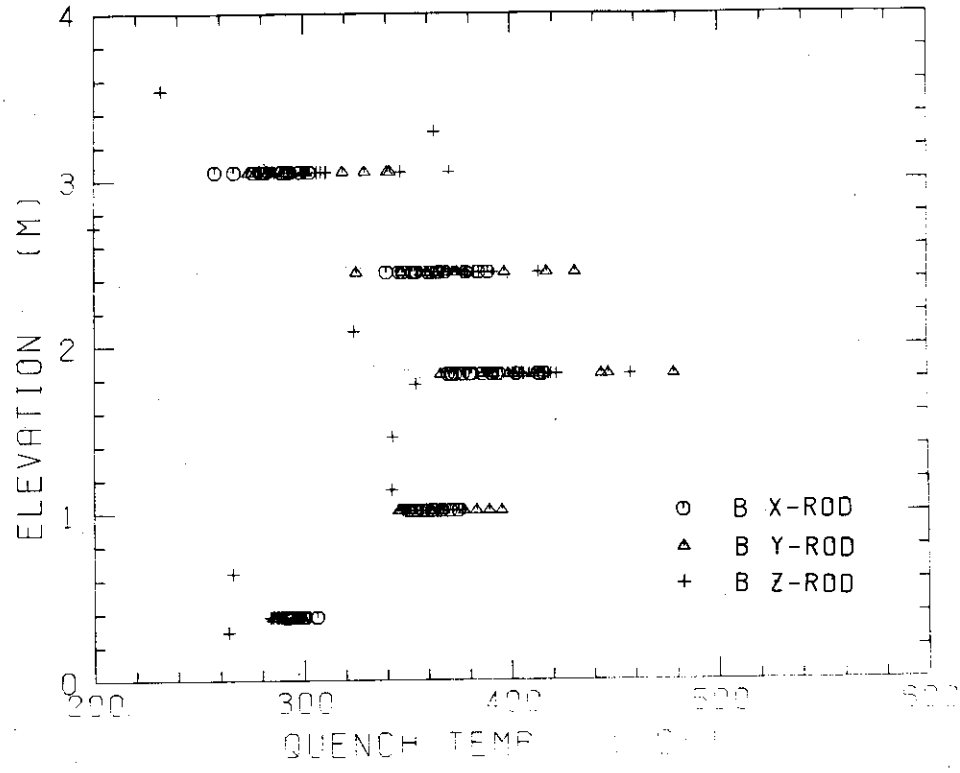

Fig. B-16 Quench temperature in medium power region (B region)

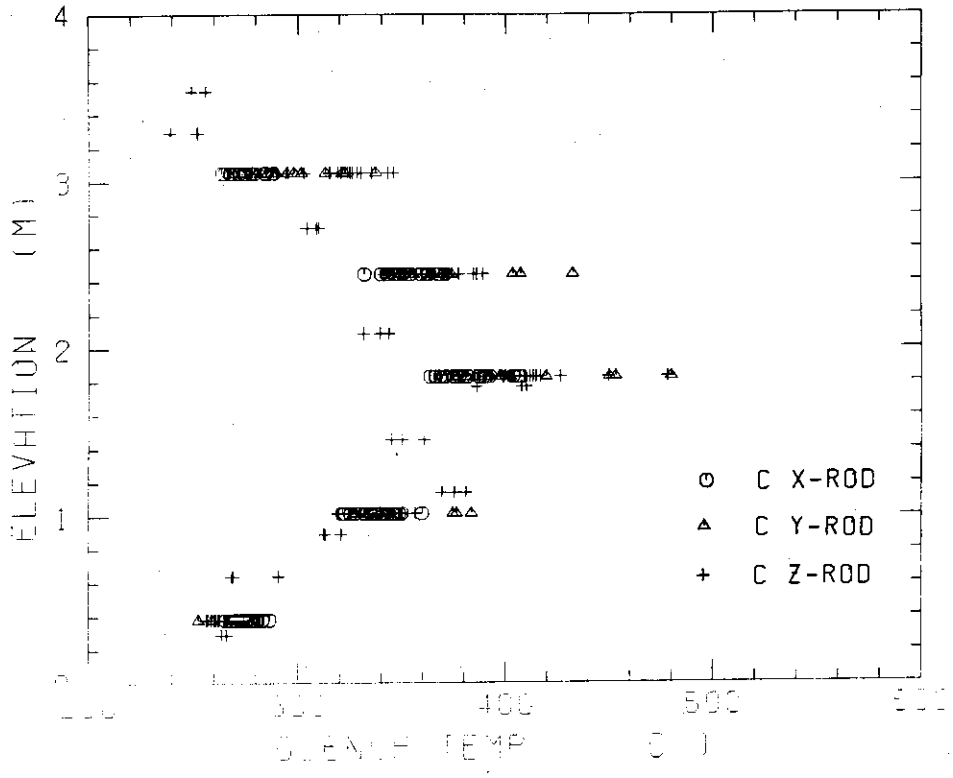

Fig. B-17 Quench temperature in low power region (C region)

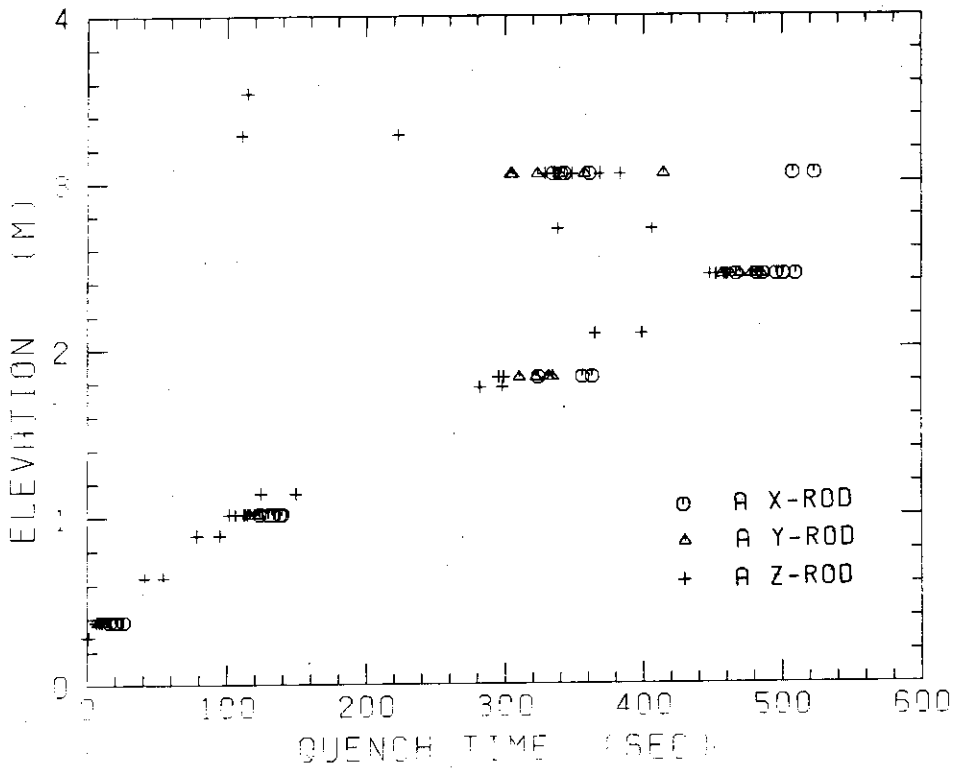

Fig. B-18 Quench time in high power region (A region)

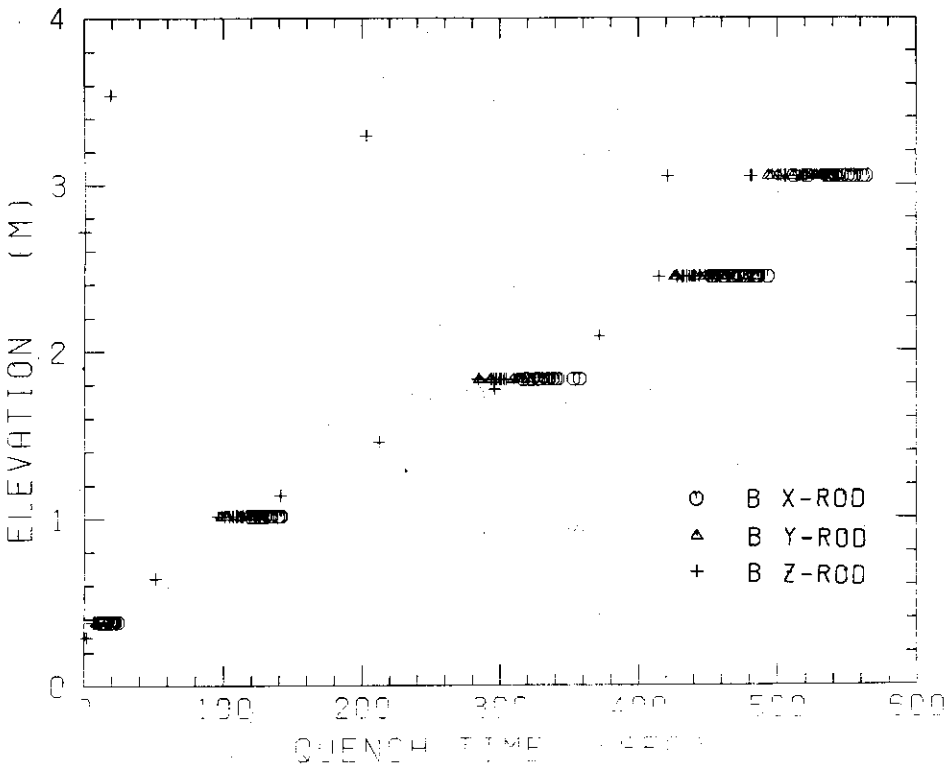

Fig. B-19 Quench time in medium power region (B region)

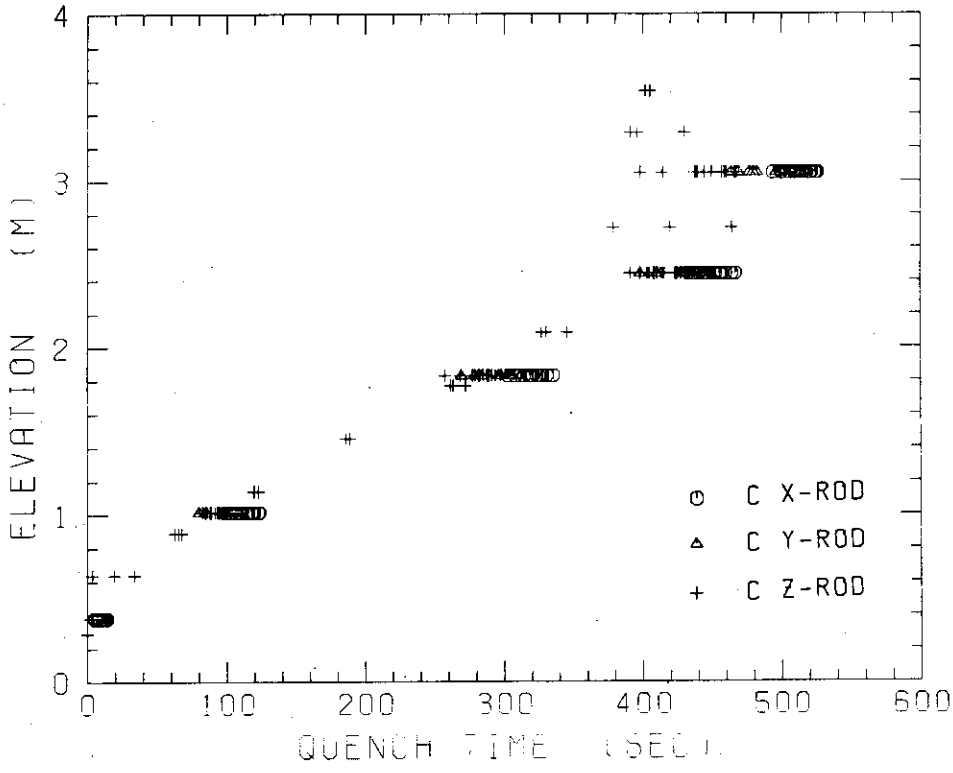

Fig. B-20 Quench time in low power region (C region)

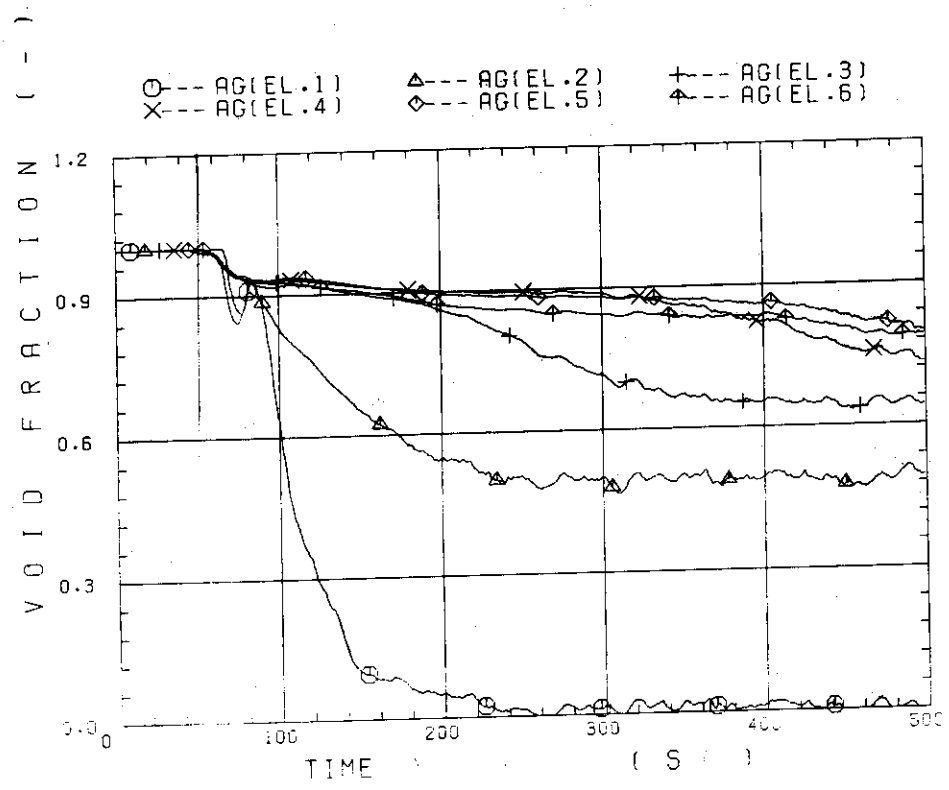

Fig. B-21 Void fraction in core

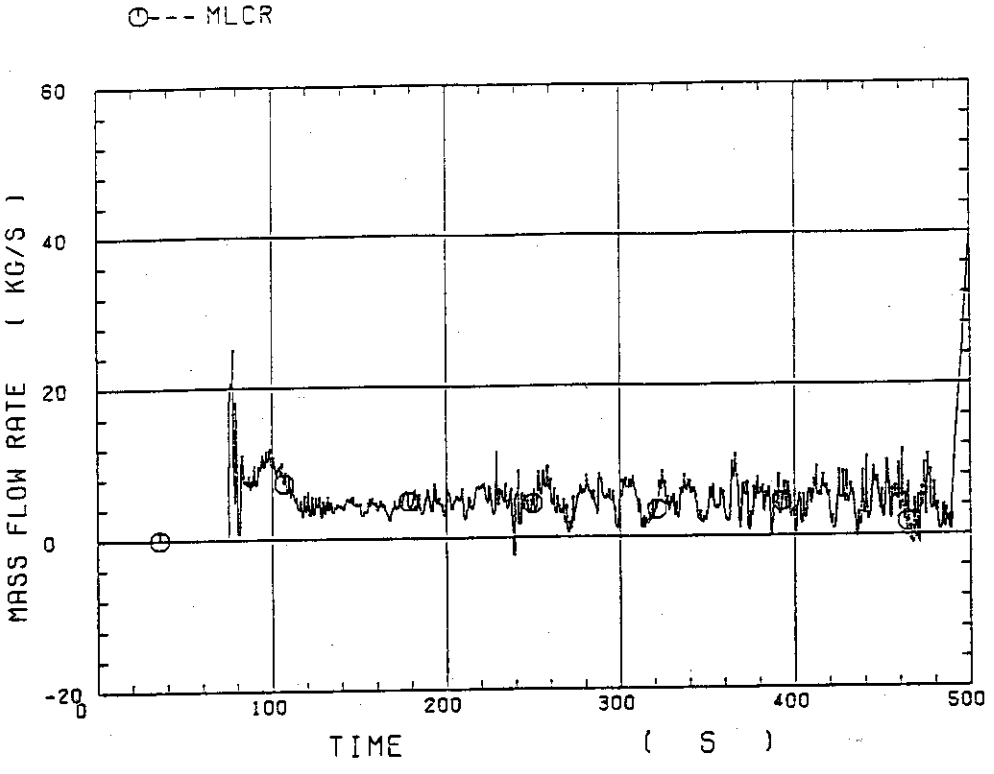

Fig. B-22 Core inlet mass flow rate

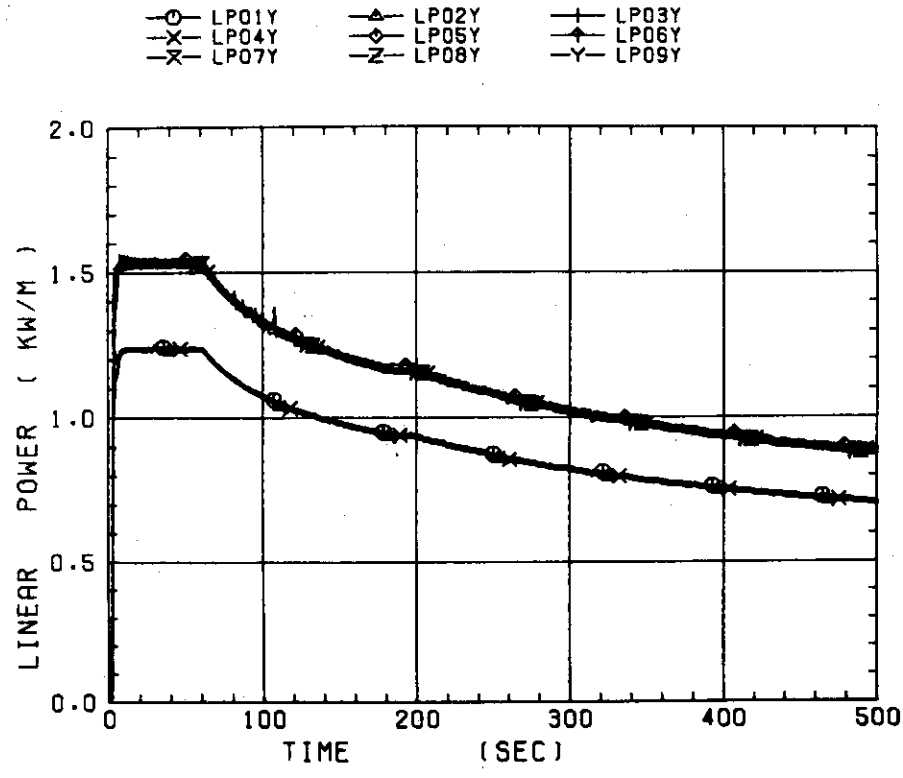

Fig. B-23 Average linear power of heater rod in each power unit zone

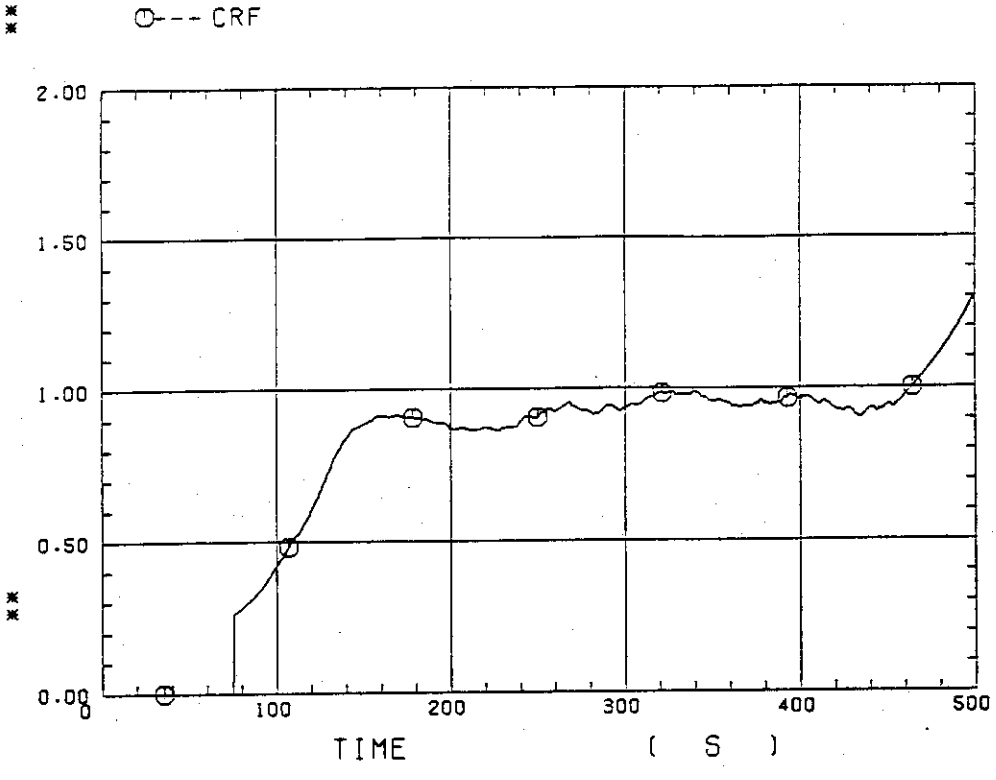

Fig. B-24 Carry-over rate fraction

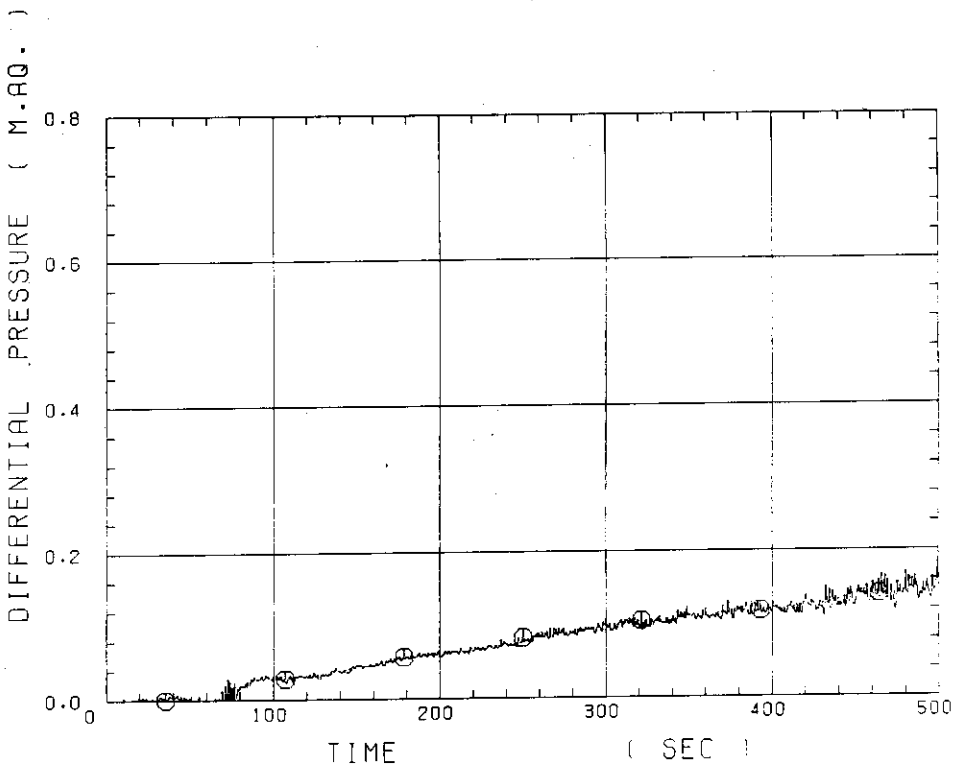

Fig. B-25 Differential pressure through upper plenum

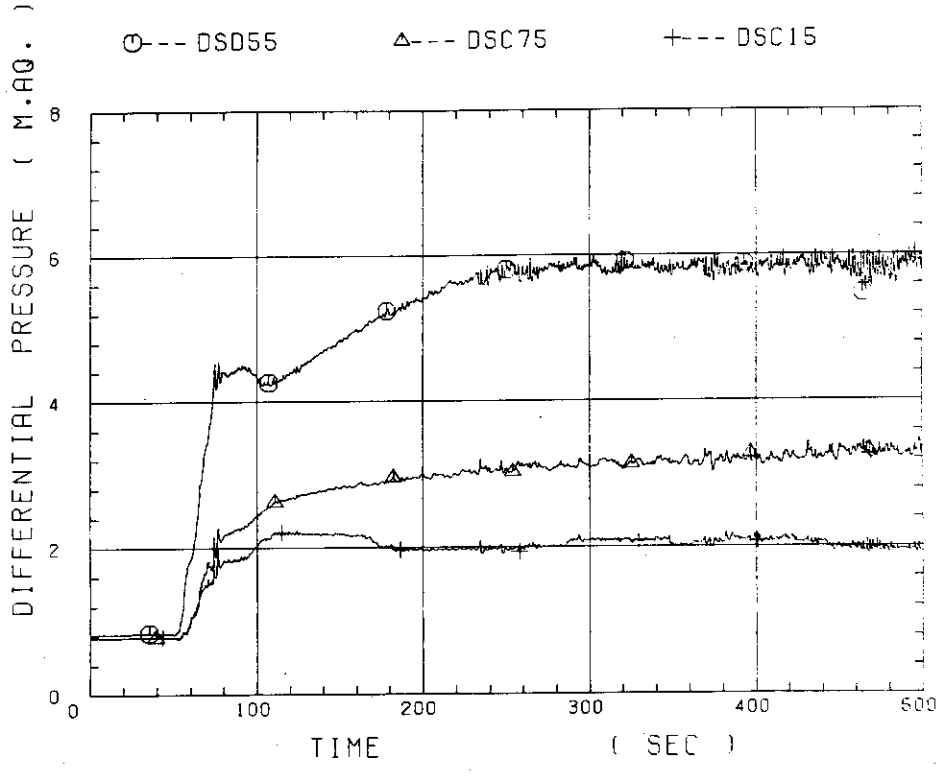

Fig. B-26 Differential pressure through downcomer, core, and lower plenum

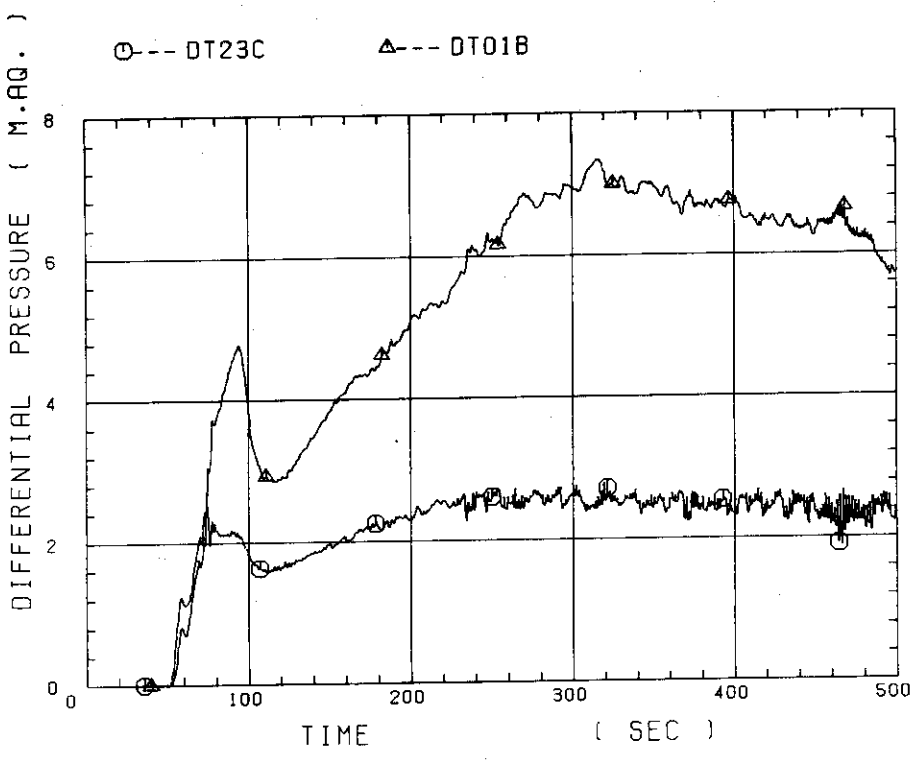

Fig. B-27 Differential pressure through intact and broken loops

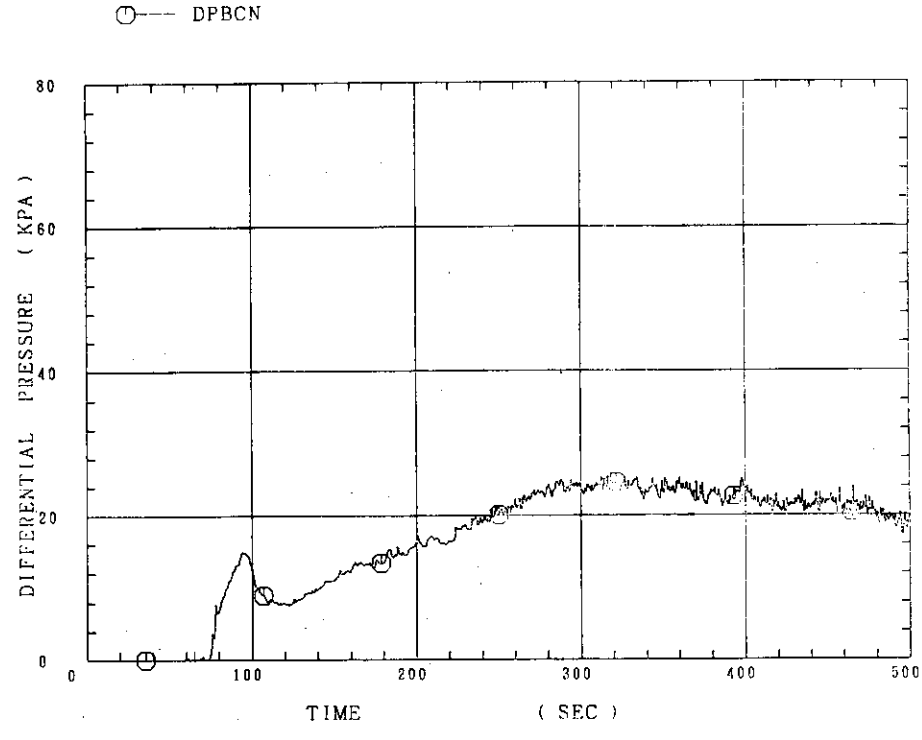

Fig. B-28 Differential pressure through broken cold leg nozzle

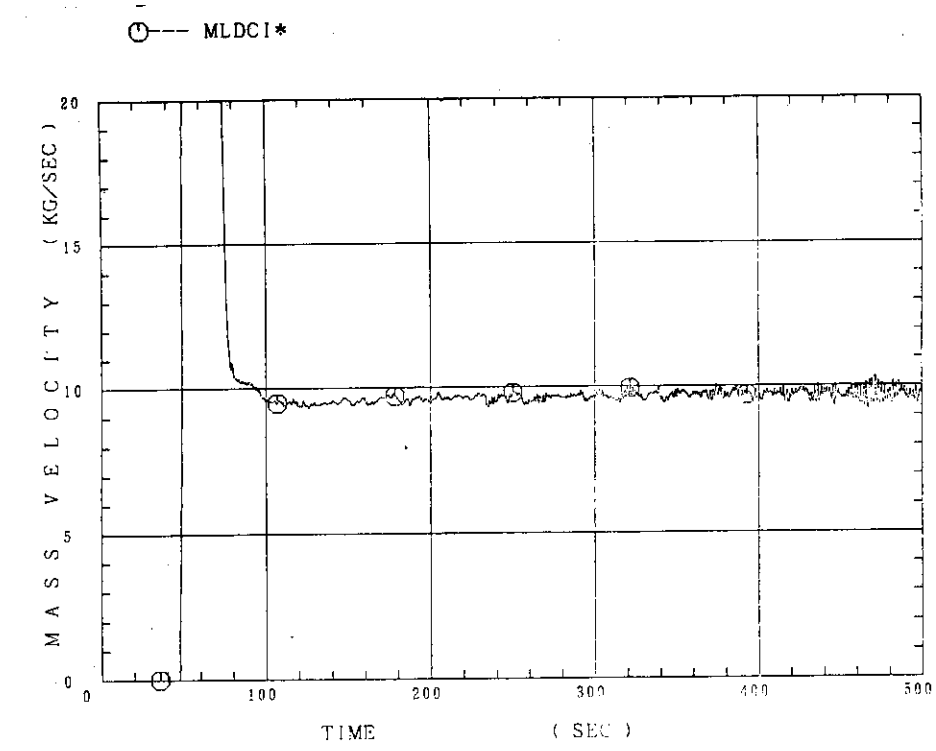

Fig. B-29 Total water mass flow rate from intact loops to downcomer

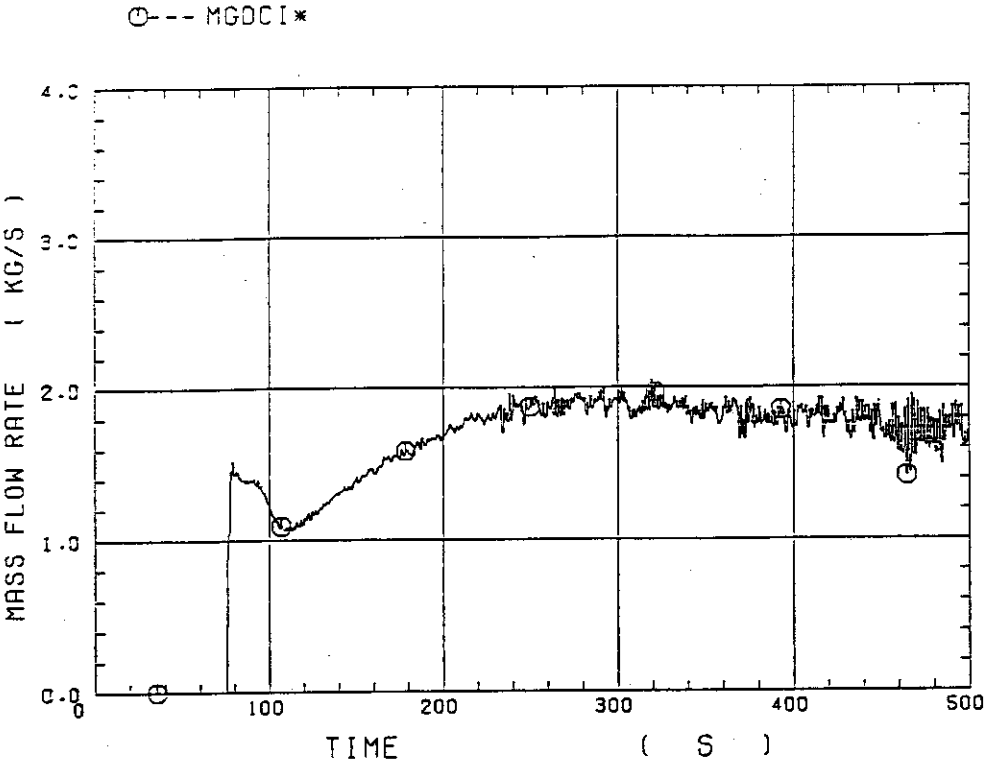

Fig. B-30 Total steam mass flow rate from intact loops to downcomer

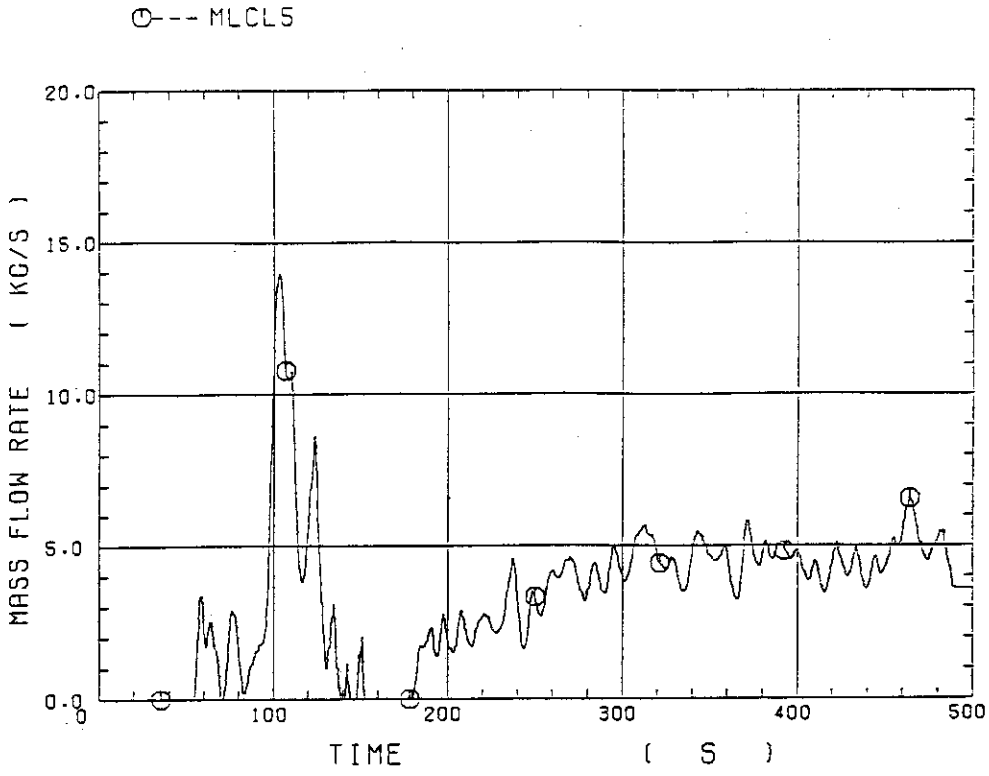

Fig. B-31 Water mass flow rate through broken cold leg nozzle

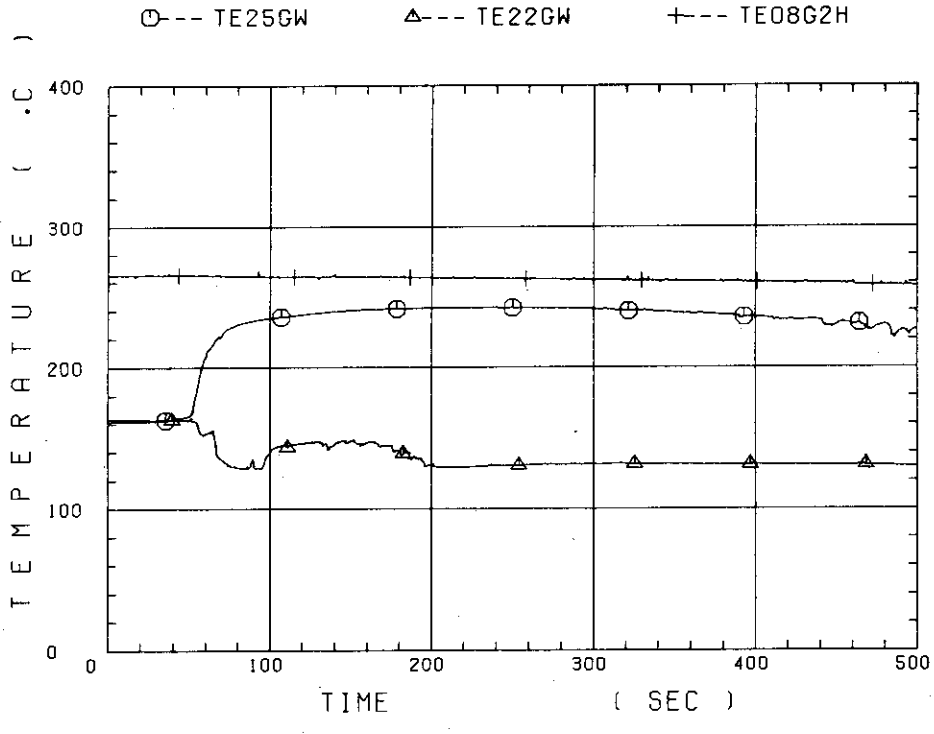

Fig. B-32 Fluid temperature in inlet plenum, outlet plenum, and secondary of steam generator 1

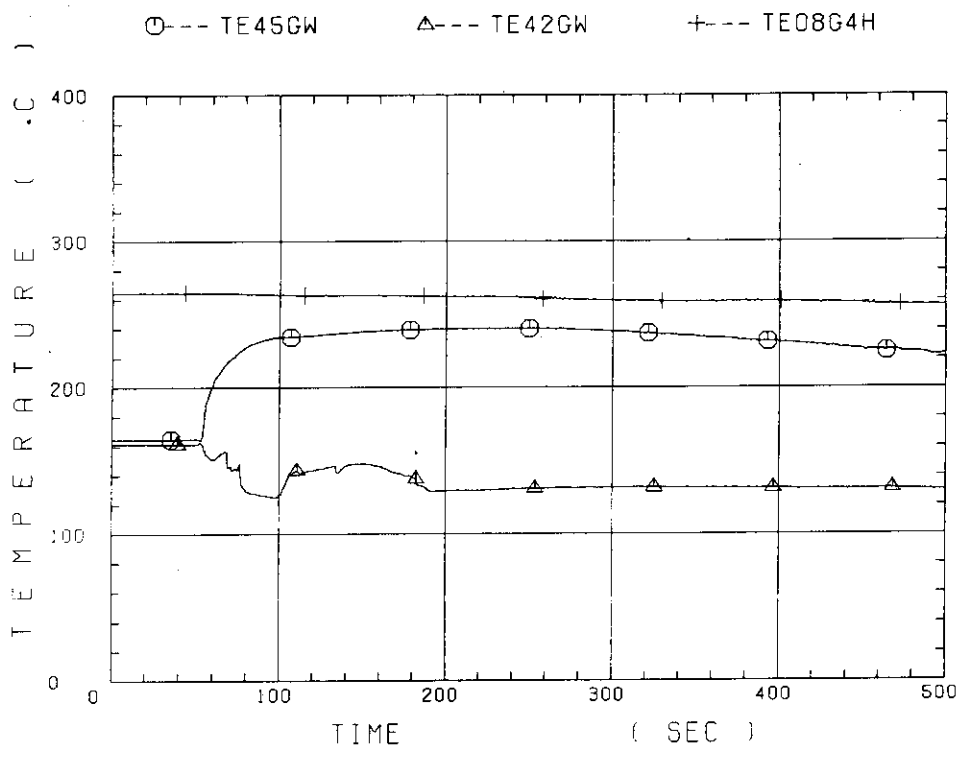

Fig. B-33 Fluid temperature in inlet plenum, output plenum, and secondary of steam generator 2

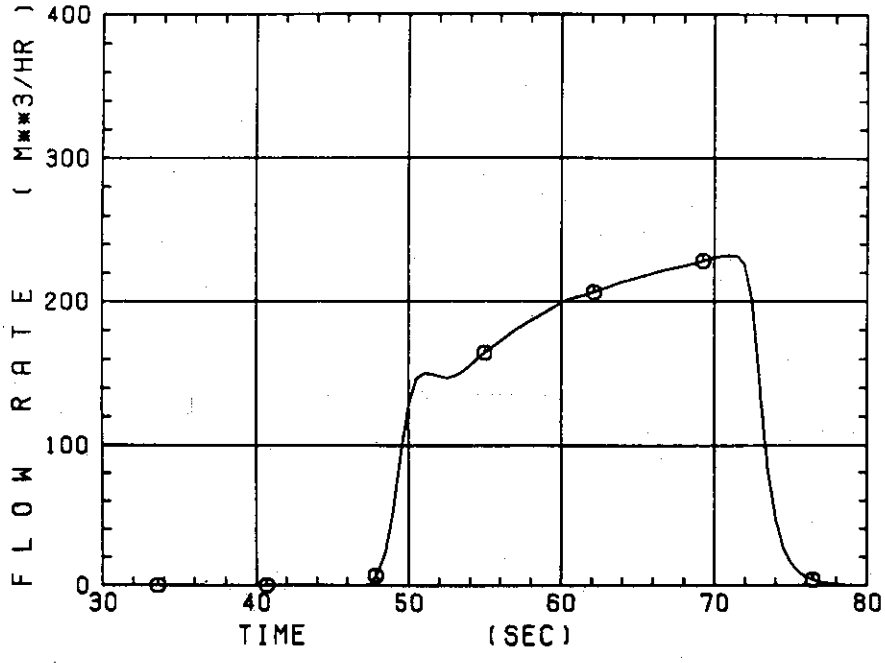

Fig. B-34 Total accumulator injection rate

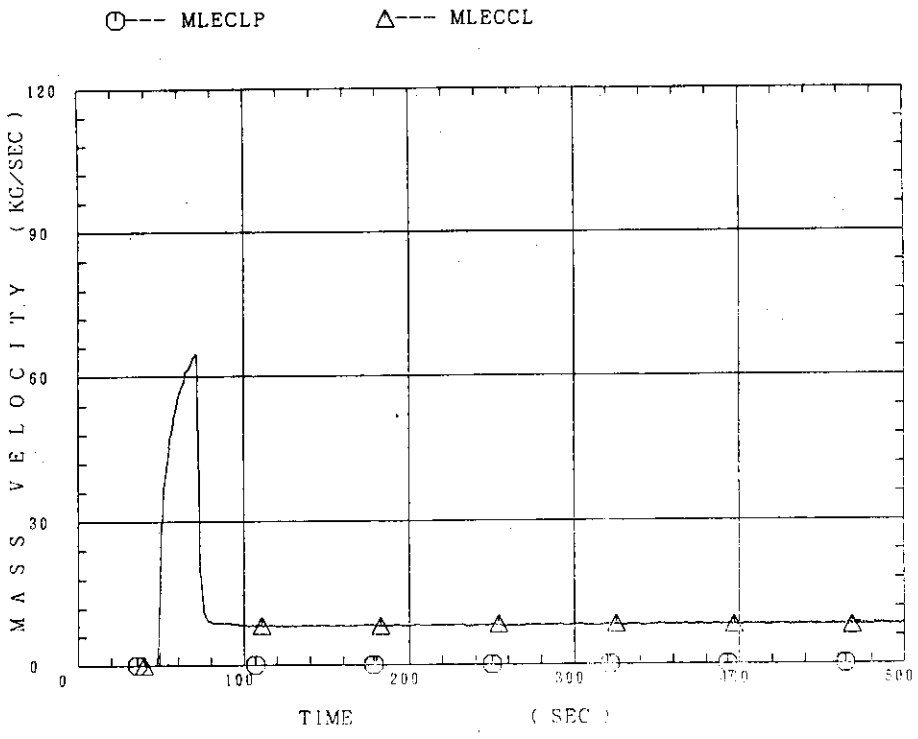

Fig. B-35 ECC water injection rates to lower plenum and to cold legs

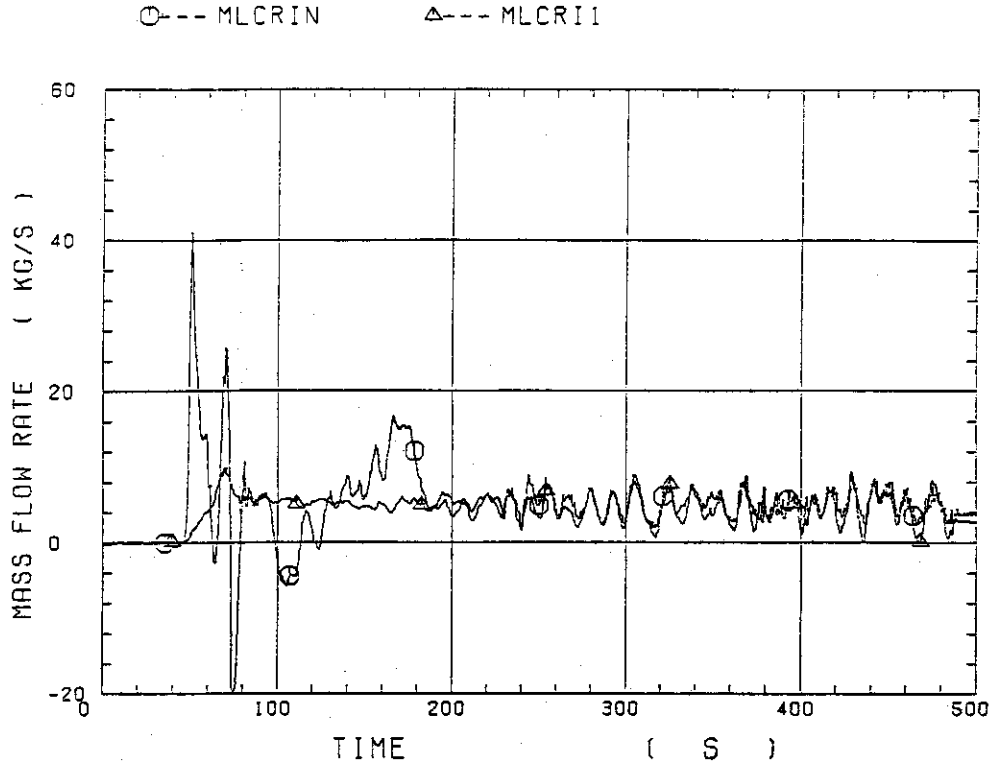

Fig. B-36 Core inlet mass flow rates estimated by mass balance downstream and upstread of core inlet

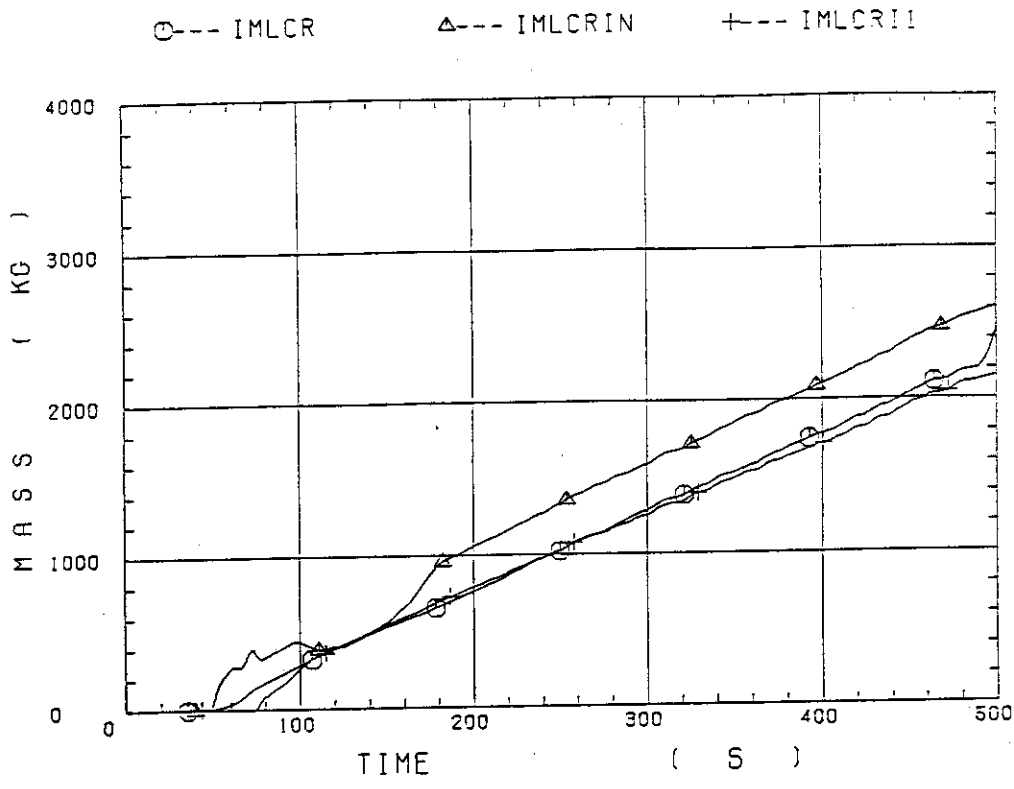

Fig. B-37 Comparison of injected mass into core among two estimation methods and evaluated mass

Appendix C

Main results of Test C1-15 (Run 24)

Table and Figure List

Table C-1 Summary of test conditions

1. TEST TYPE : NITROGEN GAS INJECTION TEST

2. TEST NUMBER : RUN 024 3. DATE : Feb. 26, 1980

4. POWER : A: TOTAL: 9.40 MW; B:LINEAR: 1.4 KW/M

5. RELATIVE RADIAL POWER SHAPE :

   A: ZONE: A B C

   B: RATIO: 1.07 : 1.0 : 0.82

6. AXIAL POWER SHAPE : CHOPPED COSINE

7. PRESSURE (KG/CM^2A) :

   A: SYSTEM: 6.06 → 2.08, B: CONTAINMENT 6.06 → 2.08,

   C: STEAM GENERATOR SECONDARY: 54

8. TEMPERATURE (DEG.C) :

   A: DOWNCOMER WALL 175, B: VESSEL INTERNALS 158,

   C: PRIMARY PIPING WALL 157, D: LOWER PELNUM LIQUID 150,

   E: ECC LIQUID 40, F: STEAM GENERATOR SECONDARY 264,

   G: CORE TEMPERATURE AT ECC INITIATION 507

9. ECC INJECTION TYPE: A

   A: COLD LEG, B: LOWER PLENUM, C: LOWER PLENUM + COLD LEG

10. PUMP K-FACTOR : ~15

11. ECC FLOW RATES AND DURATION :

   A: ACCUMULATOR 237 M^3/HR FROM 0 TO 35.5 SECONDS

   B: LPCI 29.8 M^3/HR FROM 35.5 TO 81.7 SECONDS

   C: ECC INJECTION TO LOWER PLENUM : FROM ____ TO ____ SECONDS

   (VALVE OPENING AND CLOSING TIMES ARE INCLUDED IN THE INJECTION DURATION)

12. INITIAL WATER LEVEL IN LOWER PLENUM : 0.86 M.

13. POWER CONTROL : ANS x 1.2 + ACTINIDE (30 SEC AFTER SCRAM)

14. EXPECTED BOCREC TIME FROM ECC INITIATION 13 SEC

15. EXPECTED PEAK TEMPERATURE AT BOCREC 600 C

Table C-2 Chronology of events

EVENT	TIME (sec)
Test Initiated (Heater Rods Power on) (Data Recording Initiated)	0
Accumulator Injection Initiated	47
Power Decay Initiated (Bottom of Core Recovery)	81
Accumulator Injection Switched from Lower Plenum to Cold Leg	———
Accumulator Injection Ended and LPCI Injection Initiated	82.5
All Heater Rods Quenched	628
Power Off	683
LPCI Injection Ended	864
Test Ended (Data Recording Ended)	1137

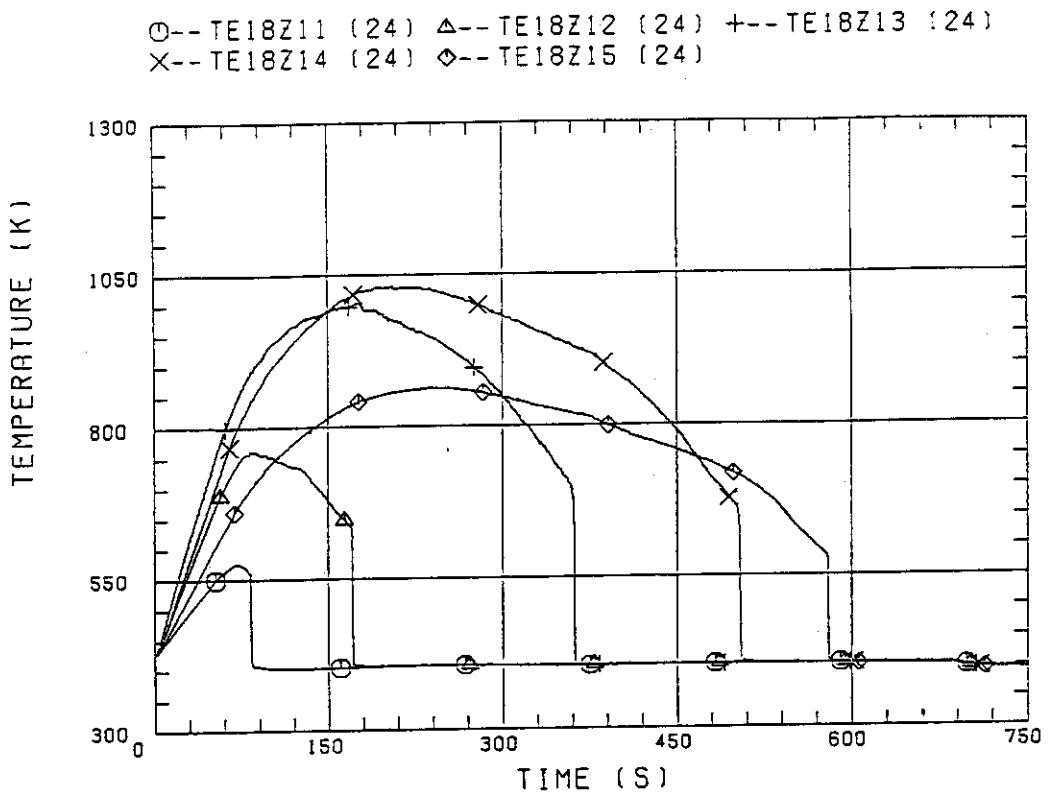

Fig. C-1 Surface temperature on low power rod (Z-rod) in medium power region (B region) (average power rod)

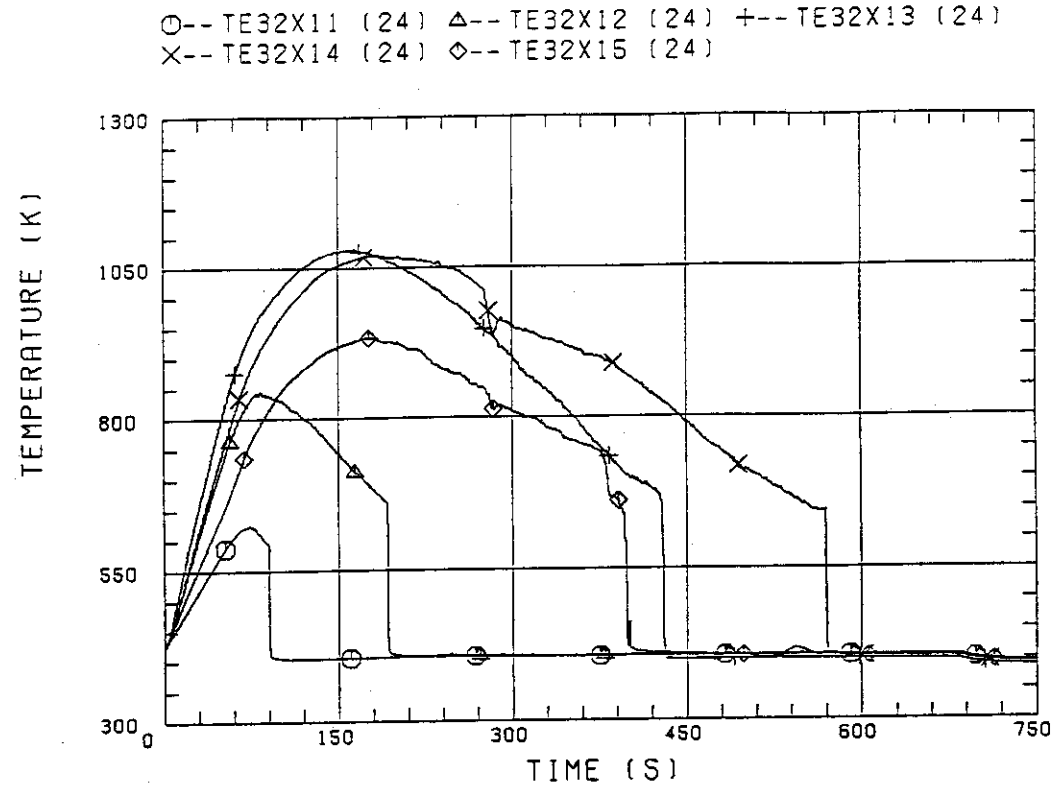

Fig. C-2 Surface temperature on high power rod (X-rod) in high power region (A region) (peak power rod)

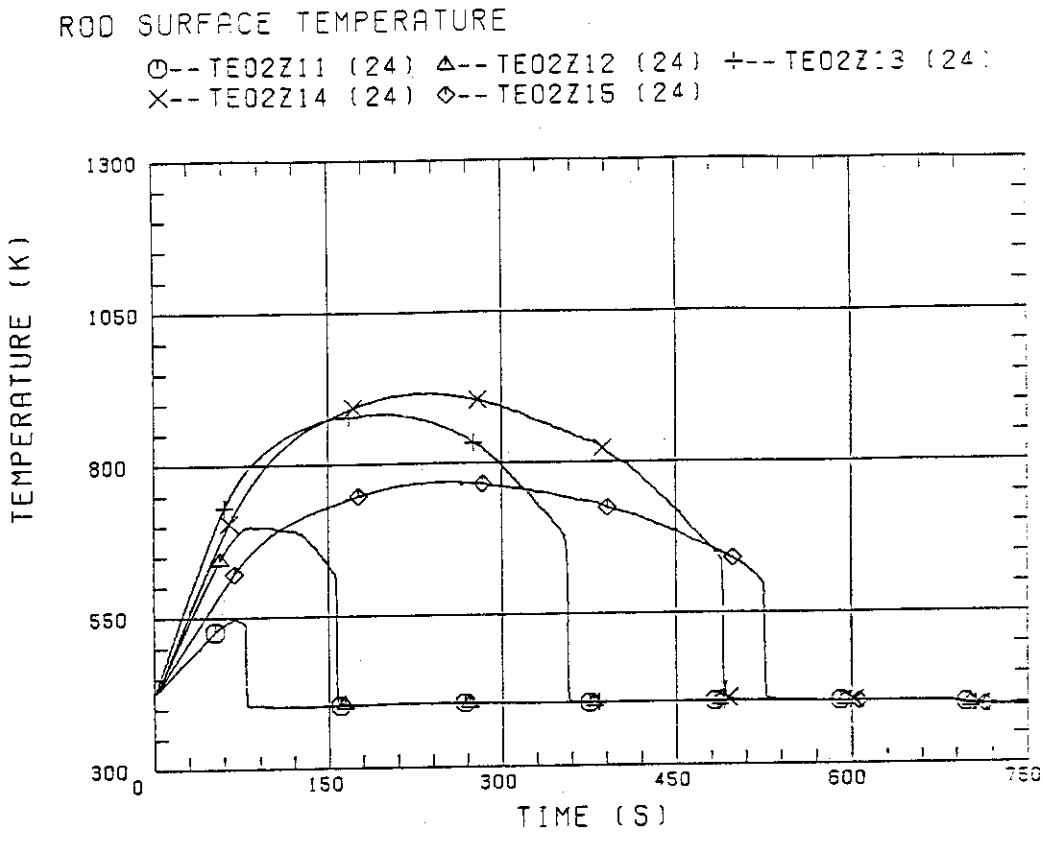

Fig. C-3 Surface temperature on low power rod (Z-rod) in low power region (C region) (lowest power rod)

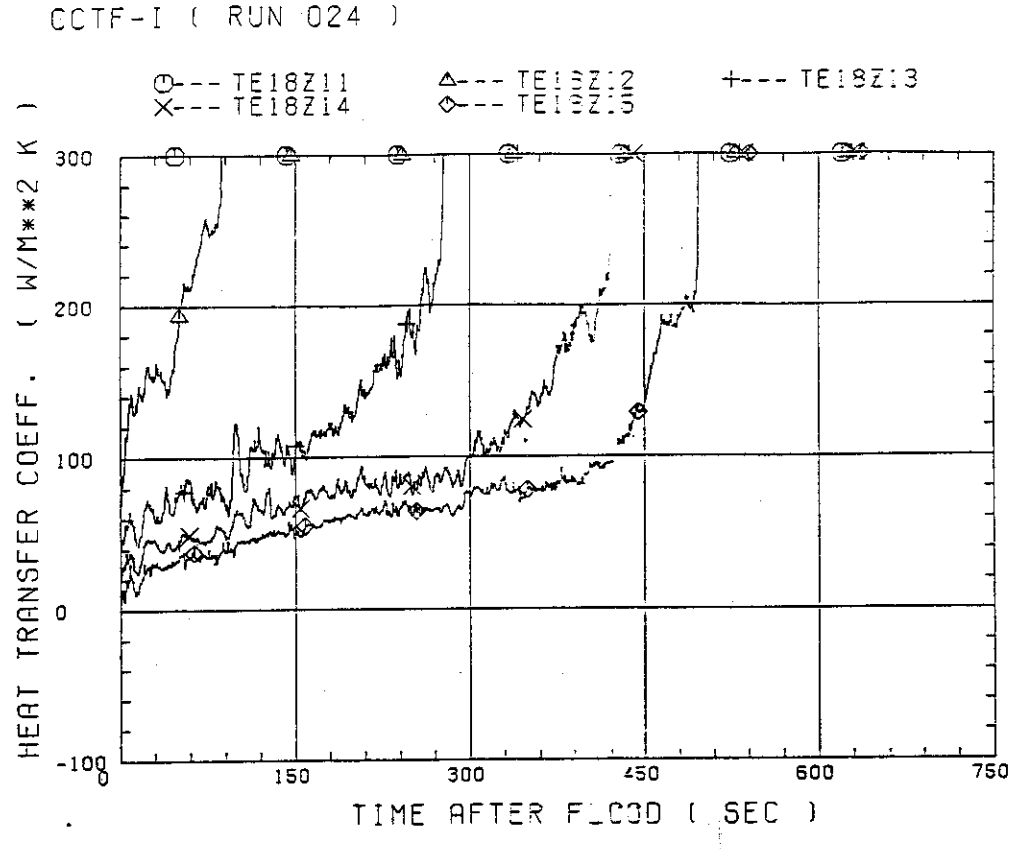

Fig. C-4 Heat transfer coefficient at midplane of low power rod (Z-rod) in medium power region (B region) (average power rod)

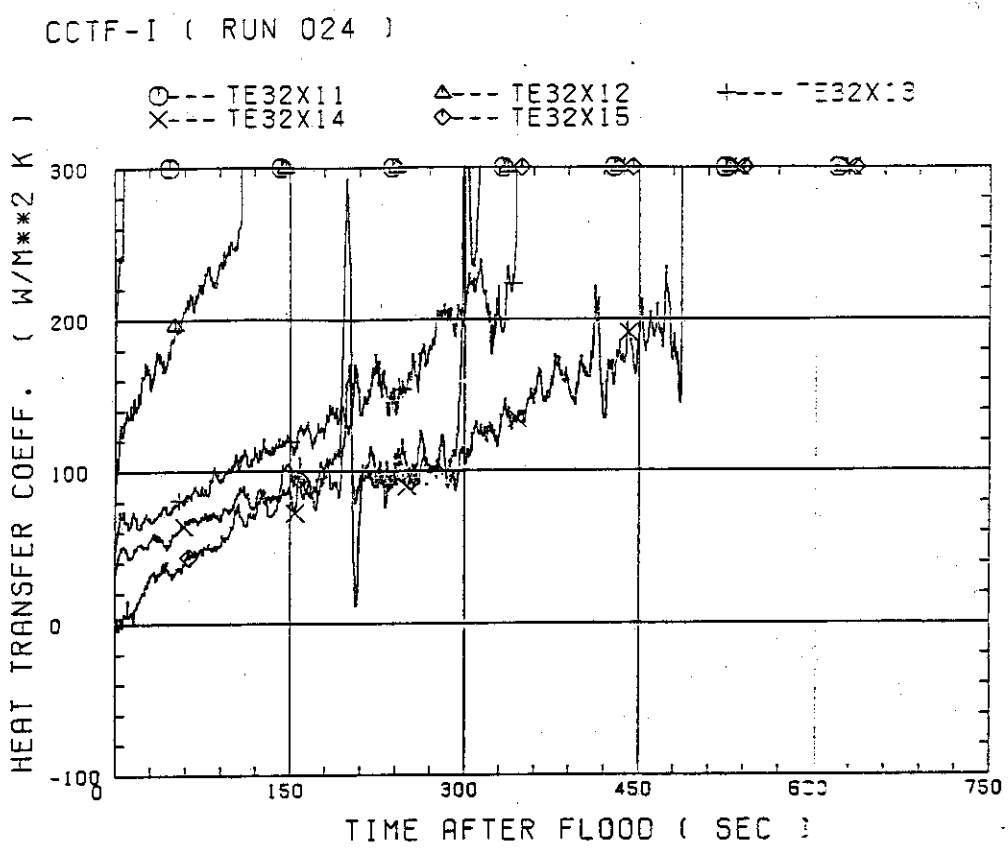

Fig. C-5 Heat transfer coefficient at midplane of high power rod (X-rod) in high power region (A region) (peak power rod)

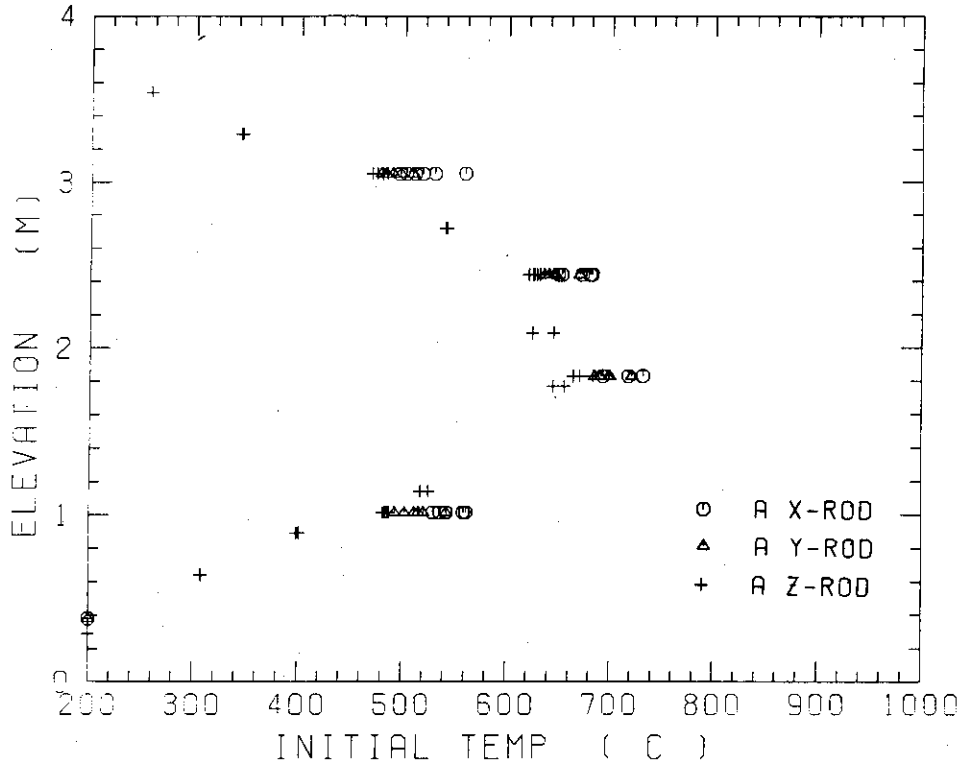

Fig. C-6 Initial rod surface temperature in high power region (A region)

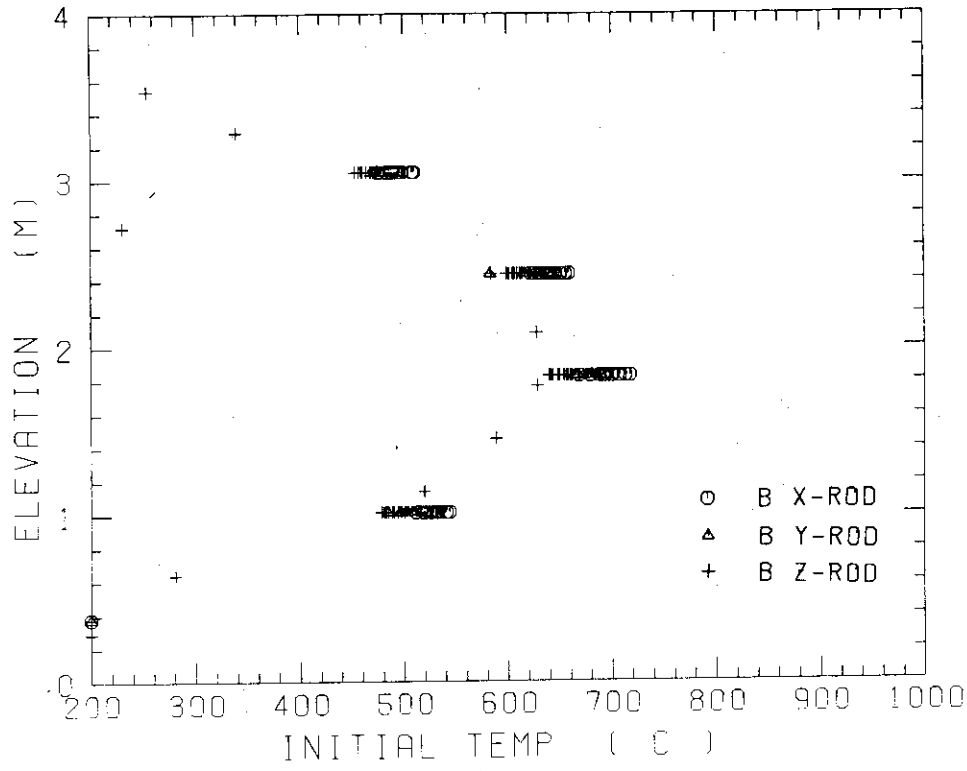

Fig. C-7 Initial rod surface temperature in medium power region (B region)

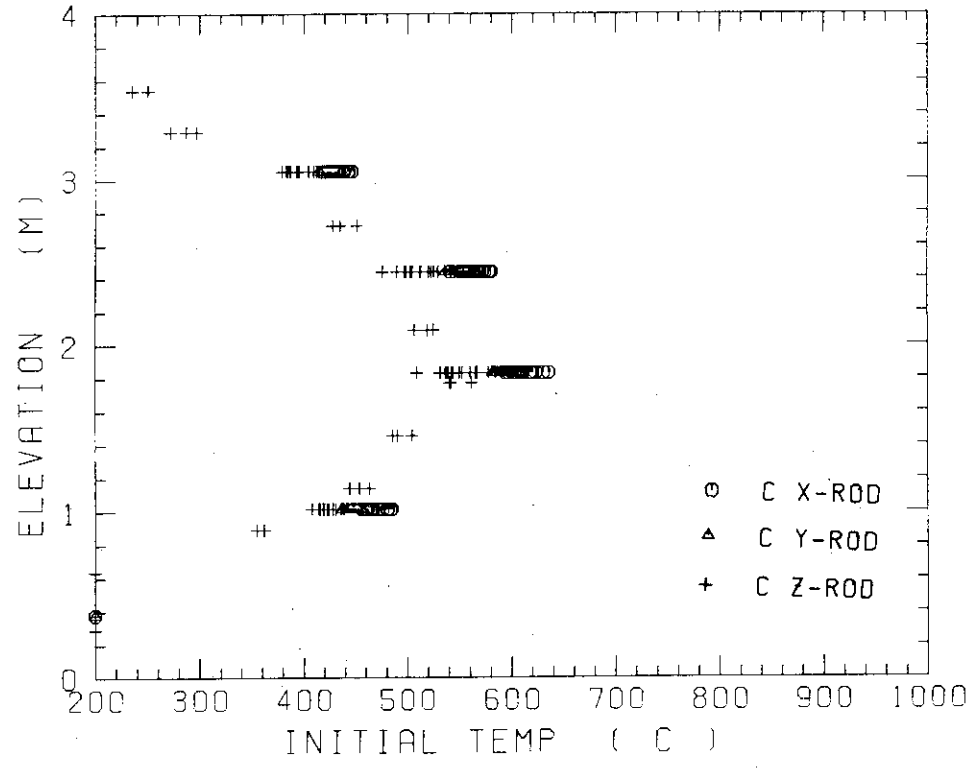

Fig. C-8 Initial rod surface temperature in low power region (C region)

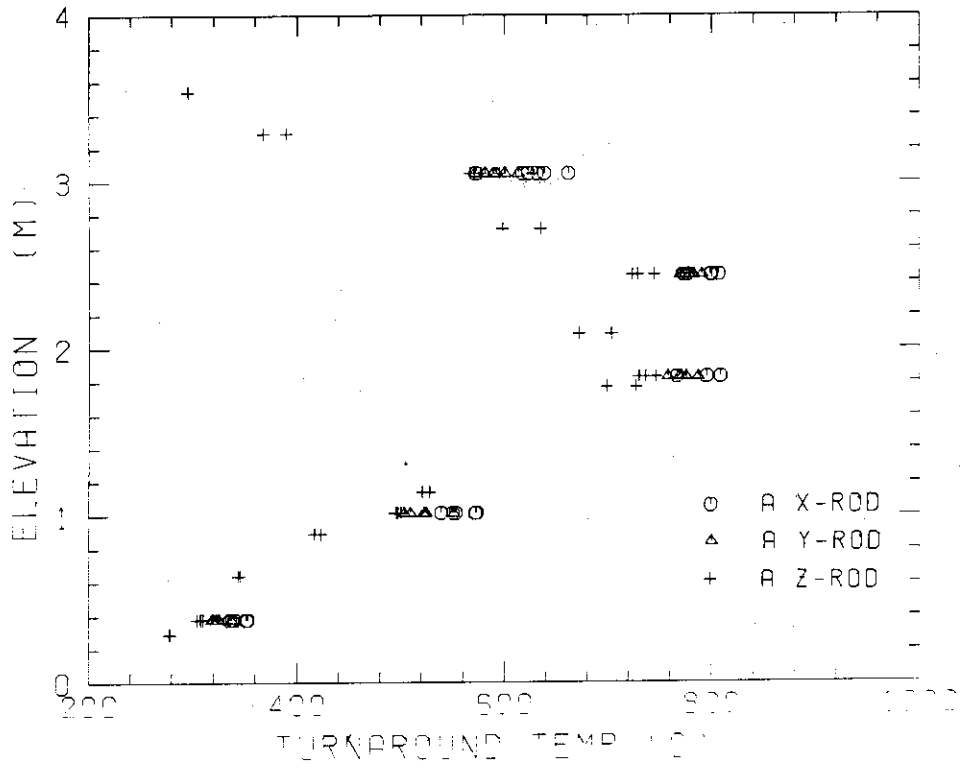

Fig. C-9 Turnaround temperature in high power region (A region)

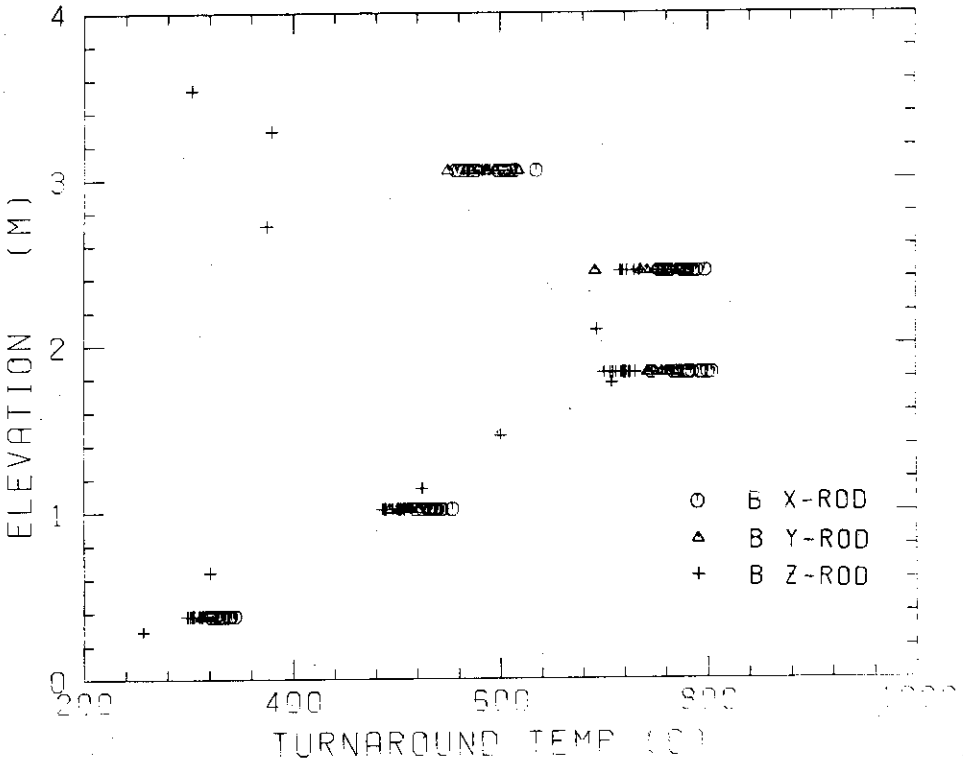

Fig. C-10 Turnaround temperature in medium power region (B region)

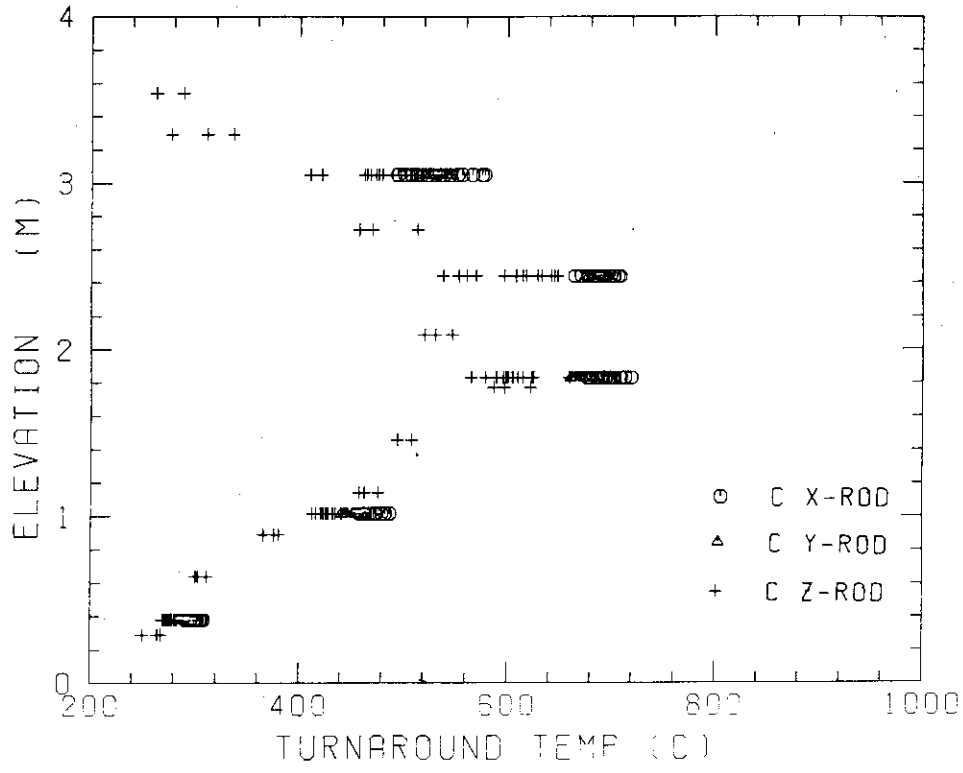

Fig. C-11 Turnaround temperature in low power region (C region)

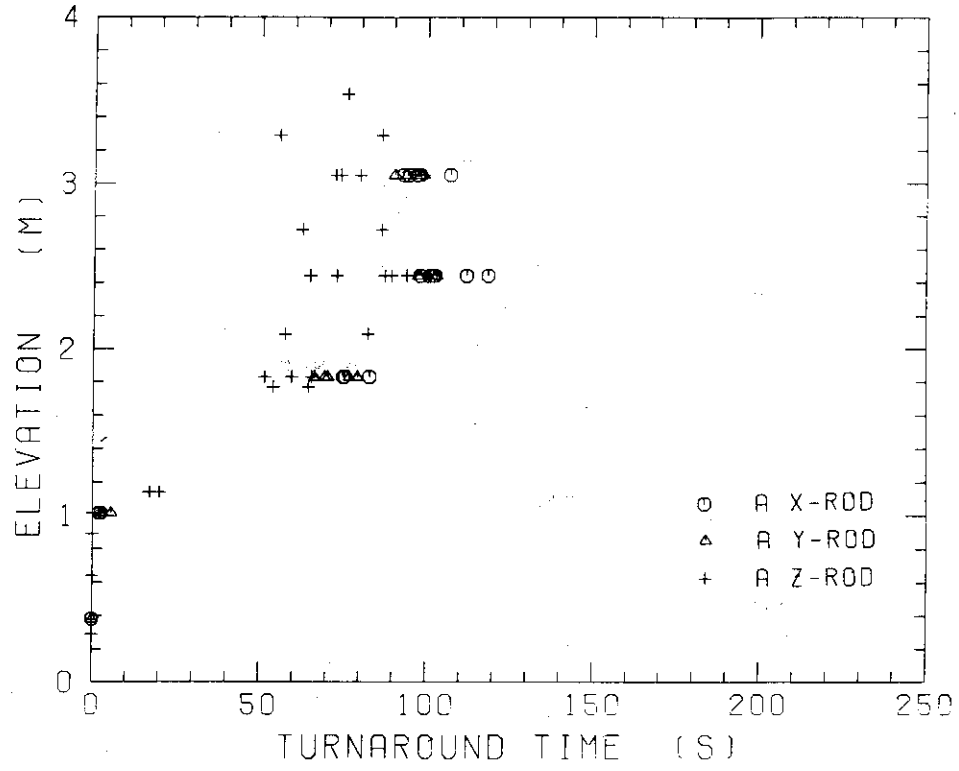

Fig. C-12 Turnaround time in high power region (A region)

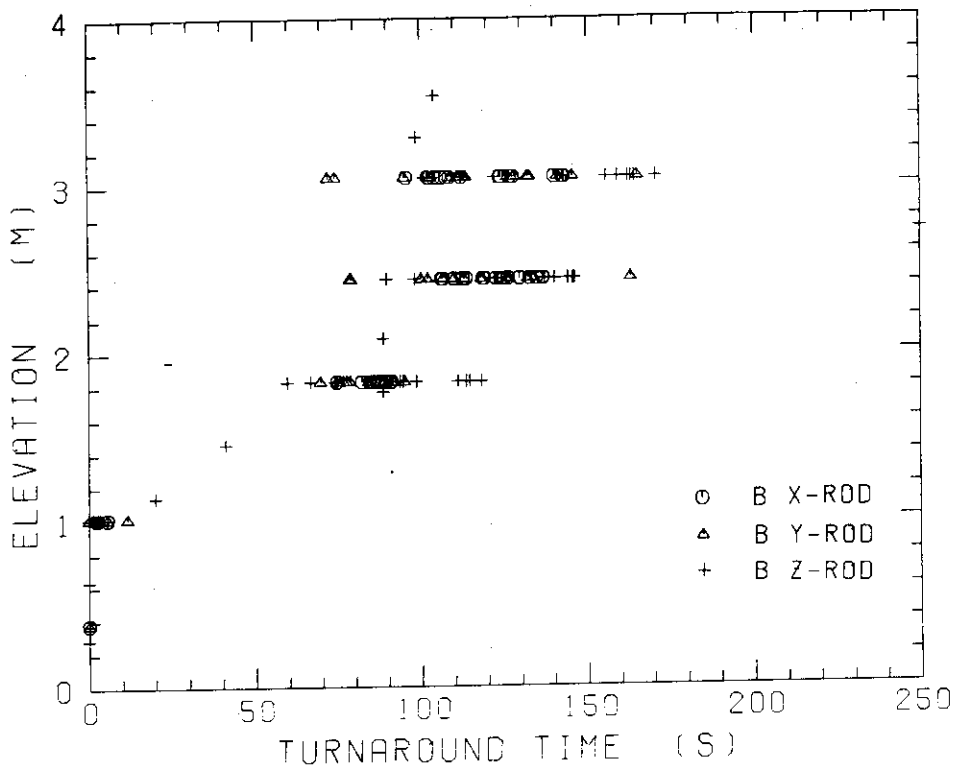

Fig. C-13 Turnaround time in medium power region (B region)

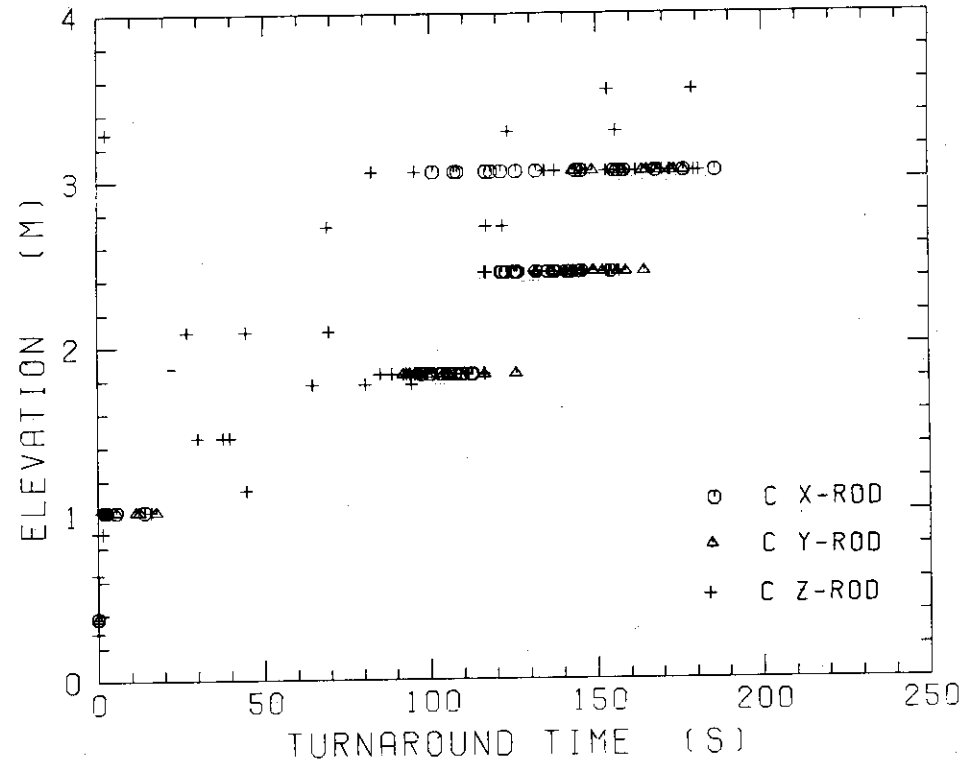

Fig. C-14 Turnaround time in low power region (C region)

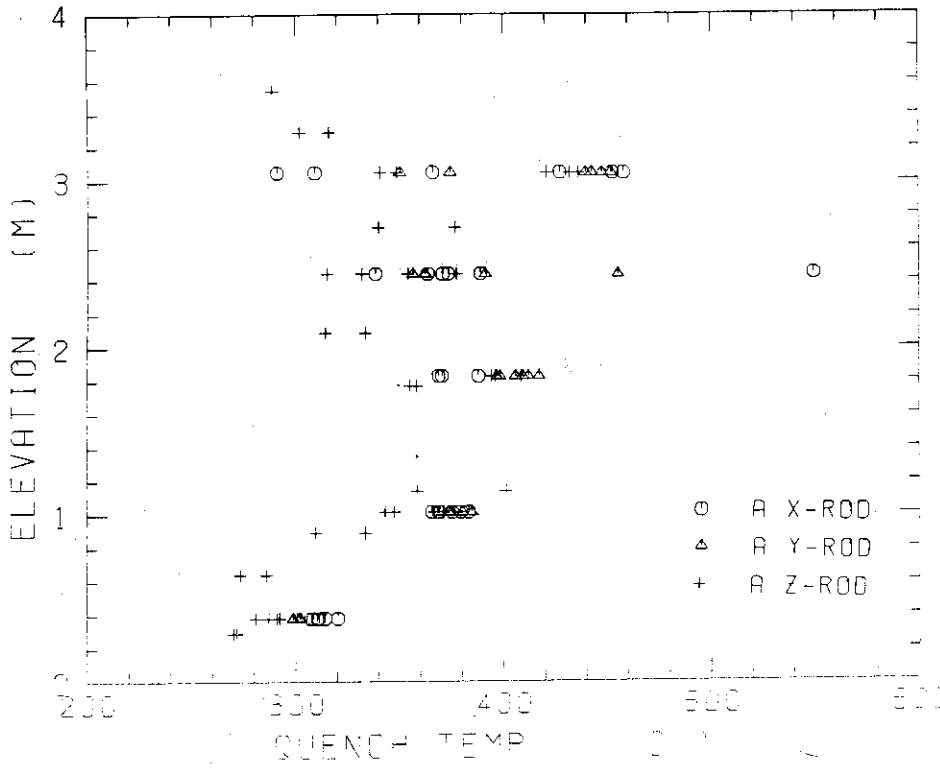

Fig. C-15 Quench temperature in high power region (A region)

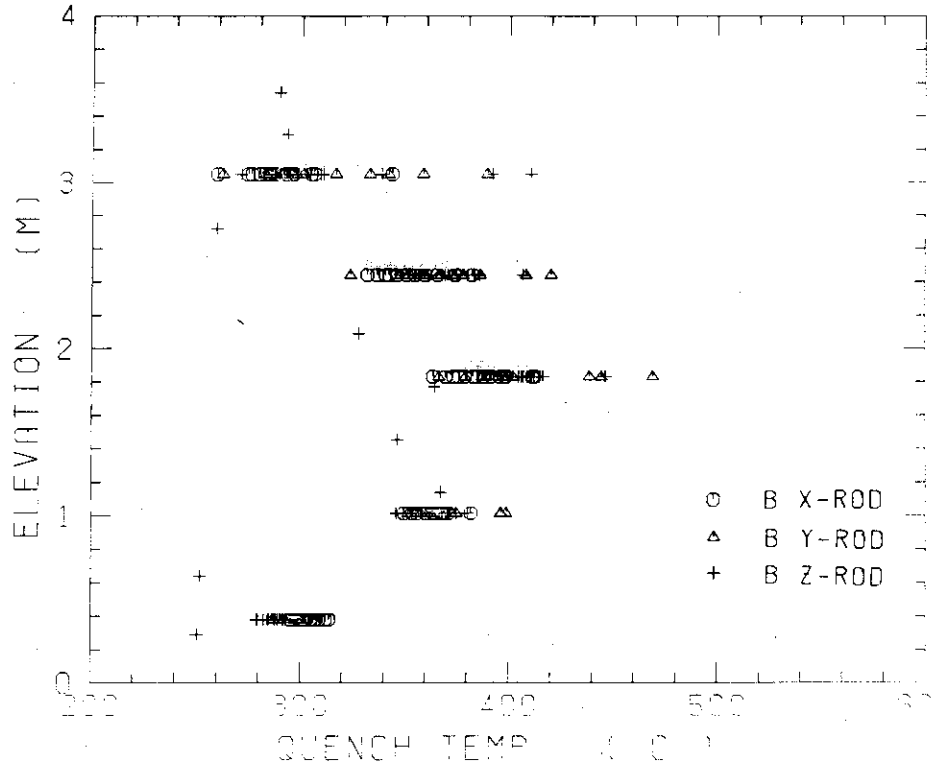

Fig. C-16 Quench temperature in medium power region (B region)

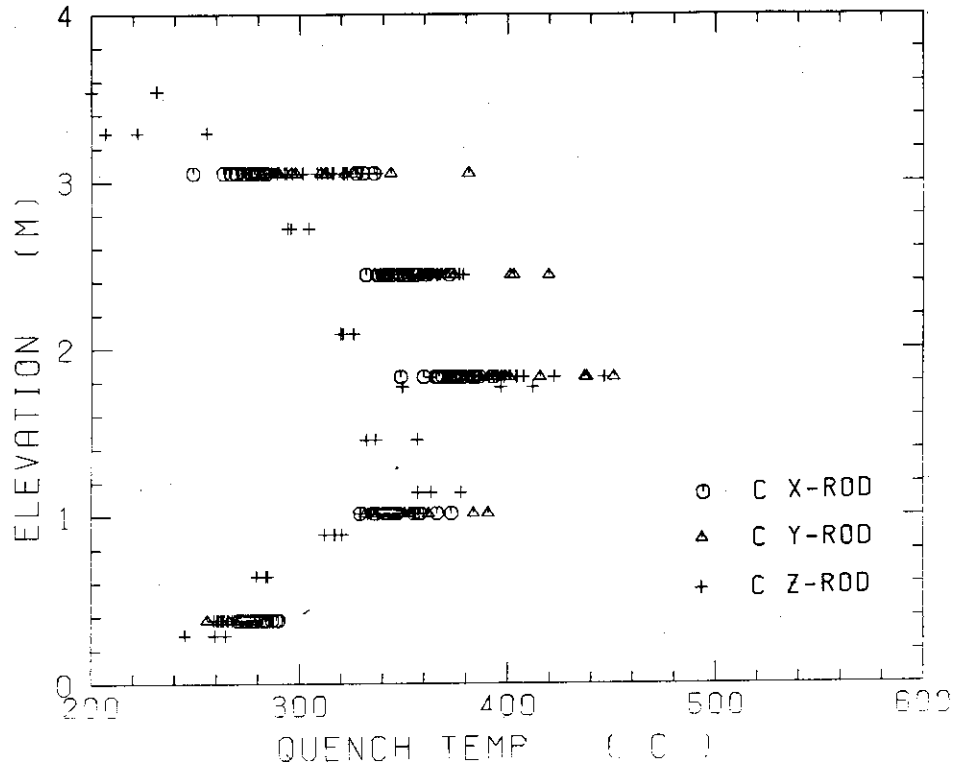

Fig. C-17 Quench temperature in low power region (C region)

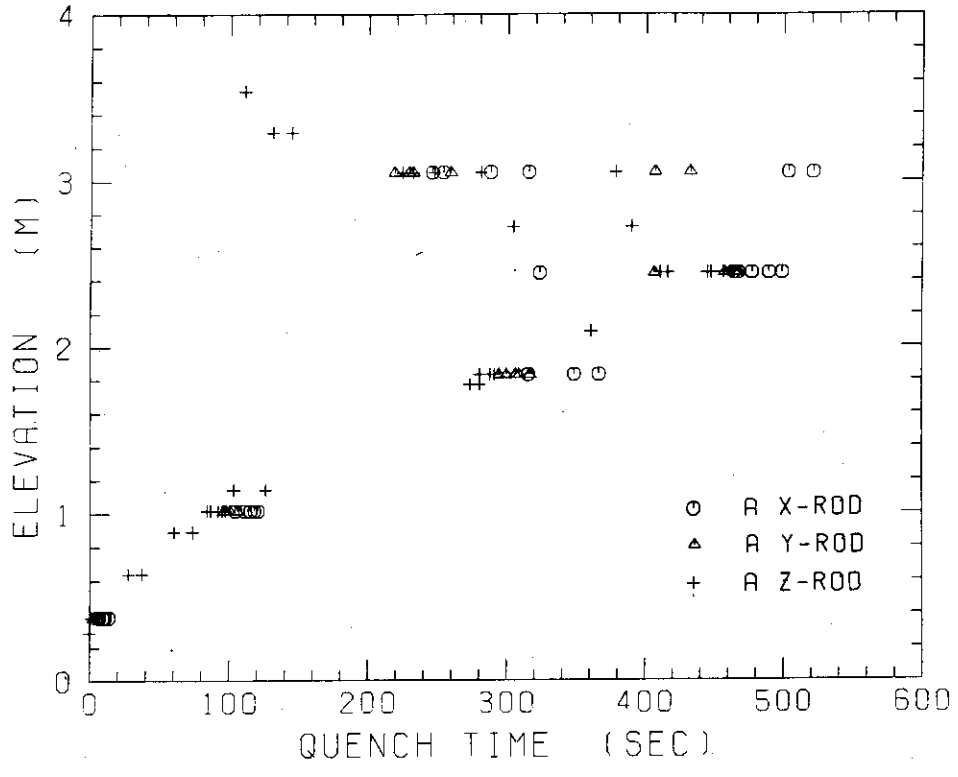

Fig. C-18 Quench time in high power region (A region)

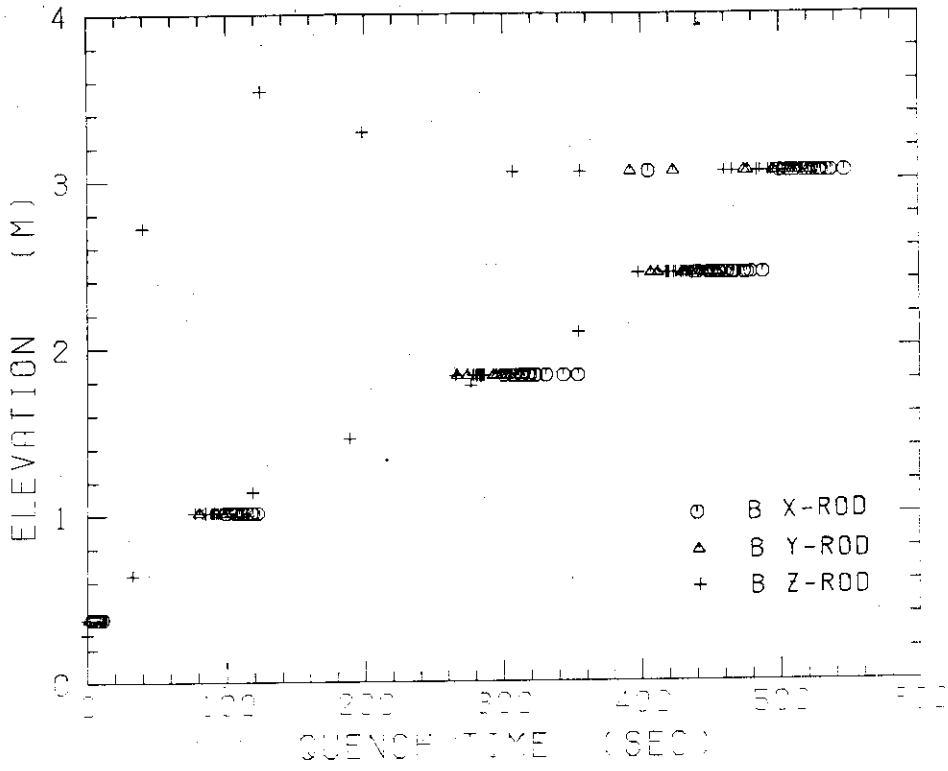

Fig. C-19 Quench time in medium power region (B region)

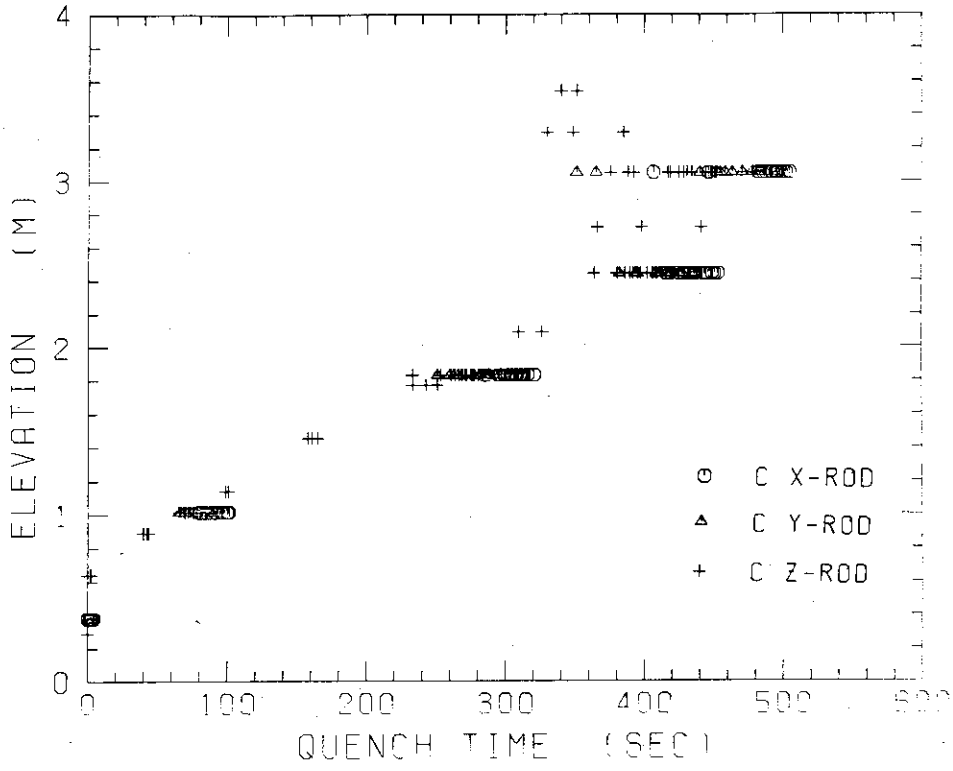

Fig. C-20 Quench time in low power region (C region)

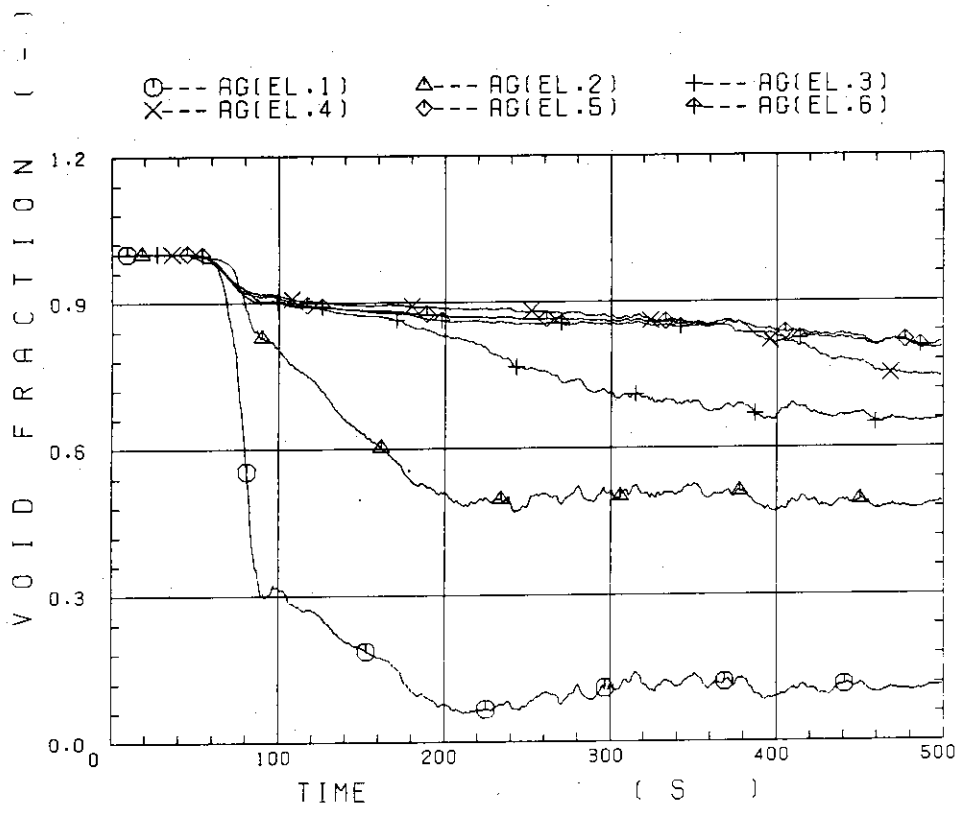

Fig. C-21 Void fraction in core

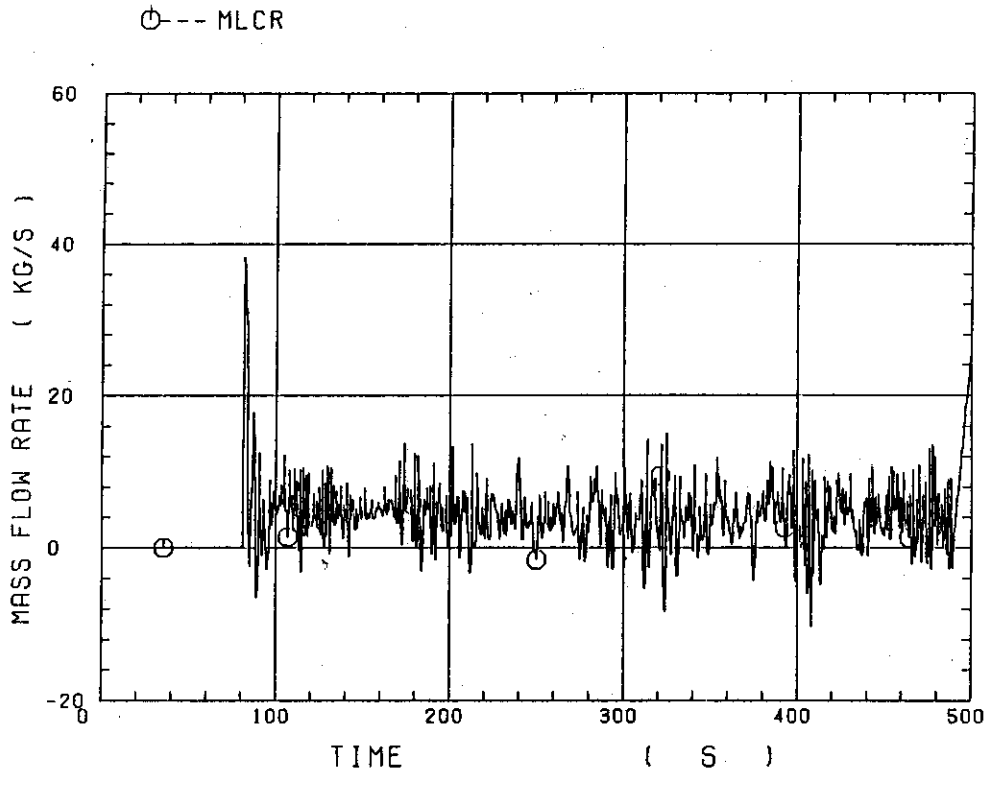

Fig. C-22 Core inlet mass flow rate

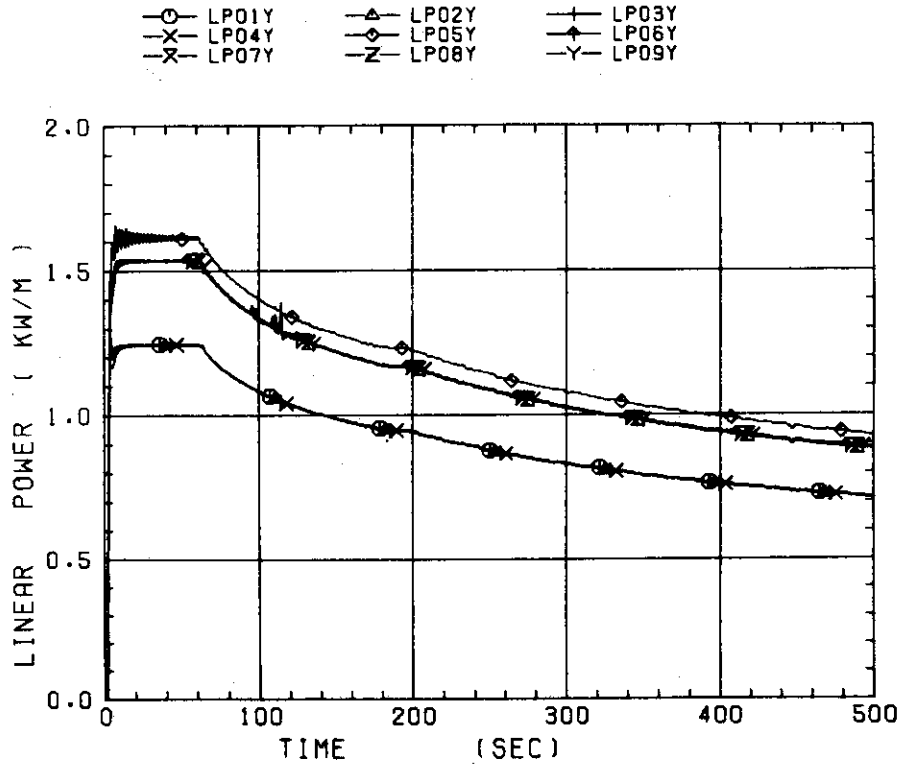

Fig. C-23 Average linear power of heater rod in each power unit zone

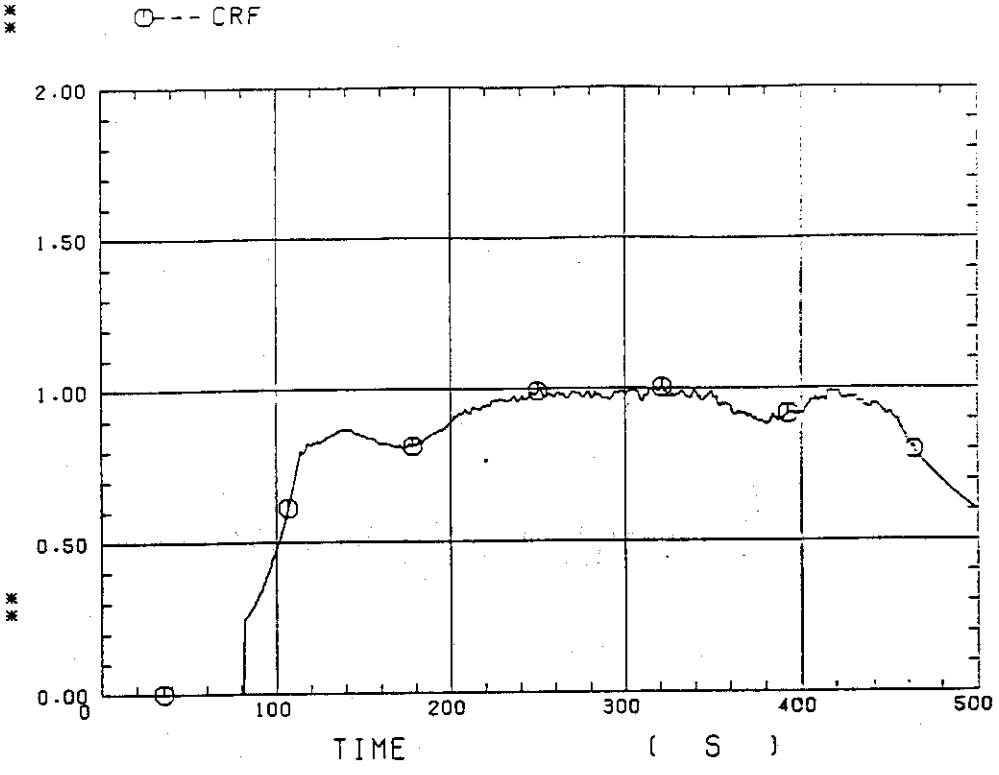

Fig. C-24 Carry-over rate fraction

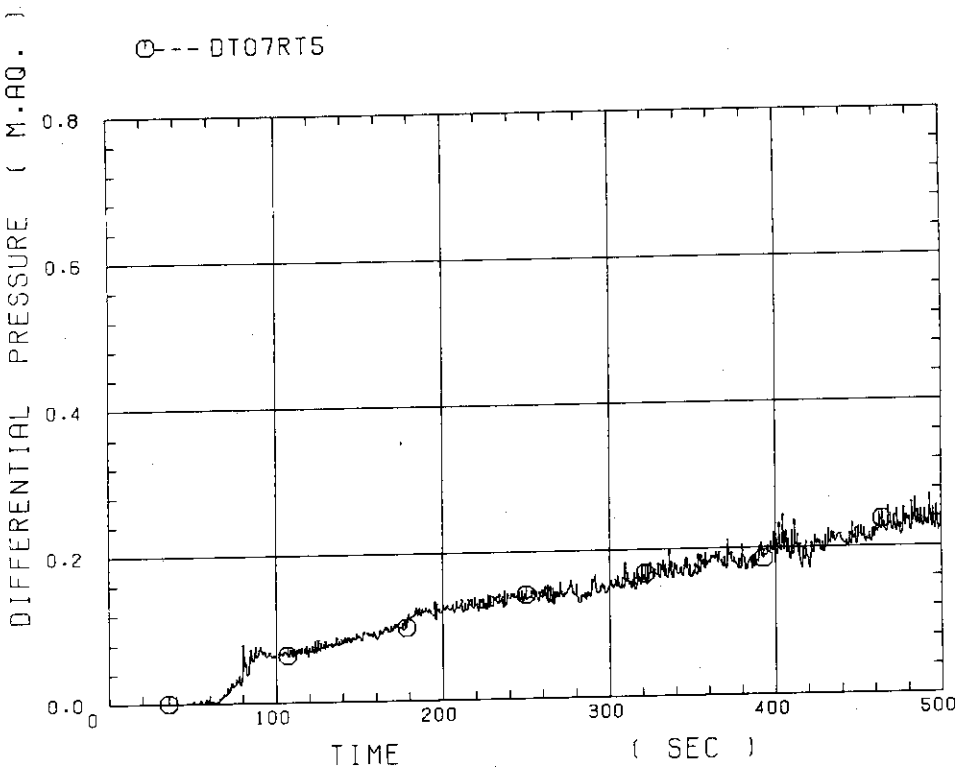

Fig. C-25 Differential pressure through upper plenum

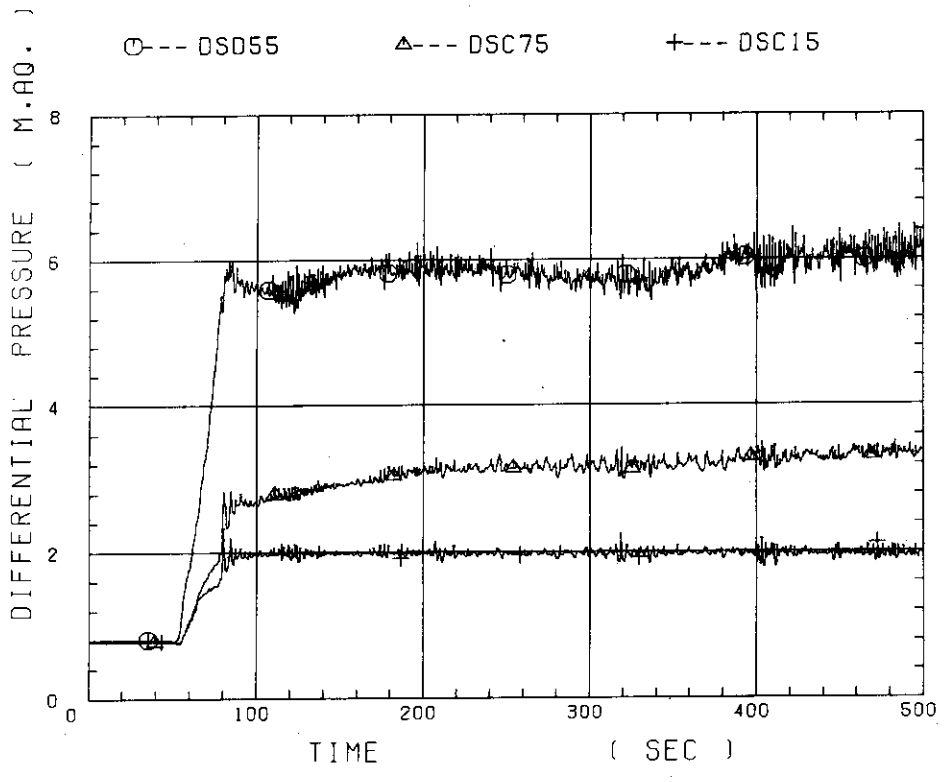

Fig. C-26 Differential pressure through downcomer, core, and lower plenum

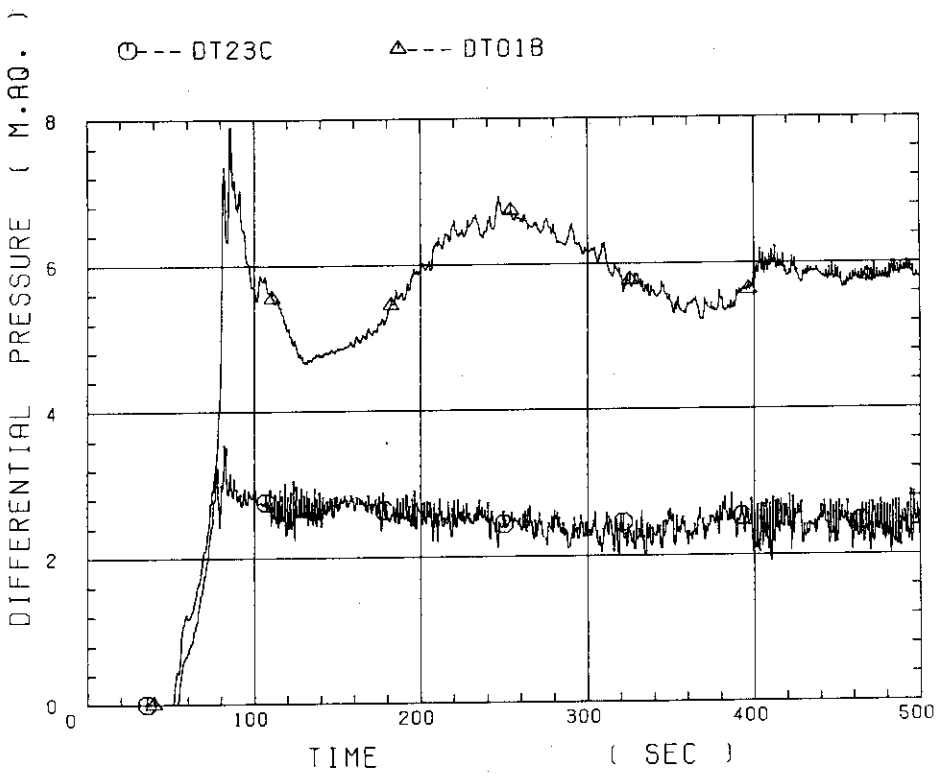

Fig. C-27 Differential pressure through intact and broken loops

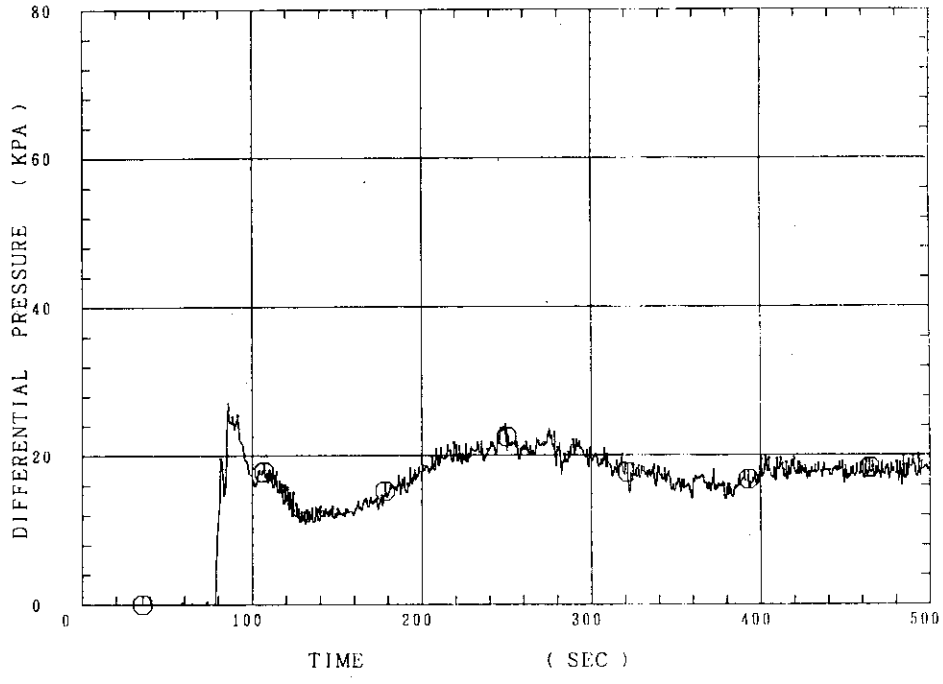

Fig. C-28 Differential pressure through broken cold leg nozzle

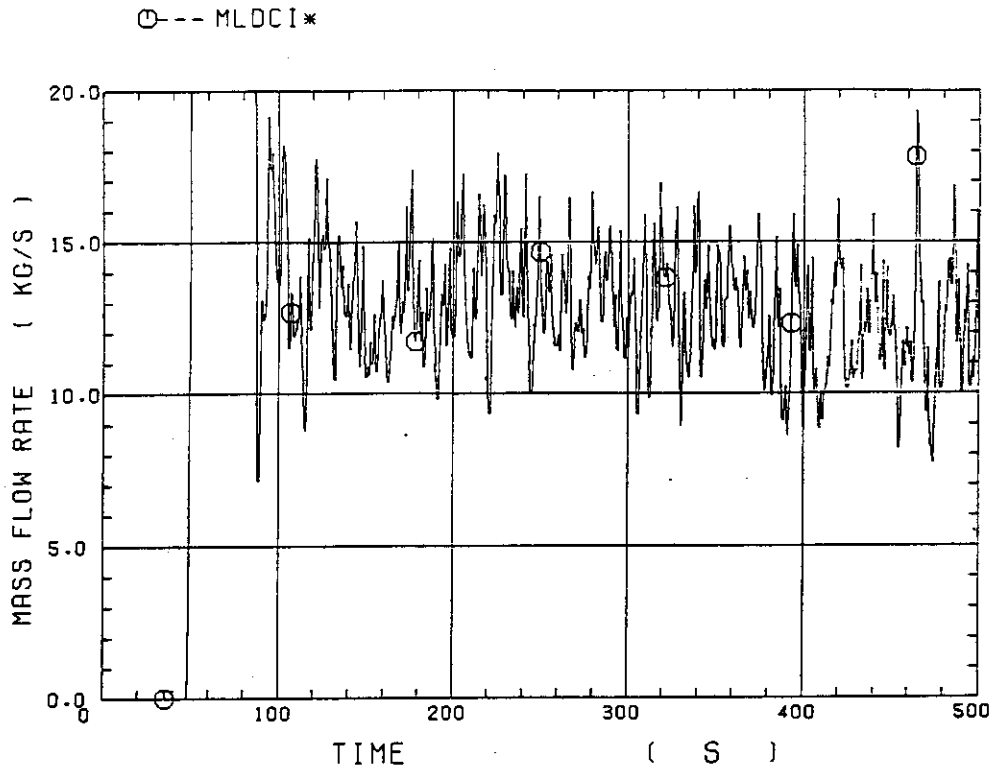

Fig. C-29 Total water mass flow rate from intact loops to downcomer

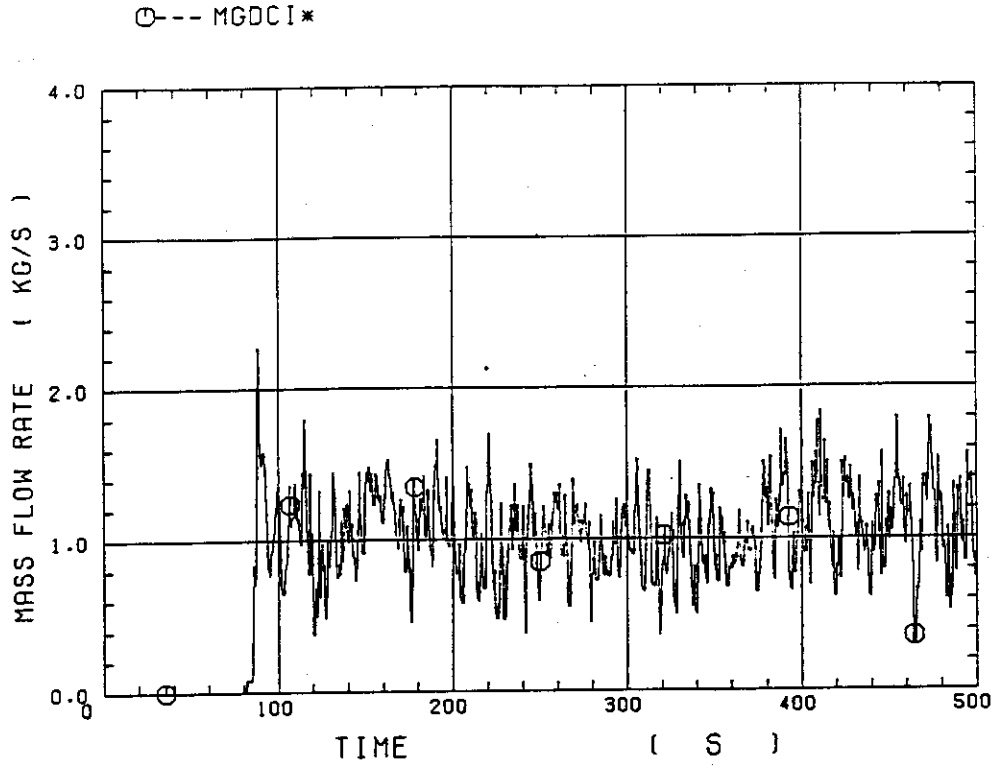

Fig. C-30 Total steam mass flow rate from intact loops to downcomer

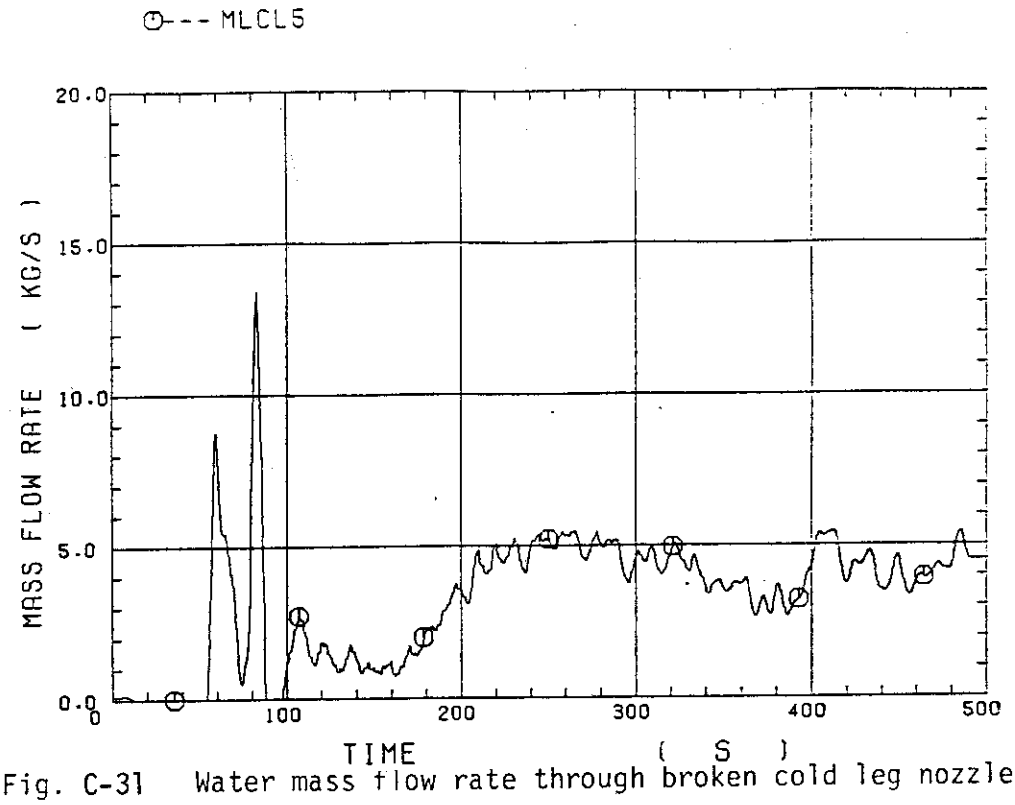

Fig. C-31 Water mass flow rate through broken cold leg nozzle

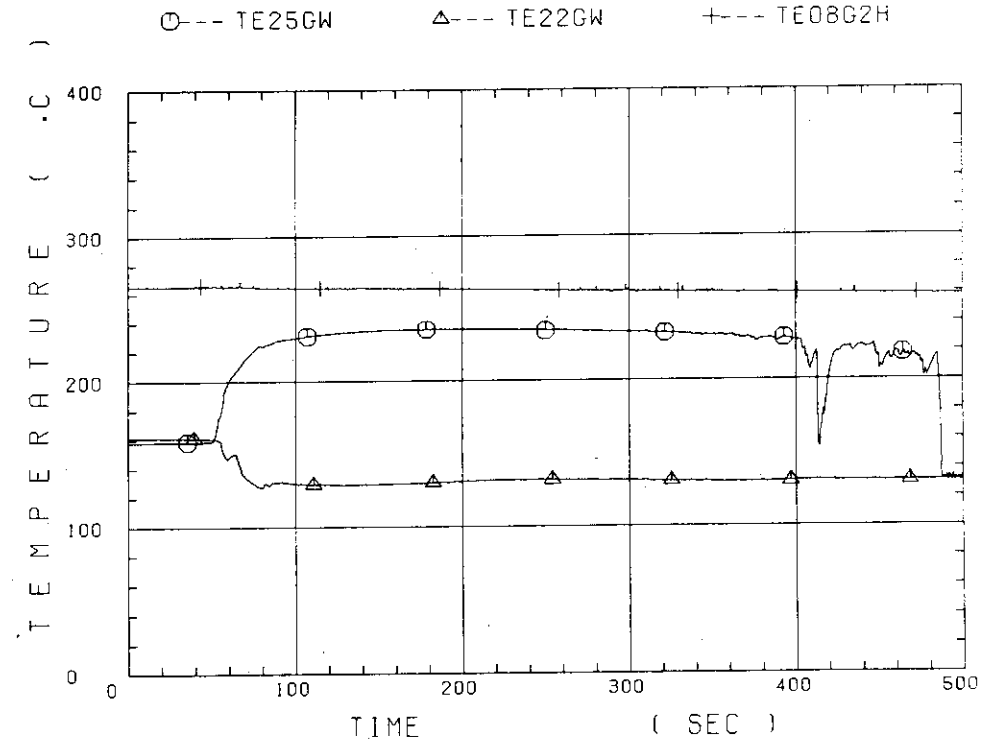

Fig. C-32 Fluid temperature in inlet plenum, outlet plenum, and secondary of steam generator 1

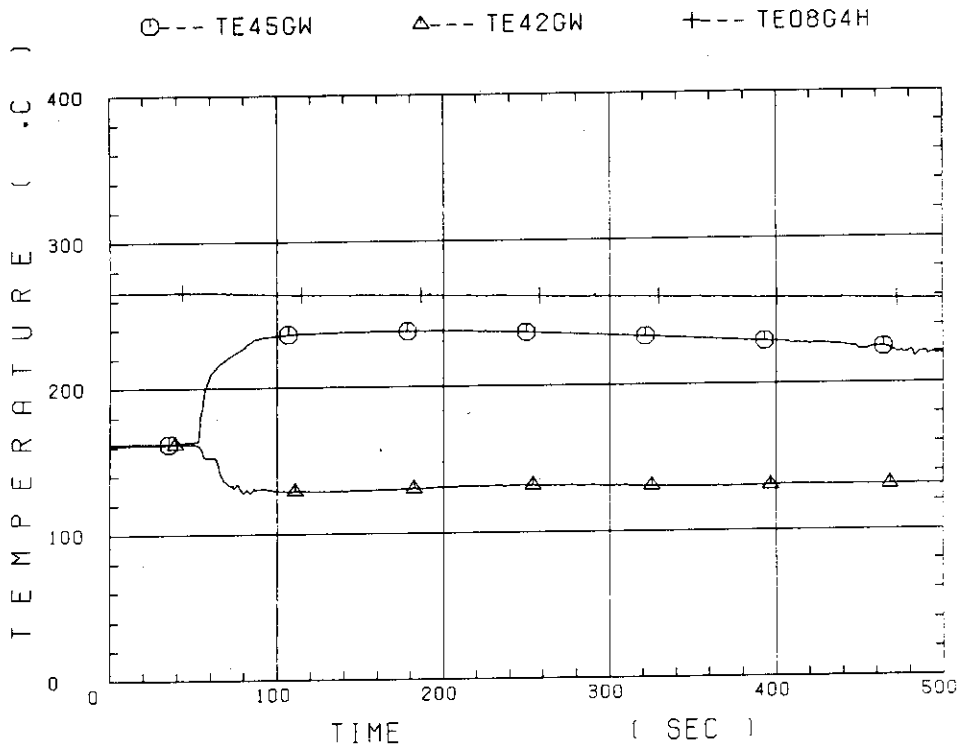

Fig. C-33 Fluid temperature in inlet plenum, output plenum, and secondary of steam generator 2

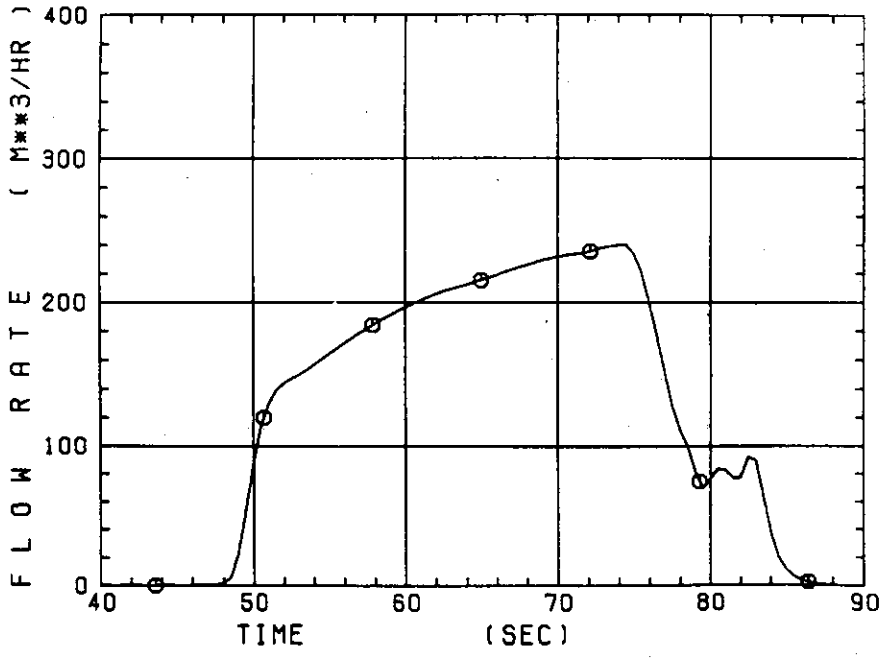

Fig. C-34 Total accumulator injection rate

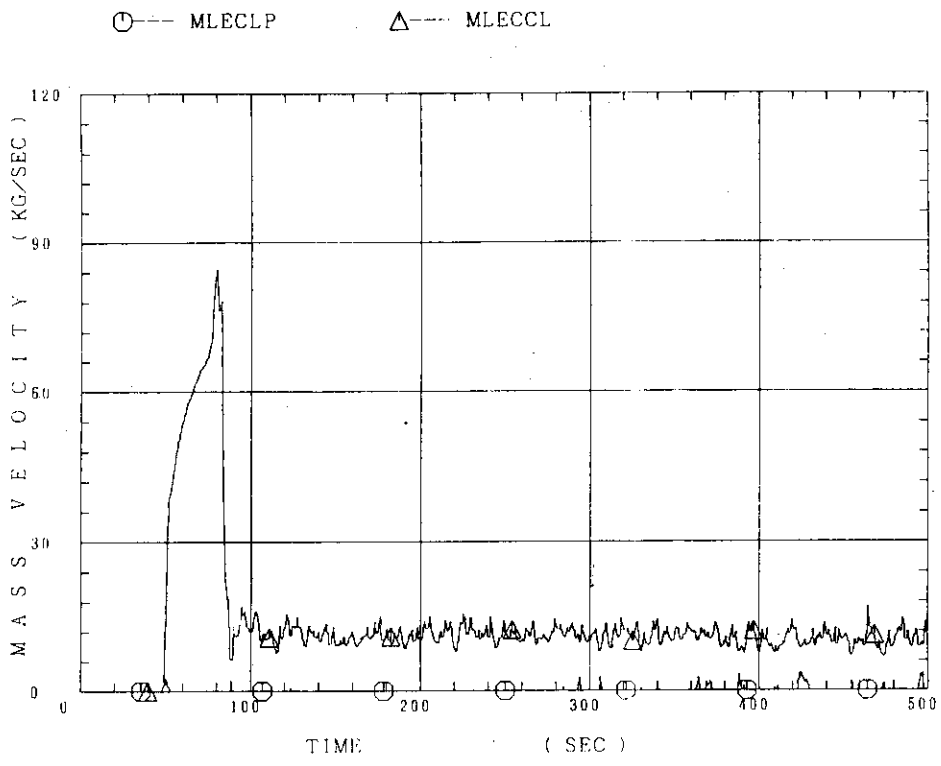

Fig. C-35 ECC water injection rates to lower plenum and to cold legs

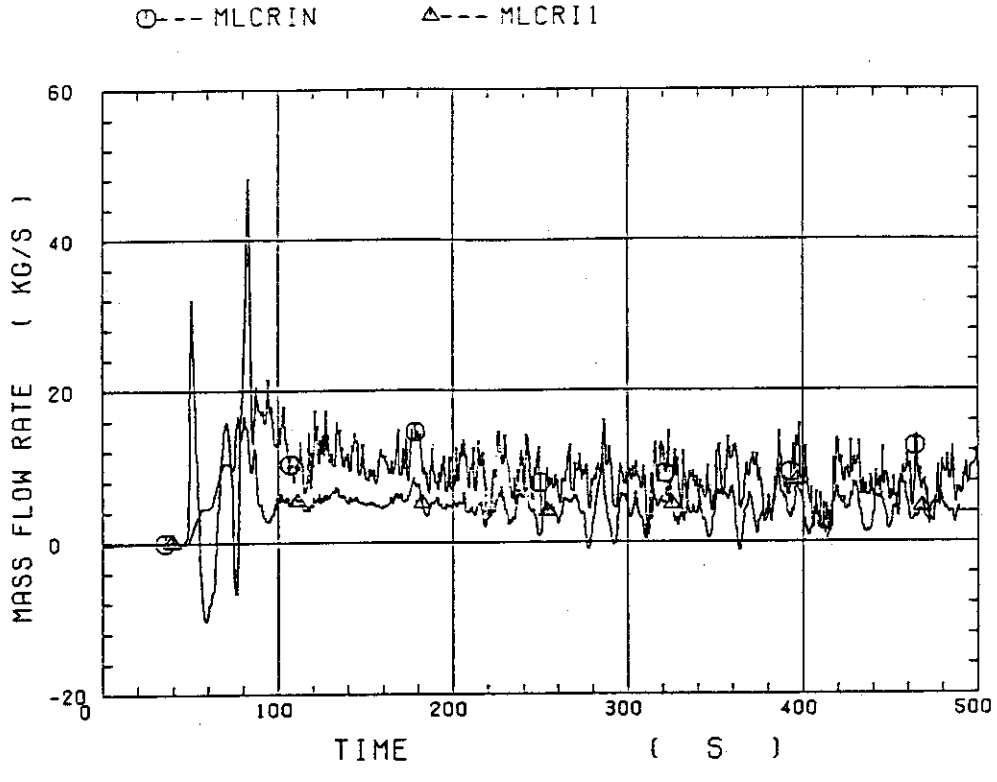

Fig. C-36 Core inlet mass flow rates estimated by mass balance downstream and upstream of core inlet

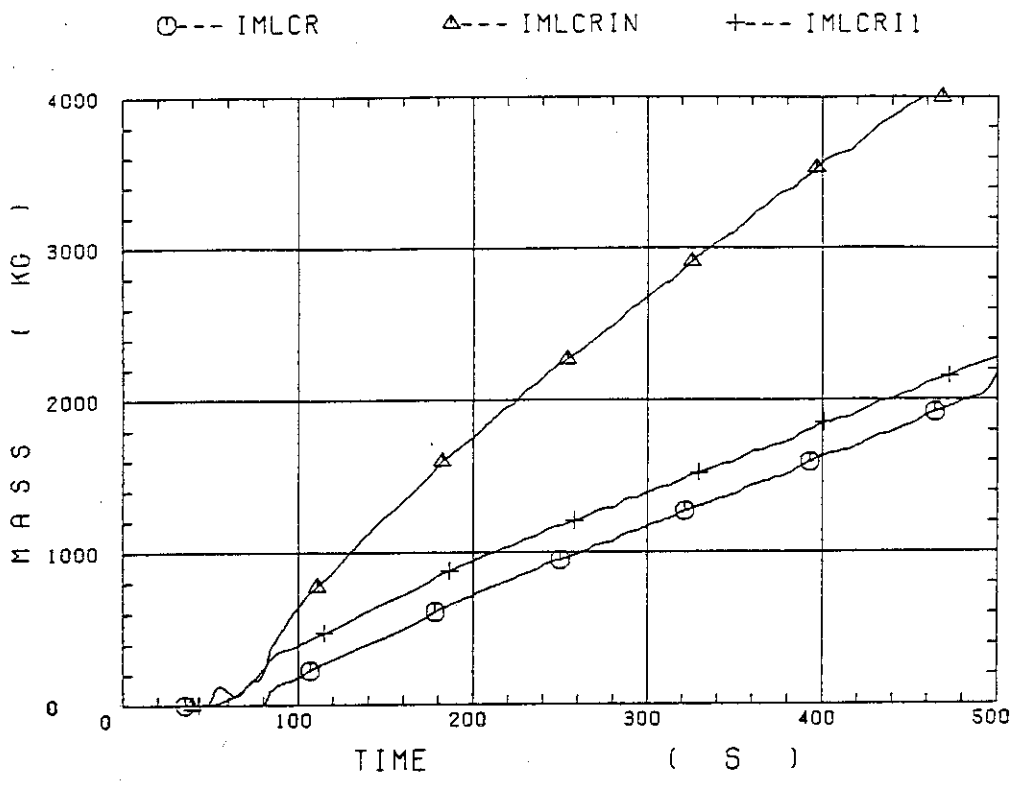

Fig. C-37 Comparison of injected mass into core among two estimation methods and evaluated mass